



**Politecnico
di Torino**

Politecnico di Torino

Corso di Laurea Magistrale in Ingegneria Biomedica
A.a. 2021/2022
Sessione di Laurea Luglio 2022

Additive manufacturing of bioactive glass scaffolds for bone repair by stereolithography

Relatori:

Prof. Francesco Baino
Prof.ssa Enrica Vernè
Dr. Martin Schwentenwein

Candidato:

Carlo Pillosu

Sommario

1	INTRODUCTION.....	1
1.1	Bone tissue	1
1.1.1	Bone tissue cells	1
1.1.2	Bone tissue morphology	3
1.1.3	Mechanical properties of bone tissue	6
1.1.4	Osteogenesis	7
1.2	Bone Tissue Engineering	10
1.2.1	Biomaterials in Bone Tissue Engineering	12
1.2.2	Ceramic biomaterials in Bone Tissue Engineering	15
1.3	Bioactive glasses	17
1.3.1	Synthesis methods	21
2	TECHNIQUES FOR MAKING SCAFFOLDS IN BONE TISSUE ENGINEERING	25
2.1	Scaffold definition	25
2.2	Scaffold requirements	25
2.2.1	Biological requirements	26
2.2.2	Structural features	27
2.2.3	Composition	28
2.3	Fabrication process	29
2.3.1	Conventional methods	29
2.4	Additive manufacturing technologies	33
2.5	Stereolithography (SLA)	39
2.5.1	Processing.....	39
2.5.2	Slurry characteristics	40
2.5.3	Main parameters	41
2.5.4	Post Processing.....	43
2.6	Digital Light Processing (DLP)-Based Stereolithography	44
2.6.1	Digital Micromirror Device (DMD)	44
2.6.2	Advantages and disadvantages of the DLP-based SLA	45
3	MATERIALS & METHODS	50
3.1	Glass preparation	50
3.2	47.5BG Slurry preparation.....	51
3.3	Manufacturing	52
3.3.1	Pre-Processing	52
3.3.2	Processing.....	53
3.3.3	CeraFab Hardware Control	56
3.3.4	Post-Processing.....	57

3.4	Slurry characterization.....	61
3.4.1	Viscosity test	61
3.4.2	Photorheology test	63
3.4.3	Curing depth test.....	64
3.4.4	Shrinkage test	64
3.5	Scaffold design & Printing job	65
3.6	Scaffold characterization	67
3.6.1	X-Ray Diffraction.....	67
3.6.2	Morphological analysis.....	69
3.6.3	Mechanical tests	72
3.6.4	Bioactivity test.....	74
4	RESULTS & DISCUSSION	77
1.1	Slurry characterization.....	77
1.1.1	Viscosity test	77
1.1.2	Photo-rheology test.....	79
1.1.3	Curing depth test.....	81
1.2	Characterization of porous scaffolds.....	83
1.2.1	Porosity.....	84
1.2.2	XRD	85
1.3	Mechanical tests	86
1.4	Bioactivity Test	89
5	CONCLUSIONS & FUTURE DEVELOPMENT.....	98

Abstract

In the field of regenerative medicine (Tissue Engineering), the repair and regeneration of bone tissue (Bone Tissue Engineering) is one of the most discussed research topics of the last decades. For small bone defects, bone is able to self-regenerate, but in the presence of more extensive defects, such as trauma, congenital diseases or gaps due to the removal of bone tumours, it is necessary to apply grafting procedures that promote healing. Currently, there is no bone grafting material that is the best solution, but each type of graft has its own advantages and disadvantages.

In this MS thesis work, for the first time, the use of the additive manufacturing technique (AM) of Digital Light Processing (DLP)-based Stereolithography has been proposed for the production of silicate bioactive glass porous scaffolds. Additive Manufacturing (AM) techniques are the most promising for scaffold fabrication as they allow obtaining highly interconnected and porous structures through selective photopolymerization, and also have the advantages of high reproducibility and easy execution of the entire production process. They are characterized by the typical layer-by-layer construction of the structure derived from the computer aided design (CAD) model.

Bioceramics and bioactive glasses represent a valid alternative to metal implants and are designed to create specific bonds with bone tissue and promote osseous regeneration. They are known to have excellent biocompatibility, low biodegradability, and mechanical properties similar to those of natural bone. This allows these materials to exhibit a perfect integrability both from the biological point of view and from the biomechanical point of view yielding an optimal transfer of the loads applied to the bone through the gap.

This thesis project focuses on the development of bioactive glass scaffolds produced by DLP-based stereolithography. The experimental activity included, firstly, the preparation of the bioactive silica-based glass powders (47.5B, composition: $47.5\text{SiO}_2-10\text{Na}_2\text{O}-10\text{K}_2\text{O}-10\text{MgO}-20\text{CaO}-2.5\text{P}_2\text{O}_5$ mol.%) at the DISAT laboratories.

The powders were then moved to the Austrian company Lithoz GmbH, operating in the field of additive manufacturing for various sectors, including aerospace, industrial and medical. During the period in Lithoz, the work involved the printing of about 80 porous cylindrical scaffolds (total porosity of $35 \pm 5\%$) starting

from the CAD model of a polymer sponge, which imitated the trabecular bone architecture through the AM technique of stereolithography DLP-based.

Three main activities were carried out:

- characterization of the slurry 47.5BG, evaluating its viscosity and photo-rheological behaviour;
- printing of the scaffolds, thanks to the use of the stereolithographic system CeraFab 7500;
- evaluation of the best heat treatment in the Nabertherm P330 furnace.

The scaffolds produced by this innovative technique display good mechanical properties, comparable with those of human bone. They show an elastic modulus $E=4.8\pm 0.9$ GPa similar to the cortical human bone one, and a Weibull modulus of 3.9 that confirms a proper reliability of the structures.

Subsequently, at the DISAT laboratories, the *in vitro* bioactivity was evaluated by immersion of the samples for 5 different periods of time (24 hours, 48 hours, 1 week, 2 weeks and 1 month) in a simulated body fluid (SBF) solution. The SEM/EDS and μ -CT analyses were then carried out, both on as-such scaffolds and on scaffolds after immersion in SBF, to assess the morphology and porosity of the scaffolds, and XRD for the evaluation of the crystalline phases. These analyses allow understanding if the hydroxyapatite layer has formed on the surface after *in vitro* bioactivity tests, thanks to the ionic exchange between material and solution, which allows bone regeneration and osteointegration. It has been noticed the thickening of the hydroxyapatite layer on the scaffold surface with increasing immersion time in SBF time, associated to a concomitant modest increase of the solution pH towards alkalinity, up to 7.8, which promotes the activity of osteoblasts in the osteogenesis process.

The use of SLA-DLP has therefore been found of great potentialities for the production of porous scaffolds and will deserve further studies and in-depth analysis.

Abstract

All'interno del settore della medicina rigenerativa (Tissue Engineering), la riparazione e rigenerazione del tessuto osseo (Bone Tissue Engineering) è uno dei temi di ricerca più trattati degli ultimi decenni. Per piccoli difetti ossei, l'osso è in grado di auto-rigenerarsi, ma in presenza di difetti più estesi dovuti a traumi, malattie congenite o lacune a seguito dell'asportazione dei tumori ossei, è necessario ricorrere all'uso della chirurgia e di un innesto che ne promuova la guarigione. Attualmente non esiste un materiale per l'innesto osseo che rappresenti la soluzione migliore ma ogni tipo di innesto ha i propri vantaggi e svantaggi. In questo lavoro di tesi, per la prima volta, è stato proposto l'utilizzo della tecnica di additive manufacturing (AM) della Stereolitografia basata sul Digital Light Processing (DLP) per la produzione di scaffold porosi in biovetro a base di silice. Per la loro realizzazione, le tecniche di Additive Manufacturing (AM) sono le più promettenti in quanto permettono, tramite la fotopolimerizzazione selettiva, l'ottenimento di strutture altamente interconnesse e porose, ed inoltre presentano il vantaggio di avere alta riproducibilità e facilità di esecuzione dell'intero processo produttivo. Esse sono caratterizzate dalla tipica costruzione layer by layer della struttura derivante dal modello di progettazione assistita (computer-aided design CAD). Le bioceramiche e i biovetri rappresentano una valida alternativa agli impianti metallici e sono progettate per creare specifici legami con il tessuto osseo e promuoverne la rigenerazione. Sono note per avere una eccellente biocompatibilità, bassa biodegradabilità e proprietà meccaniche simili a quelle dell'osso naturale. Questo permette a questi tali materiali una perfetta integrabilità sia dal punto di vista biologico sia dal punto di vista puramente biomeccanico che permette un ottimale trasferimento dei carichi applicati all'osso attraverso la lacuna.

In primo luogo, si è proceduto con la preparazione delle polveri di vetro bioattivo a base di silice (47.5B, composizione: $47.5\text{SiO}_2\text{-}10\text{Na}_2\text{O-}10\text{K}_2\text{O-}10\text{MgO-}20\text{CaO-}2.5\text{P}_2\text{O}_5$ mol.%) presso i laboratori del DISAT.

Le polveri sono poi state trasportate presso l'azienda austriaca Lithoz GmbH, operante nel campo dell'additive manufacturing per diversi settori, tra cui quello aerospaziale, industriale e medico.

Parte dell'attività sperimentale di tesi è stata svolta in Lithoz, dove sono stati realizzati circa 80 scaffold cilindrici porosi (porosità totale $35 \pm 5\%$) partendo dal modello CAD di una spugna polimerica, che imitasse l'architettura trabecolare dell'osso e fosse in grado di favorire la rigenerazione ossea attraverso la tecnica

AM della stereolitografia basata sul digital light processing. È stata effettuata la caratterizzazione dello slurry a base del vetro 47.5B, valutandone la viscosità e il comportamento foto-reologico, la stampa degli scaffold grazie all'utilizzo del sistema stereolitografico CeraFab 7500 e la valutazione del miglior trattamento termico nel forno Nabertherm P330 per la rimozione della componente organica e la sinterizzazione delle particelle vetrose. Gli scaffold prodotti con questa tecnica innovativa hanno dimostrato eccellenti proprietà meccaniche, confrontabili con quelle dell'osso umano. Presentano un modulo elastico di $E=4.8\pm 0.9$ GPa confrontabile con quello dell'osso corticale umano e un modulo di Weibull pari a 3.9, il quale dimostra una buona affidabilità delle strutture prodotte.

Successivamente, presso i laboratori del DISAT, i campioni sono stati valutati dal punto di vista della bioattività in vitro tramite l'immersione per 5 periodi di tempo diversi (24 ore, 48 ore, 1 settimana, 2 settimane e 1 mese) in soluzione SBF (simulated body fluid). Sono poi state effettuate, sia sugli scaffold tal quali, sia sugli scaffold dopo immersione in SBF, le analisi SEM/EDS e μ -CT, per valutare la morfologia e il grado di porosità degli scaffold, e XRD per la valutazione delle fasi cristalline presenti. Queste analisi sono particolarmente importanti per lo studio della bioattività in quanto consentono di capire se si è formato uno strato di idrossiapatite sulla superficie del campione dopo immersione in SBF, grazie allo scambio ionico tra materiale e soluzione, che permette la rigenerazione dell'osso e l'osteointegrazione.

È stato notato l'ispessimento dello strato di idrossiapatite sulla superficie all'aumentare del tempo di immersione in SBF con un contestuale modesto aumento del valore di pH della soluzione verso l'alcalinità, fino a 7.8, che promuove l'azione degli osteoblasti nel processo di osteogenesi.

L'utilizzo della stereolitografia-DLP è dunque risultata di grandi potenzialità per la produzione di scaffold porosi e meritevole di ulteriori studi e approfondimenti.

1 INTRODUCTION

1.1 BONE TISSUE

Bone tissue is a dynamic and plastic tissue that provides for modelling its own structure following organic and mechanics stimuli. It is made of an organic and one inorganic part. The organic part is composed of bone cells (osteoprogenitor cells, osteoblasts, osteocytes and osteoclasts that provide growth, production and reabsorption of bone tissue) and extracellular matrix (amorphous substance and type I collagen fibres). The inorganic part is composed of lots of minerals like calcium and magnesium phosphates and Na citrates, Mn, K. The organic component of the extracellular matrix represents 35% of the dry weight of the bone and determines its strength and elasticity while the mineralized inorganic component represents 65% of the dry weight and gives the bone compactness and hardness. Bone tissue is subjected of several structural and functional changes caused by age, nutrition and general person's condition.

Calcium	34.8
Phosphorus	15.2
Sodium	0.9
Magnesium	0.72
Potassium	0.03
Carbonates	7.4
Fluorine	0.03
Chlorine	0.13
Pyrophosphates	0.07
Other elements	0.04

Table 1: Bone composition (%) of adults

1.1.1 Bone tissue cells

The bone tissue cells are osteoprogenitor cells, osteoblasts, osteocytes and osteoclasts and are described below:

- **Osteoprogenitor cells:** are mesenchymal cells with stem properties, in fact they can proliferate and differentiate into osteoblasts. They are located in the periosteum and endosteum: reactivated provide for the formation of new bone tissue.
- **Osteoblasts:** are the precursors of osteocytes; they are bulky, highly polarized cells with a slightly displaced ovoid nucleus at the periphery and with intensely basophilic cytoplasm. They provide both the production of the organic matrix (called osteoid) and the deposition of the inorganic one, therefore have osteogenic functions. They produce type I collagen, osteocalcin, osteopontin and sialoprotein of the bone. When the osteoblasts have finished the formation of the bone remaining trapped inside gaps in the matrix produced by them, they become osteocytes.
- **Osteocytes:** are irregularly shaped cells, with a well-evident nucleus and a cytoplasm that has several extensions. They are lodged in the bony gaps from which depart, in every direction, numerous microscopic channels. Through these channels the cytoplasmic prolongations of different osteocytes come in contact with each other through communicating junctions and with blood capillaries present in the bone channels, thus allowing metabolic exchanges between the osteocytes themselves and between osteocytes and blood. Furthermore, osteocytes maintain the extracellular matrix of the bone.
- **Osteoclasts:** they do not belong to the osteoprogenitor line but derive from the fusion of numerous monocities precursors (until 30) and are delegated to the destruction (resorption) and to the reshaping of the bone tissue. They are very big cells, being able to exceed even the 100 μm of diameter and have numerous nuclei. Osteoclasts too are highly polarized cells: when activated, they have a cytoplasmic face near the bone with very mobile ripples and adhere to the surface of the bone creating a microenvironment isolated from the surrounding (sealed area) which is acidified for the subsequent activation of lysosomal (protein and phosphatase) and non-lysosomal (metalloproteinase) derived enzymes. This process leads to the erosion of the bone matrix and the formation of a depression called Howship gap.

1.1.2 Bone tissue morphology

Bone tissue can be divided into two main categories: trabecular bone and lamellar bone tissue. The first category represents the primary bone tissue, and it is present during prenatal life and in adults in cases of bone neo-deposition (for example in case of fractures); lamellar bone constitutes the majority of bone tissue in adult mammals and is organized into gills.

Trabecular bone tissue

In the prenatal life and in the adult under particular conditions the function of the bone tissue is not so much to perform the task of strong resistance to pressure or traction, but rather to be as light as possible, elastic and plastic. Non-lamellar bone tissue is divided into non-lamellar bone tissue with braided fibres and non-lamellar bone tissue with parallel fibres (mainly found in birds). In the non-lamellar woven tissue, the collagen fibres are intertwined to form a dense network, the fundamental substance, arranged irregularly, is poorly represented both in its organic and inorganic part, Bone gaps are globose and tend to be larger than lamellar bone. The non-lamellar tissue of intertwined fibres is also present in the adult at the level of sutures due to fractures, in ligament and tendon insertions, on the surfaces close to the periosteum, in all bone neo-depositions in general and in particular in the tooth cement. The bony tissue is not lamellar with parallel fibres is, on the contrary, rare in the mammals: it can be found in the insertion zones of the tendons.

Lamellar bone tissue

The lamellar bone, thanks to its chemical composition and its particular structural organization, has a strong resistance to traction, pressure and mechanical stress in general. Thanks to its organization in lamellas, in fact, this tissue guarantees a good resistance to stress, although not weighing down the skeleton. Lamellar bone tissue is divided into:

- **compact lamellar bone tissue** if it is composed predominantly of complete concentric lamellae, such as in diaphysis;

- **spongy lamellar bone tissue** if instead it is composed of incomplete gills that form many small fragments embedded between them (trabecular bones), as for example in the epiphysis.

The compact bone tissue is very hard, crossed by numerous channels containing blood vessels and lymphatic ducts visible only under a microscope. The spongy bone is presented as a three-dimensional network of trabecular bones that comes to delimit a labyrinthine space filled with bone marrow. In the long bones are distinguished the epiphysis, short and roundish, localized at the extremities and formed mainly by spongy bone, and an elongated part, central, shaped like a hollow cylinder called diaphysis, formed by compact bone, extremely resistant to shocks and pressures and containing bone marrow. In flat bones, however, we distinguish two surfaces of compact bone tissue, called inner and outer plank. A layer of spongy bone is included in the middle.

Compact lamellar bone tissue

It constitutes the diaphysis in the long bones, the superficial layer of the epiphysis, the planktops of the flat bones and generally covers all the bony surfaces. The bony gills are organized in concentric layers to form the osteons, in which the osteocytes are placed circularly, after different orbits, around channels, called Havers channels, containing one or two small blood capillaries. The number of gills surrounding a single Havers channel can vary from 4 to 20. The various channels of Havers communicate with each other thanks to other channels placed, however, transversally or obliquely, called channels of Wolkman, also containing blood capillaries. The nutrients reach the osteocytes through the capillary network and distributed through the dense network of cytoplasmic extensions that connect them. The spaces created between the different osteons are occupied by fragments of lamellar bone of variable shape and size called interstitial systems. The boundaries between osteons and interstitial systems are easily detected by a layer of refracting connective tissue called a cementing line. The bone surface in contact with the periosteum and the endostasis is formed by gills arranged parallel to the free surface of the bone; these gills are called circumferential gills.

Spongy lamellar bone tissue

It is formed by incomplete gills associated with forming trabeculae (such as in the epiphysis of long bones). This spatial arrangement provides better resistance to multidirectional pressures, and generates

intercommunicating spaces in which the bone marrow is housed. The gills are more or less woven and of variable thickness. The osteocytes are distributed in the gills unevenly and with variable size and shape.

Periosteum

The outer surfaces of the bone are covered by a thick connective capsule consisting of dense connective tissue to intertwined fibres, the periosteum. It has the task of protecting the bone and supporting the trophic action mediated by the blood vessels of which it is rich. In the outer face of the periosteum are present few cells and many collagen fibres (fibrous layer), in the inner face, instead, there are few fibres, numerous blood capillaries and osteoprogenitor cells with osteogenic potential (osteogenic layer). From the periosteum they depart transversally, towards the bone tissue, connective fibres, called Sharpey fibres, which have the task, penetrating into the system of external circumferential lamellae, to provide a good anchoring system to the bone. The periosteum is not present in the joints and in the insertion points of muscles and ligaments.

Endosteum

The endosteum is formed by a layer of pavementous cells and connective fibres that cover all the internal surfaces of the bone (bone trabecular of the spongy bone, medullary cavities of the compact bone, Havers and Wolkmann channels). The cells that form the endostasis have a high osteogenic potential.[1]

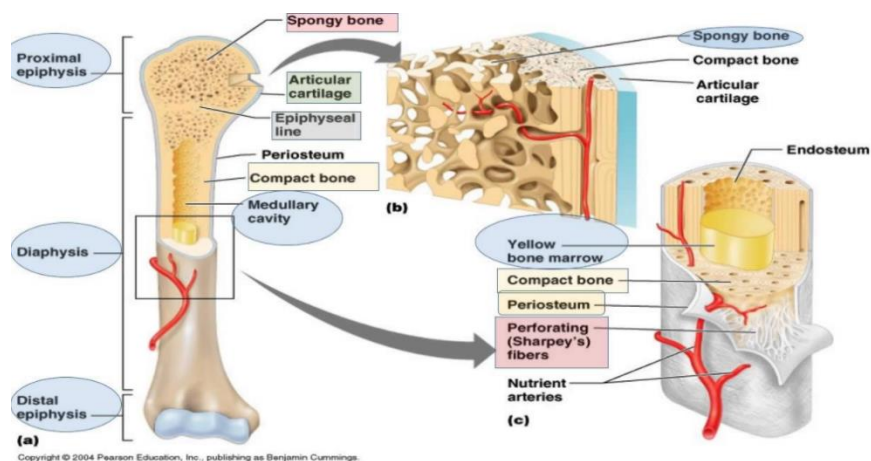


Figure 1: Bone structure

1.1.3 Mechanical properties of bone tissue

Biological materials can have different mechanical properties in different conditions of subject, load conditions and age of the patient.

Bone is an anisotropic and non-homogeneous material because its behaviour changes according to the direction of the applied load. In addition, thanks to the phenomenon of remodelling, it is able to vary its shape dynamically depending on the stress to which it is subjected. You can define the bone tissue as a visco-elastic material: its predominant quality is fragility. Bone can be assimilated to a very rigid spring and when it is deformed even only 2% of its length, it breaks. The Young module (or elastic module) of bone is between 10-20 GPa but you can notice a different behaviour between the compact bone and the trabecular one. This last one, despite having the task to transfer and to distribute the loads in the surrounding cortical bone, is less rigid, presenting a stiffness of about 1/5-1/10 of the cortical bone in compression. It is in fact less resistant to mechanical stresses and subject to breakage even for lower efforts and this is the reason why it always needs a stronger layer of compact and durable bone.

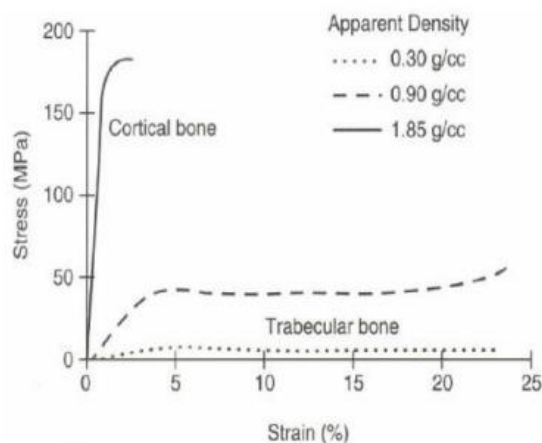


Figure 2: Stress-strain plot of bone under compression: Cortical bone vs. Trabecular bone

Most tests to study bone behaviour are carried out on non-viable bone, and the values obtained in vitro are not always corresponding to in vivo behaviour. Resistance to stress does not provide a unique value but depends a lot on the type of load that impacts on it, the type of bone involved but also the test that is being

applied in the test. In general, it can be considered as a material with good fatigue strength and compression and with high flexibility, guaranteed by the trabecular bones.

<i>Property</i>	<i>MPa</i>
<i>Tensile strength</i>	89-118
<i>Flexural strength</i>	76
<i>Compressive strength</i>	125-166
<i>Parallel delamination strength</i>	116
<i>Perpendicular delamination strength</i>	40-92
<i>Torsion strength</i>	65
<i>Elastic modulus</i>	19500-20500

Table 2: Mechanical properties of the bone

1.1.4 Osteogenesis

Osteogenesis or ossification is the process that lead to new bone tissue formation. This process start from a pre-existing mesenchymal tissue that is transformed into bone tissue.

There are two types of osteogenesis:

- **Direct ossification** (or intramembranous) in which bone tissue is formed from mesenchymal tissue;
- **Indirect ossification** (or chondral) in which bone tissue is formed from hyaline cartilage.

Both ossification types originate non-lamellar bone that is subsequently transformed into lamellar bone.

Direct ossification

During the process of direct or intramembranous ossification the mesenchymal cells of the embryo are organized into aggregates (ossification centres) where they differ in osteoblasts that deposit osteoid tissue (extracellular matrix of bone), subsequently mineralized to form primitive bone tissue also called non-lamellar bone tissue to braided fibres which will then be replaced, following remodelling, by lamellar bone tissue. Examples of intramembranous ossification are those of frontal, parietal, part of temporal and maxillary bones. In the jaw, the direct ossification process (called mantle ossification) is initiated and guided by the presence of a cartilaginous button that acts as a catalyst and allows the transformation of the surrounding mesenchymal tissue into bone tissue.

Indirect or chondral ossification

When the ossification process takes place through an intermediate cartilage passage, it is called indirect ossification or chondral. This type of ossification is typical of long bones, those of the spine, the pelvis, part of the facial ones and the ribs. For the mechanism from which this type of ossification originates is called "replacement bone". The calcified bone reflects roughly the same architecture as the previous cartilage model, varying significantly only in size. Indirect ossification occurs in two different ways

- perichondral ossification
- endochondral ossification

Perichondral ossification

In the cartilage model we see a thickening of the perichondrium present on the diaphysis (long part of the bone) for a significant increase of the osteoblasts present in the connective capsule. Subsequently they begin to penetrate inside the cartilage vessels carrying other osteoblasts along with chondroclasts used for the destruction of cartilage tissue. From the outside towards the inside of the diaphysis a thin reticular web is formed that will provide the first osteoid tissue model (primary ossification centre). Much of the cartilage tissue degenerates as neoformed bone tissue begins to settle. This process takes place through the formation of a ossification front in which cartilaginous cells are placed along columns, disperse chromatin and hypertrophying to the point of destruction. At the same time the osteoblasts of the opposite front will deposit

in the intracellular spaces osteoid tissue that, subsequently, will organize in gills and will form the bone tissue itself. This will result in the elongation of the bone model.

Endochondral ossification

When most of the diaphysis is ossified, the vessels enter first one epiphysis (the proximal one), and then the other, forming secondary ossification centres. In this second phase the deposition of the osteoid tissue begins from the inside of the epiphysial model and proceeds outwards allowing an increase of the bone in width. In the diaphysis, meanwhile, there will be a remodelling of the already formed bone tissue, by macrophages, thus allowing the osteoblasts present in the endosteum the deposition of other osteoid tissue. This will increase the thickness of the diaphysis itself. At the end of the indirect ossification process the two layers of epiphyseal cartilage will be reabsorbed, first of the lower and then of the upper ones.

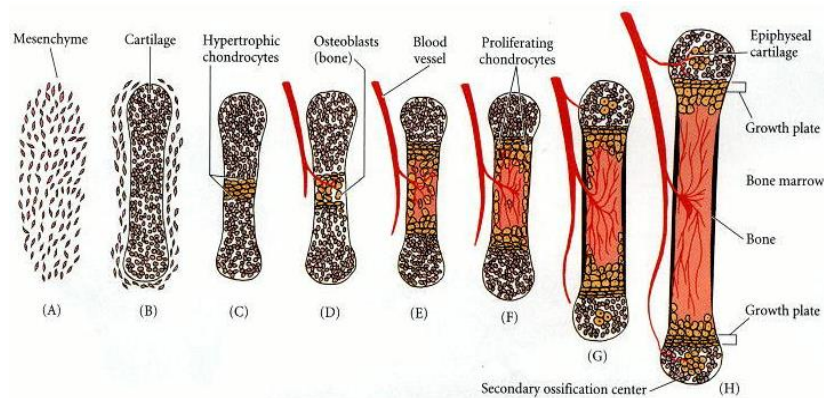


Figure 3: Stages of ossification

Stages of indirect ossification

The indirect ossification process is carried out in successive phases. Typical example is the ossification at the level of the metaphysis of the long bone. There are different areas:

1. The **resting or reserve cartilage area** shall consist of reserve chondrocytes bordering on the epiphysis.
2. A **proliferation zone**, it consists of active proliferative chondrocytes arranged in columns.

3. The **ripening zone** is formed by chondrocytes which increase in size.
4. A **hypertrophic zone**, where chondrocytes have reached their maximum size, the extracellular matrix is progressively calcified, reducing its permeability to nutrients.
5. **Zone of degeneration**, calcification of the matrix leads to degeneration of chondrocytes. The spaces of the gaps left empty are populated by blood vessels and cells osteoprogenitors that then regroup on the formation of residual calcified cartilage and on which will deposit non-lamellar bone tissue to intertwined fibres that will then reorganize into lamellar bone tissue.

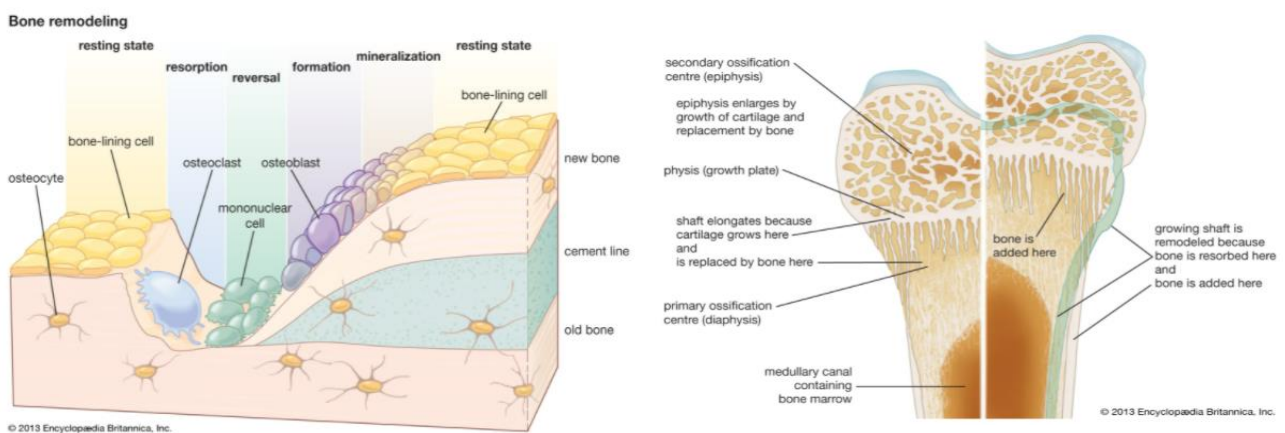


Figure 4. Different areas of bone remodelling

1.2 BONE TISSUE ENGINEERING

Medical advances have led to an increasing life expectancy even if this introduces new challenges: increases in age-related diseases and associated reductions in quality of life. Trauma, injury, diseases or advancing years can bring to the loss or dysfunction of skeletal tissue and consequently significant morbidity as well as a variety of socio-economic issues. In addition, changing patient's demographics, together with rising patient's expectations and increasing complexity of resulting clinical scenarios, provide the task for new, more reliable skeletal regeneration strategies. In the current approaches to replace or lost skeletal tissue there are several substantial limitations and disadvantages that may be harmful. Tissue engineering and regenerative medicine have come ahead in the recent years with new approaches to take care of loss or

dysfunction of skeletal tissue caused by trauma, injuries, diseases or advancing patient age. This type of engineering aim to create robust, reproducible and enhanced bone formation scaffolds or grafts to repair the patient's bone defects.[2]

The field of bone tissue engineering (BTE) was initiated nearly three decades ago. Interest and progress in the BTE field has seen enormous growth over the years, with an exponentially increasing number of studies and reviews published on the PubMed database since the mid-1980s . The field of BTE focuses on alternative treatment options that will eliminate issues related to current clinically used treatments like donor site morbidity, limited availability, immune rejection or pathogen transfer. BTE requires the work of scientists, engineers, and surgeons to achieve this goal of creating bone grafts that enhance bone repair and regeneration.[3]

The BTE concept highlights several main points:

- a biocompatible scaffold that mimics the natural bone extracellular matrix;
- osteo-genic cells to lay down the bone tissue matrix;
- activation of morphogenic signals that help to direct the cells to the phenotypically desirable type;
- sufficient vascularization to bring the growing tissue nutrient supply.

Specifically, upon implantation, the graft may influence the host by releasing osteogenic and/or vasculo-genic growth factors (i.e., growth factor-releasing scaffold, scaffold with growth factor analogs, or seeding with platelet-enriched plasma), or by housing cells that are genetically engineered to or naturally release growth factors. As a consequence, accelerated cell homing, vascularization, and regeneration of the defect site can be achieved. [4]

1.2.1 Biomaterials in Bone Tissue Engineering

Biomaterial is a non-living substance used in the manufacture of a medical device that at some point has an interface with living tissue”.

(Consensus Development Conference, Chester, UK, 1986)

“A biomaterial is a substance that has been engineered to take a form which, alone or as part of a complex system, is used to direct, by control of interactions with components of living systems, the course of any therapeutic or diagnostic procedure, in human or veterinary medicine”

(Williams DF. On the nature of biomaterials, Biomaterials 2009)

Biomaterials are a class of materials that can be used in contact with biological tissues, without causing adverse reactions in the host organism and designed to evaluate, support or replace any tissue, organ or function of the body. Thanks to this ability they are used for the construction of medical devices intended to perform different functions. In particular, they can be applied in permanent structures such as artificial prostheses and artificial organs or in devices that remain in contact with the human body for a limited period of time such as sutures or scaffolds. Different types of materials such as polymers, metals, glass and ceramics fall inside this category, provided that they meet the following requirements:

1. Biofunctionality: ability of a material to reproduce a certain physical and mechanical function.
2. Sterilizability: the ability of a material to maintain unchanged its biofunctional characteristics following the sterilization process.
3. Biocompatibility: Ability of the material to determine by the host organism a favourable reaction to its presence.

A fundamental distinction in the field of biomaterials consists in the stability that they demonstrate in their reaction with the organism: if they do not undergo substantial chemical or physical transformation as a result of grafting, they are bio-stable; or biodegradable if they are degraded by the human body until they are

completely eliminated: of the latter class are part of the scaffolds produced with glass-ceramic materials. A further distinction applied to biomaterials evaluates reactions with the organism, focusing on the effects on the tissues themselves; bioinert, bioabsorbable and bioactive materials can be highlighted.

Bioinert materials: are chemically and physically stable and have minimal interactions with the organism and surrounding tissues, allowing them to be used to avoid the development of adverse reactions. Some examples can be found in alumina, zirconia and titanium oxide (Al_2O_3 , ZrO_2 , TiO_2) and it should be noted that in the absence of a chemical bond established between the implant and the tissue, specific cement binders can be used as joining agents.

Bioabsorbable materials: consist of substances that are metabolized by the organism until they are dissolved and expelled in such a way that at the end of the reabsorption process the grafted plants are completely replaced by biological tissue. They are bioabsorbable ceramics such as calcium phosphate and bioactive glasses and polymeric materials such as polylactic acid (PLA) and polyglycol (PGA).

Bioactive materials: cause a positive reaction after implantation, exhibiting an intermediate behaviour between bioresorbable and bioinert materials. Bioactive materials cause a reaction that may be categorized as being between that of bioabsorbable materials and bioinert materials. A bioactive material is able to create a compatible environment with the growth of healthy tissue (osteogenesis, if we refer to bone tissue), resulting in a mineralized interface that acts as a natural junction between tissue and material. Bonding mechanisms, bonding times, interface thickness and bonding strength change depending on the type of material chosen.

Biomaterials for bone regeneration are able to speed up and strengthen growth of new bone. Examples of bioactive materials are bioactive glasses, calcium carbonate, calcium phosphates (tricalcium phosphate (TCP), hydroxyapatite (HA) and several formulations of calcium sulphate (CS)). [5]

Bioactive material for bone regeneration can be divided into two different categories:

Class A: osteoproliferative material (e.g. bioactive glasses). The implant is colonized by the osteogenic cells present in the surrounding biological space. These materials can bind to both soft tissue and hard tissue and exert an osteostimulatory effect on bone cells [6].

Class B: osteoconductive material (e.g. hydroxyapatite). The implants provide a biocompatible interface on which tissue of bone can grow.

Biomaterials commonly used in BTE can be grouped into four major classes [7,8]:

1. **Metals:** are inert and are mainly used for applications subjected to heavy loads, with sufficient fatigue strength to withstand the daily activity of the individual. Metals have several disadvantages such as a lack of adhesion capacity of tissue cells and slow and poor degradation of the implant.[9] To replace or repair damaged bone, the most commonly used metals are stainless steel, titanium-based alloys, tantalum and cobalt alloys.
2. **Synthetic polymers and natural polymers:** Natural and synthetic polymers are applied in different BTE fields of application, especially for scaffold construction. They are easier to process than metals. The natural polymers are biocompatible and biodegradable and are very similar to the structure constituents of different kinds of tissues (e.g. collagen).[10] Synthetic polymers can be obtained in the laboratory under monitored conditions. They have well known and reproducible physical and mechanical qualities like degradation rate, tensile strength and elastic modulus. There are different classes of synthetic polymers that are used in the manufacture of scaffolds as bone substitutes, for example: polyesters, polyorthoesters, polyanhydrides, polycaprolactone.[11]
3. **Ceramics and glasses:** are biomimetic materials famous in BTE because the majority of them have a mineralogical composition similar to that of human bone and good biocompatibility and osteoconductive properties. [12] Thanks to these characteristics, they are utilized to repair, reconstruction and replacement of damaged and sick parts of the body's human skeletal structure.
4. **Composites:** Composites are materials consisting of two or more elements whose physical properties differ considerably from those of the individual constituents which, acting in uneven and asymmetrical synergy, give anisotropic properties to the resulting material. The composite materials, to properly emulate the mechanical behaviour of natural tissues, must have structures with different stiffnesses, a very interesting design challenge. The application of structural composite materials is

mainly aimed at the orthopaedic sector, where the mechanical performance of the material is a primary requirement.

1.2.2 Ceramic biomaterials in Bone Tissue Engineering

Bioceramics can have a natural or synthetic origin and are born to create bonds with the bones in alternative to metallic implants. They have good properties for the biomedical field also due to their matchable physio-chemical properties with some of the human body parts.

Bioceramics, synthetic or naturally derived, are designed to form bonds with bone and are emerging as an alternative to metal implants.[13] Ceramics are defined as oxides, nitrides, sulfides, carbides of metals, and metalloids. [14] These are important in the biomedical field due to their excellent physicochemical properties that are compatible with certain parts of the human body. Initially, bioceramic porcelain was used in the processing of crowns in the 18th century. Then, in the 19th century, plaster from Paris was used for dental purposes. [15,16] The use of ceramics has expanded in the medical field in the 20th century due to advances in therapeutic technology. [17]

Bioceramic materials have excellent biocompatibility, low degradability, high melting point, non-corrosive properties, and poor plasticity than metal-based biomaterials. The bioceramics are solid and fragile, and have fracture toughness similar to the bone tissue module. [18-21] Synthetic bioceramics such as aluminium oxide, zirconium dioxide, titanium, Ca-P-based porous materials, bioactive glasses/glass-ceramics are used in dentistry, orthopaedics, calcified tissues, coatings, medical sensors and many other areas.[22-25] The use of bioceramics also opens to new horizons for the recovery and regeneration of soft tissues.[26] Bioactive glasses/glass-ceramics have become universal materials that can be developed with a great extent of versatility according to the user's needs. Silica based bioactive glass has been widely studied in recent decades. Borates, borosilicates, and other combinations of different compositions based on therapeutic elements offer new approaches for different applications. This will also result in increased penetration into the orthopaedic and dental fields. Advanced approaches also include the use of bioactive glass / glass-ceramic as a 3D scaffold, as a coating of implants and composites that exhibit mechanical properties comparable to natural bone.[27] All biomaterials must be biocompatible and exhibit antibacterial properties.

Developing the right biomaterials for your needs and applications can be a daunting task. For example, adding a dopant to the main composition of glass and glass-ceramics affects various properties, but at the same time they delays other properties. Therefore, proper selection of materials, their composition, concentration, parameters, and design are required io order to balance different properties. For example, in the case of bioactive glass, the antibacterial biocompatibility activity can be increased by doping the matrix.

However, a high dose of doped ions may cause intoxication. Ceramic-based biomaterials have some advantages over metals and alloys, such as density, porosity, high elastic modulus, hardness and cost. But they also have deficiencies, such as poor sinterability, ductility, and machinability. These properties limit their use as biomaterials. In most cases, these original bioactive glasses/glass-ceramics are manufactured using expensive minerals. Recently, sustainable natural bioceramics, such as waste ash, rice husk ash, sugar cane ash, corn reeds, have also been used as an attractive source of silica, which can be converted into valuable biogenic silica nanoparticles and bioactive glass/glass-ceramic.[28] Similarly, food waste such as eggshell powder, egg membrane containing calcium, banana crust containing potassium, polyphenolics, and essential acids can be used to produce beta-tricalcium phosphate, hydroxyapatite, and mesoporous bioactive glasses, an alternative to bioactive glasses used for prostheses and medical treatments. It has also been shown that synthetic minerals combined with agricultural food waste, act as alternatives to biomaterials for various biomedical applications.[29,30]

	Application	Material
Orthopedics	Bone filler	HA, α/β -TCP granules, bioglass
	Total knee arthroplasty	Al_2O_3 , ZrO_2 , $Al_2O_3 + ZrO_2$ composite
	Femoral stem fixation	Bone cement or HA coating
	Bone scaffold	HA, α/β -TCP, bioglass
	Bone screw	Al_2O_3
	Femoral head	Al_2O_3 , ZrO_2 , $Al_2O_3 + ZrO_2$ composite
	Acetabular cup fixation	Bone cement or HA coating
Dental	Posterolateral spinal fusion	α/β -TCP
	Fixed partial denture	Al_2O_3 , ZrO_2 , $Al_2O_3 + ZrO_2$ composite
	Periodontal pocket obliteration	Al_2O_3 , HA
	Dental crown	ZrO_2
Cranio-maxillofacial	Coating on dental screw	HA
	Facial reconstruction	HA, α/β -TCP, bone cement, bioglass
ENT ¹	Alveolar ridge Reconstruction	Al_2O_3
	Middle ear ossicular replacements	Al_2O_3 , HA
Drug delivery	Osteomyelitis	Al_2O_3
	Bone tumor/cancer	Nano HA as drug carrier Nano HA with cancer drugs, bone cement loaded with cancer drugs

ENT¹: ear, nose, and throat.

Figure 5: Applications of the main used materials for BTE

The bioactive glass/glass-ceramics derived from agricultural food waste is more advanced than artificial bioactive glasses. The choice of the primary components and their quantity plays a vital role in qualifying as a biomaterial. By changing the parameters of the process and the advent of artificial techniques, have improved and overcomes the disadvantages of ceramic material.

1.3 BIOACTIVE GLASSES

The first bioactive glass (BG), trade named as 45S5 Bioglass, was discovered by Hench et al.[32] in the early 1970s and addressed to bone replacement applications. After this discovery, a lot of bio glasses have been reported for various medical applications like the drug delivery, hyperthermia treatments or even implants and fillers etc.[33] . The original BG composition (45SiO₂-24.5CaO-24.5Na₂O-6P₂O₅ in wt%) is based on silica (Si) as a glass primary former that has the ability to create bonds with the bone after implantations in-vivo.

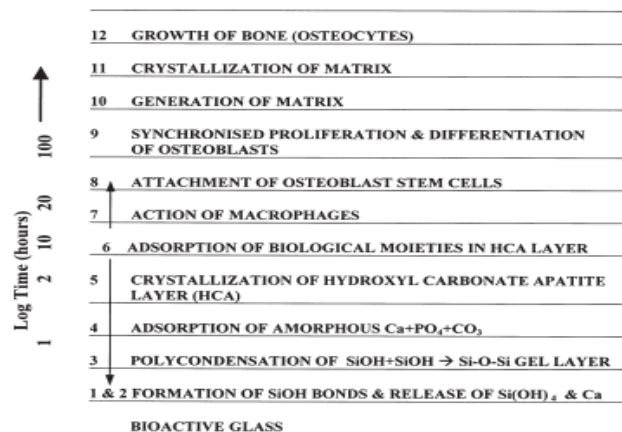


Figure 6: Steps of in-vivo reaction of Bioglass

A sequence of 11 reactions steps is included in the bonding processes of BG to living tissue [34] where the 1–5 steps are essentials for the formation of the (hydroxycarbonate apatite) HCA layer on the surface of glasses.

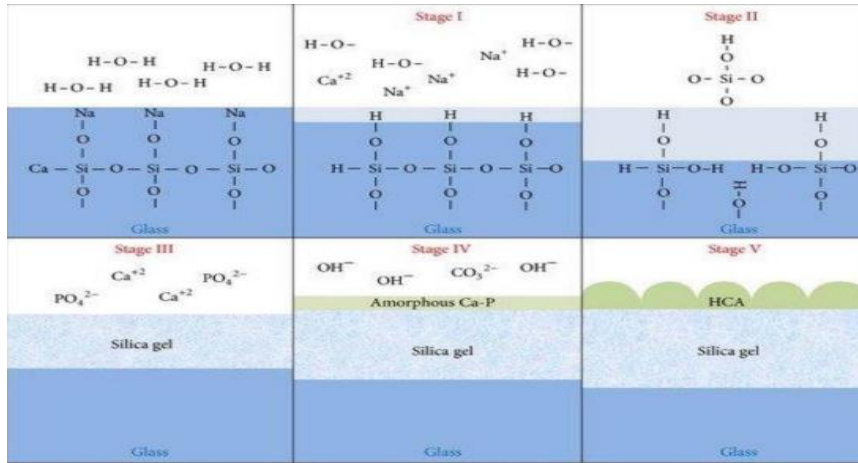


Figure 7: Steps 1 to 5 shows the formation of the HCA layer on the glass surface

BGs are found to be “bioactive” on the basis of these mechanisms:

(i) the formation of an apatite layer on the surface of BG when it is dissolved in a physiological environment, (ii) the release of biologically active ions in simulated body fluids (SBF)/plasma during in-vitro and in-vivo testing, respectively. The interaction of BG surfaces with body fluids begins with an exchange of ions that leads to an increase in the testing medium’s pH, resulting in the development of a silica-rich layer and then the growth of a Ca–P rich layer on the BG surface. This layer is further combined with carbonates and then crystallizes to form HCA, which ultimately helps to bond with the bone [35].

The HCA layer also provides an optimal biological environment for next 6–11 biological reaction stages, which include cell colonization, proliferation and differentiation to form new bone with good mechanical bond to implant surface. The HCA layer thickness has a major impact on bone bonding ability of the BG as well as on the interface shear strength. Generally, an interface thickness of 20 μm offers strong shear strength and interfacial bonding [36]. Porosity, surface area and the morphology of the bio glass in general, control the creation of new soft or hard tissue.

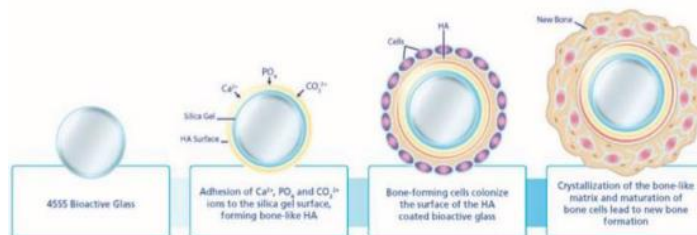


Figure 8: Bioactive glass surface in-vivo reaction

The pore size $<1 \mu\text{m}$ is responsible for better bioactivity, and attachment of cells [37-45]. It could be achieved by change in process parameters, constituents, and chemical route like sol-gel method or melt-quench method. Another class of bioceramics is bioactive glass-ceramics that are formed through the controlled crystallization of glass at an appropriate temperature. Most of the bioactive glass-ceramics are made with similar compositions to BG, but bioglass-ceramics exhibit better mechanical properties and poor bioactive properties than BG[46]. For example, commercial **Cerabone** (A-W) ($\text{SiO}_2\text{-CaO-MgO-P}_2\text{O}_5\text{-F}$) is produced by controlled heat treatment having 38 wt% apatite, 34 wt% of wollastonite and 28 wt% of residual glass phase that is used as coating for Ti alloys, artificial vertebrae and bone fillers [47-49]. The action of A-W glass ceramic depends upon different parameters such as porosity (5.0 ± 0.3), percentage of vitreous phase (28%), hardness (6.9 ± 0.3) and bending strength (215 MPa; 3 points). Particularly, bending strength of A-W glass ceramic is higher than that of typical human cortical bone (160 MPa), but the fracture toughness is three times lower than human cortical bone i.e. $6 \text{ MPam}^{1/2}$ [50].

Other common examples of bioactive glass-ceramic are **Ceravital**, wollastonite diopside (WD), diopside and combeite. Ceravital ($\text{SiO}_2\text{-CaO-MgO-Na}_2\text{O-K}_2\text{O-P}_2\text{O}_5$) has an analogous bioactivity mechanism to the Hench's BG and it has good mechanical properties and better stability in the long period. After the implantation of Ceravital scaffold there is a first degradation of the surface caused by ionic exchanges, followed by the formation of reaction layers that protect the material from further chemical attacks. Wollastonite and diopside phase formed when parent glass heat treatment is above $900 \text{ }^\circ\text{C}$. Wollastonite also has high thermal, mechanical and biological properties. But it has a high dissolution rate in in-vitro conditions. On the other hand, diopside has a slower dissolution rate and high mechanical properties. Therefore, composites of wollastonite and diopside have been used in tissue engineering applications. These bioactive glass-ceramics has been used in bulk, granular and porous form, and are used for bone graft applications [51]. Therefore, it concluded that properly selected glass ceramics could meet most of the required properties for bone graft and tissue engineering applications.

In general bioactive glasses can exhibit a different behaviour in vitro and in vivo depending on the composition, for example:

- Inert bioglass: SiO₂ rich glasses that forms only a hydration layer on the surface when in contact with physiological solution (region B on the diagram);
- Non-bioactive glasses: glasses with SiO₂ < 60% but still high. The superficial reaction layer could form a silica gel but it protects from chemical attacks (centre of B region);
- Bioactive silicate glasses: a silica gel layer is formed on the surface and it is rich in Ca²⁺ and (PO₄)³⁻. Apatite can precipitate (region A);
- Silicate glasses with multivalent cations like Al³⁺, Fe³⁺, Ti⁴⁺. Salts of these ions multiple layers are formed on the surface and apatite cannot be formed, so they are not bioactive (region B);
- Silicate glasses that lend rapid ion very exchange: a very thick and non-protective silica gel is formed;
- Resorbable glass: if locally pH>9 there is a faster silica gel layer dissolution and a progressive dissolution of the glass (region C);
- Region S is part of region A where bioactive glasses bond to both bone and soft tissue and are gene activating;
- Region E refers to the Bioglass composition;
- In region D bioglass is not formed.

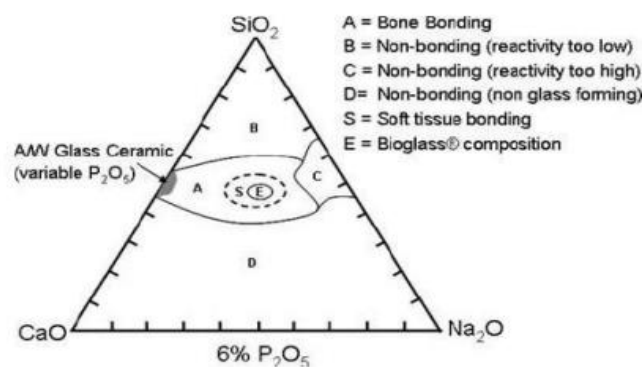


Figure 9: SiO₂-CaO-Na₂O ternary plot

1.3.1 Synthesis methods

Several methods have been developed for the synthesis of bioactive glass, its composites, and other bioactive glasses, including conventional melt-quenching, sol-gel, flame synthesis and microwave irradiation. The original Bioglass developed by Hench has been prepared through a conventional high-temperature melting process, through the melting of oxides mixed together at more than 1300°C followed by a quenching step [52]. In the 1990s, soft chemistry strategies and particularly the sol-gel process emerged, providing a more versatile method to design bioactive glass. In contrast to the previously described method, sol-gel technology allows the synthesis of bioactive glasses of equivalent composition but at a lower temperature. This process is based on hydrolysis and condensation of molecular precursors (alkoxydes or salts), which lead to the formation at room temperature and ambient pressure of an inorganic polymeric network. Solvent being trapped within the network explains the gel-like texture. The last two methods are gaining attention in the last few years. The flame synthesis method consist of baking precursors directly in a flame reactor [53], instead, microwave method works dissolving precursors in water, transferring to an ultrasonic bath and then irradiated. This last method is faster and cheaper than the others methods.[54]

References

- [1]“Atlante di istologia” © 2011-2021 Dipartimento di Medicina Sperimentale/Department of Experimental Medicine - Università di Genova/University of Genoa (<http://www.istologia.unige.it/page13/page35/page42/>)
- [2]Black, C.R.M., Goriainov, V., Gibbs, D. et al. Bone Tissue Engineering. *Curr Mol Bio Rep* 1, 132–140 (2015). <https://doi.org/10.1007/s40610-015-0022-2>
- [3]. O’Keefe RJ, Mao J. Bone tissue engineering and regeneration: from discovery to the clinic--anoverview. *Tissue Eng Part B Rev.* 2011; 17(6):389–392. [PubMed: 21902614]
- [4]Amini, A. R., Laurencin, C. T., & Nukavarapu, S. P. (2012). Bone tissue engineering: recent advances and challenges. *Critical reviews in biomedical engineering*, 40(5), 363–408. <https://doi.org/10.1615/critrevbiomedeng.v40.i5.10>
- [5]R. A. Horowitz, Z. I. V Mazor, C. Foitzik, H. Prasad, M. Rohrer, and A. D. Y. Palti, “ β -Tricalcium Phosphate As Bone Substitute Material,” *J. Osseointegration*, vol. 1, no. 1, pp. 60–68, 2010. [3]H. Qu, H. Fu, Z. Han, and Y. Sun, “Biomaterials for bone tissue engineering scaffolds: A review,” *RSC Adv.*, vol. 9, no. 45, pp. 26252–26262, 2019.
- [6]E. Verné, “Slide Corso Materiali per la Bioingegneria: ‘Bioceramici’, Politecnico di Torino.” Torino, Italy, 2018..
- [7]J. Jeong, J. H. Kim, J. H. Shim, N. S. Hwang, and C. Y. Heo, “Bioactive calcium phosphate materials and applications in bone regeneration,” *Biomater. Res.*, vol. 23, no. 1, pp. 1–11, 2019.
- [8]R. Albuлесcu et al., “Comprehensive In Vitro Testing of Calcium Phosphate-Based Bioceramics with Orthopedic and Dentistry Applications,” *Materials (Basel).*, vol. 10, pp. 1–41, 2019
- [9]A. R. Amini, C. T. Laurencin, and S. P. Nukavarapu, “Bone tissue engineering: Recent advances and challenges,” *Crit. Rev. Biomed. Eng.*, vol. 40, no. 5, pp. 363–408, 2012.
- [10]D. Mohamad Yunos, O. Bretcanu, and A. R. Boccaccini, “Polymer-bioceramic composites for tissue engineering scaffolds,” *J. Mater. Sci.*, vol. 43, no. 13, pp. 4433–4442, 2008
- [11]K. Rezwan, Q. Z. Chen, J. J. Blaker, and A. R. Boccaccini, “Biodegradable and bioactive porous polymer/inorganic composite scaffolds for bone tissue engineering,” *Biomaterials*, vol. 27, no. 18, pp. 3413–3431, 2006.
- [12]H. E. Jazayeri et al., “The cross-disciplinary emergence of 3D printed bioceramic scaffolds in orthopedic bioengineering,” *Ceram. Int.*, vol. 44, no. 1, pp. 1–9, 2018.
- [13] S. Pina, R. Rebelo, V.M. Correlo, J.M. Oliveira, R.L. Reis, Bioceramics for osteochondral tissue engineering and regeneration, *Adv. Exp. Med. Biol.* 1058 (2018) 53–75.
- [14] M.M. Subedi, Ceramics and its importance, *Himal. Geol.* 4 (2013) 80–82.
- [15] J. Chevalier, L. Gremillard, Ceramics for medical applications: a picture for the next 20 years, *J. Eur. Ceram. Soc.* 29 (7) (2009) 1245–1255.
- [16] Z. Abbasi, M. Bahrololoom, M. Shariat, R. Bagheri, Bioactive glasses in dentistry: a review, *J. Dent. Biomater.* 2 (1) (2015) 1–9.
- [17] W. Rieger, Ceramics in Orthopedics-30 Years of Evolution and Experience, *World Tribology Forum in Arthroplasty*, Hans Huber Verlag Bern, Suisse, 2001, pp. 283–294.
- [18] M. Kaur, K. Singh, Review on titanium and titanium based alloys as biomaterials for orthopedic applications, *Mater. Sci. Eng. C* 109 (2019) 844–862.

- [19] P. Kurinjinathan, K.T. Arul, J.R. Ramya, Cobalt ions doped bioactive ceramics for biosensor biomedical applications, *Int. J. Cur. Res. Rev.* 10 (21) (2018) 49.
- [20] A. Ravaglioli, A. Krajewski, *Bioceramics: Materials· Properties Applications*, Springer Science & Business Media 1992.
- [21] H.E. Jazayeri, M. Rodriguez-Romero, M. Razavi, M. Tahriri, K. Ganjawalla, M. Rasoulianboroujeni, M.H. Malekshoaraie, K. Khoshroo, L. Tayebi, The cross- disciplinary emergence of 3D printed bioceramic scaffolds in orthopedic bioengineering, *Ceram. Int.* 44 (1) (2018) 1–9
- [22] K. Shanmugam, R. Sahadevan, *Bioceramics-an introductory overview, fundamental biomaterials*, *Ceram. Int.* (2018) 1–46
- [23] S. Balasubramanian, B. Gurumurthy, A. Balasubramanian, Biomedical applications of ceramic nanomaterials: a review, *Int. J. Pharma Sci. Res.* 8 (12) (2017) 4950–4959.
- [24] B. McEntire, B.S. Bal, M. Rahaman, J. Chevalier, G. Pezzotti, Ceramics and ceramic coatings in orthopaedics, *J. Eur. Ceram. Soc.* 35 (16) (2015) 4327–4369.
- [25] S.S. Danewalia, K. Singh, Bioactive glasses and glass-ceramics for hyperthermia treatment of cancer: state of art, challenges and future perspectives, *Mater. Today Bio* (2021) 100.
- [26] S. Kargozar, R.K. Singh, H.-W. Kim, F. Baino, “Hard” ceramics for “soft” tissue engineering: paradox or opportunity? *Acta Biomater.* 115 (2020) 1–28.
- [27] F. Baino, J. Barberi, E. Fiume, G. Orlygsson, J. Massera, E.J. Verne, Robocasting of bioactive SiO₂-P₂O₅-CaO-MgO-Na₂O-K₂O glass scaffolds, *J. Healthc. Eng.* (2019), 2019.
- [28] A.A. Alshatwi, J. Athinarayanan, V.S. Periasamy, Biocompatibility assessment of rice husk-derived biogenic silica nanoparticles for biomedical applications, *Mater. Sci. Eng. C* 47 (2015) 8–16. [29] G. Sharma, M. Kaur, S. Punj, K. Singh, Biomass as a sustainable resource for value-added modern materials: a review, *Biofuel. Bioprod. Bioref.* (2020) 1–23.
- [29] S.S. Danewalia, G. Sharma, S. Thakur, K. Singh, Agricultural wastes as a resource of raw materials for developing low-dielectric glass-ceramics, *Sci. Rep.* 6 (2016) 24617.
- [30] G. Sharma, K. Singh, Recycling and utilization of agro-food waste ashes: syntheses of the glasses for wide-band gap semiconductor applications, *J. Mater. Cycles Waste Manag.* 21 (4) (2019) 801–809.
- [32] L.L. Hench, I.D. Xynos, J.M. Polak, Bioactive glasses for in situ tissue regeneration, *J. Biomater. Sci. Polym. Ed.* 15 (4) (2004) 543–562.
- [33] S.S. Danewalia, K. Singh, Bioactive glasses and glass-ceramics for hyperthermia treatment of cancer: state of art, challenges and future perspectives, *Mater. Today Bio* (2021) 100
- [34] J.R.J.A.b. Jones, Reprint of: review of bioactive glass, *From Hench to hybrids* 23 (2015) S53–S82.
- [35] J.R.J.A.b. Jones, Reprint of: review of bioactive glass, *From Hench to hybrids* 23 (2015) S53–S82.
- [36] M. Roy, A. Bandyopadhyay, S. Bose, *Ceramics in Bone Grafts and Coated Implants, Materials for Bone Disorders*, Elsevier, 2017, pp. 265–314.
- [37] J.R. Jones, D.S. Brauer, L. Hupa, D.C. Greenspan, Bioglass and bioactive glasses and their impact on healthcare, *Int. J. Appl. Glass Sci.* 7 (4) (2016) 423–434.
- [38] A.F. Brito, B. Antunes, F. dos Santos, H.R. Fernandes, J.M. Ferreira, Osteogenic capacity of alkali-free bioactive glasses. In-vitro studies, *J. Biomed. Mater. Res. B Appl. Biomater.* 105 (8) (2017) 2360–2365.
- [39] S. Schmitz, B. Widholz, C. Essers, M. Becker, D. Tulyaganov, A. Moghaddam, I. G. de Juan, F. Westhauser, Superior biocompatibility and comparable osteoinductive properties: sodium-reduced fluoride-containing bioactive glass belonging to the CaO-MgO-SiO₂ system as a promising alternative to 45S5 bioactive glass, *Bioact. Mater.* 5 (1) (2020) 55–65.

- [40]H. Li, Z. Wu, Y. Zhou, J. Chang, *Bioglass for Skin Regeneration, Biomaterials for Skin Repair and Regeneration*, Woodhead Publishing, Cambridge, 2019, pp. 225–250.
- [41]H.E. Skallevoid, D. Rokaya, Z. Khurshid, M.S. Zafar, Bioactive glass applications in dentistry, *Int. J. Mol. Sci.* 20 (23) (2019) 5960.
- [42]J. Chen, L. Zeng, X. Chen, T. Liao, J. Zheng, Preparation and characterization of bioactive glass tablets and evaluation of bioactivity and cytotoxicity in-vitro, *Bioact. Mater.* 3 (3) (2018) 315–321.
- [43]Z. Abbasi, M. Bahrololoom, M. Shariat, R. Bagheri, Bioactive glasses in dentistry: a review, *J. Dent. Biomater.* 2 (1) (2015) 1–9.
- [44]W.C. Lepry, S.N. Nazhat, Highly bioactive sol-gel-derived borate glasses, *Chem. Mater.* 27 (13) (2015) 4821–4831.
- [45]V. Miguez-Pacheco, L.L. Hench, A.R. Boccaccini, Bioactive glasses beyond bone and teeth: emerging applications in contact with soft tissues, *Acta Biomater.* 13 (2015) 1–15.
- [46]S.S. Danewalia, K. Singh, Magnetic and bioactive properties of MnO₂/Fe₂O₃ modified Na₂O-CaO-P₂O₅-SiO₂ glasses and nanocrystalline glass-ceramics, *Ceram. Int.* 42 (10) (2016) 11858–11865.
- [47]K. Shanmugam, R. Sahadevan, Bioceramics-an introductory overview, fundamental biomaterials, *Ceram. Int.* (2018) 1–46.
- [48]S. Balasubramanian, B. Gurumurthy, A. Balasubramanian, Biomedical applications of ceramic nanomaterials: a review, *Int. J. Pharma Sci. Res.* 8 (12) (2017) 4950–4959.
- [49]B. McEntire, B.S. Bal, M. Rahaman, J. Chevalier, G. Pezzotti, Ceramics and ceramic coatings in orthopaedics, *J. Eur. Ceram. Soc.* 35 (16) (2015) 4327–4369.
- [50]K. Shanmugam, R. Sahadevan, Bioceramics-an introductory overview, fundamental biomaterials, *Ceram. Int.* (2018) 1–46
- [51]A.J. Salinas, M. Vallet-Regí, Bioactive ceramics: from bone grafts to tissue engineering, *RSC Adv.* 3 (28) (2013) 11116–11131.
- [52] Vichery C, Nedelec J-M. Bioactive Glass Nanoparticles: From Synthesis to Materials Design for Biomedical Applications. *Materials*. 2016; 9(4):288. <https://doi.org/10.3390/ma9040288>
- [53] Brunner, Tobias J.; Grass, Robert N.; Stark, Wendelin J. (2006). "Glass and bioglass nanopowders by flame synthesis". *Chemical Communications* (13): 1384–6. [doi:10.1039/b517501a](https://doi.org/10.1039/b517501a). [PMID 16550274](https://pubmed.ncbi.nlm.nih.gov/16550274/).
- [54]ESSIEN, ENOBONG R; ATASIE, VIOLETTE N; UDOBANG, ESTHER U (27 July 2016). [ias.ac.in/public/Volumes/boms/039/04/0989-0995.pdf "Microwave energy-assisted formation of bioactive CaO–MgO–SiO₂ ternary glass from bio-wastes"] (PDF). *Bulletin of Materials Science*. 39 (4): 989–995. [doi:10.1007/s12034-016-1251-6](https://doi.org/10.1007/s12034-016-1251-6). [S2CID 100064762](https://scid.org/100064762)

2 TECHNIQUES FOR MAKING SCAFFOLDS IN BONE TISSUE ENGINEERING

In the previous chapter has been described how the advancing of BTE technologies were based on the use of synthetic grafts for the treatment and regeneration of major bone defects in order to get over limits associated to the implantation of natural origin grafts. In this chapter, the focus is on porous ceramic scaffolds and an overview on ceramic scaffolds for bone tissue engineering will be provided, giving particular attention to additive manufacturing technologies. The functional and structural complexity of natural bone, makes the design of scaffolds an hard challenge, as both chemical and structural properties have to meet very specific requirements, like effective support properties and a macro-and micro-porous structure to promote angiogenesis, cell colonization and proliferation. Many fabrication techniques are currently available to produce porous artificial matrixes. Among these, rapid prototyping turned out to be one of the most promising for the development of mechanically competent and structurally highly-defined scaffolds with tailored properties for bone tissue engineering applications.

2.1 SCAFFOLD DEFINITION

A scaffold is an artificial structure used to support three dimensional (3D) tissue formation [1,2]. An ideal scaffold suitable for BTE applications should allow or improve cell viability, attachment, proliferation and homing, osteogenic differentiation, vascularization, host integration and, where necessary, load bearing [3].

2.2 SCAFFOLD REQUIREMENTS

The main scaffold characteristics for BTE applications can be divided into 4 groups: biological requirements, structural features, biomaterial composition and type of fabrication process.

➤ BIOLOGICAL REQUIREMENTS

- Non-toxic
- Biocompatible
- Bioresorbable

- Biodegradable
- Non-immunogenic
- Bioactive
- *STRUCTURAL FEATURES*
 - Biomimetic
 - Bioinspired
 - Customize architecture and shape
 - High porosity
 - Pore interconnection
 - Mechanical properties
 - Surface topography
- *COMPOSITION*
 - Ceramics
 - Polymeric
 - Composites
- *FABRICATION PROCESS*
 - Conventional
 - Advanced

2.2.1 Biological requirements

Scaffolds have to be biocompatible, and they do not have to create adverse reaction in the host body due to their toxicity. In order to create new bone matrix, cells have to adhere on the surface without any change in their work, proliferate and start the osteogenesis process. [4-6] The osteogenesis process must also be concomitant with the degradation process and the degradation products should be non-toxic and the body could excrete it without problems. However, the degradation process, leads to a loss of mechanical strength of the scaffolds, so there is a critical situation in which the load is gradually transferred from the implant to the new bone tissue. [7,8] Regarding the immunogenic features, the scaffolds have to avoid host immune response even with the recent use of immune-modulatory biomaterials that regulate the immune response

(*i.e.* decreased NK cell activity and T and B cells mediated immunity).[9] Bioactivity is the ability to interact positively with the surrounding living tissues or organs and it is a primary importance feature for the scaffold for the purpose to promote the formation of new tissue.[10,11]

recently, the attention has been directed to the “osteoinductive or smart biomaterials” that have a great potential for bone tissue regeneration. They show the ability to instruct and respond to the surrounding *in vivo* environment to ectopically form bone. The biological mechanisms of this phenomenon have not been fully understood yet and two main hypotheses have been proposed: the first is based on the ability of the biomaterial surface to absorb and present osteoinductive factors to the surrounding cells, while the second concerns calcium and phosphate ions release from calcium phosphate-based materials, which can induce stem cell differentiation towards bone phenotype [12-15]. Methods for controlling the scaffold biocompatibility can be found in ISO 10993 –1 [16].

2.2.2 Structural features

The main challenge in the development of scaffolds for BTE is to create something that better mimics the bone structure, with the same mechanical properties and osteogenic features. That’s why is so important to create vascularized engineered scaffolds to avoid ineffective osteointegration. [17,18] Mechanical properties of the scaffolds have to be tailored to those found in the site of implantation; elastic modulus, tensile strength, fracture toughness, fatigue and elongation percentage are crucial to match properly in order to avoid risks of stress shielding, osteopenia and subsequent re-fracture. [19,20]. The compressive strength is the most common test done for ceramic scaffolds and it is done in accordance with ASTM F2883-11 in order to calculate the stress –strain curve [21]. For example, to replace cortical bone a good scaffold should have a compressive strength ~ 130 -180 MPa and Young’s module ~ 12 -18 GPa .Furthermore, it has been tested that the mechanical strength of the scaffold influences the mechanotransduction properties of the bone cells attached to the surface. There seems to be a correlation between mechanotransduction and the potential osteoinductive properties of the scaffold [22].

Porosity and scaffold micro-architecture has a main role in osteointegration: scaffolds should exhibit high porosity and interconnectivity of the pores to an adequate cell penetration, vascularization, diffusion of the

nutrients and waste products elimination [23,24]. The ideal scaffold for cancellous bone tissue should have an interconnected porous structure with porosity > 80% [24], where more than 60% of the pores should have a size between 100 -400 μm and at least 20 % is expected to be smaller than 20 μm [25]. Large pores (around 200-300 μm), lead to direct osteogenic pathways, but larger pores leads to a decrease of mechanical properties and general mechanical resistance of the scaffold [24,25,28]. The prevailing opinion in the literature is that pore size must be between 200-400 μm [22]. Smaller pores (closer 100 μm), in fact, were found to be beneficial to chondrogenesis [29], even if too small pores, lead to poor vascularisation [30]and limited cell migration, causing the formation of cell capsules around the edges of the scaffold [28].

Surface topography influences bone tissue regeneration but also can modulate the immune system; it can be modulated by the incorporation of artificial ECM. If biomaterial surface is well engineered, it can limit macrophages adhesion and activation [19].

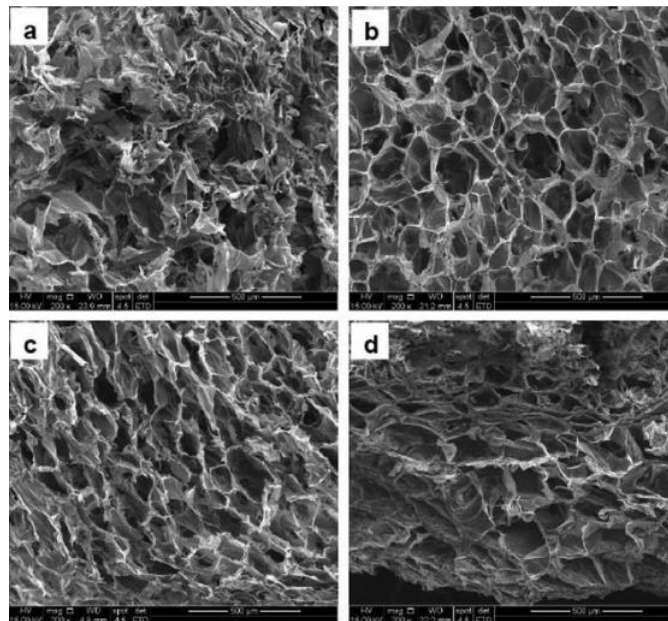


Figure 1: Microstructure of bioactive glass scaffold – Pores interconnectivity

2.2.3 Composition

The most used materials used for BTE nowadays are polymers, bioactive glasses (ceramics) or composites materials [31,32]. Polymers could be natural or synthetic and obviously have some advantages and

disadvantages. Natural polymers, derived from human system, like fibrin, collagen or hyaluronic acid have optimal biocompatibility but it's harder to control the degradation rate which is easier for synthetic polymers like polyanhydride, polypropylene fumarate (PPF), polycaprolactone (PCL), polylactic acid (PLA), polyether ether ketone (PEEK) and poly(glycolic acid) (PGA). This type of polymeric scaffolds present the possibility to have tailored design based on bone structure and mechanical properties, to have complex shapes and an improve in cell attachment [33]. Hydrogels are an important type into the synthetic polymers class because are able to increase the adhesion, proliferation and differentiation of cells thanks to their structure that can mimics the ECM topography [31].

Bioactive ceramics could be of natural or synthetic origin too. They show chemical composition similar to that of the bone and good mechanical properties as previously described but they are also fragile [34]. This materials, like HA, tricalcium phosphate (TCP), bioactive glass (BG) and calcium silicate, display optimal capability to enhance osteogenesis as confirmed by several studies [35] with an high quality of the new tissue.

Composites materials are a combination of two or more materials that mix advantages and drawbacks of each [31,32]. The combinations could be of co-polymers type, polymer-polymer or even polymer-ceramic. This last type of blend shows an excellent biomimetic feature due to the fact that the bone structure basically is a mix of inorganic HA crystals and organic collagen fibres.

2.3 FABRICATION PROCESS

2.3.1 Conventional methods

In this section a general view on the major conventional methods for the scaffold production will be given. The conventional technologies include all the manufacturing methods that don't involve the replication of a CAD/CAM model. This particular type of methods are considered in the additive manufacturing methods, and will be described in the next section. In the Table 1 an overview of the conventional manufacturing techniques for the production of glass-based scaffolds is presented.

Major group	Technological class	Specific methods
Conventional	Foaming techniques	Gel-casting foaming, sol-gel foaming, H ₂ O ₂ foaming
	Thermal consolidation of particles	Organic phase burning-out: polymeric porogens, starch consolidation, rice husk method
	Porous polymer replication	Coating methods, foam replication
	Freeze-drying	Freeze-casting of suspensions, ice-segregation-induced self-assembly
	Thermally induced phase separation	
	Solvent-casting and particulate leaching	

Table 1: Overview of the main conventional methods to produce glass-based scaffold for BTE

2.3.1.1 Foaming techniques

For this method a slurry of bioactive glass is prepared and the foaming agent is added in order to create air bubbles and consequently the porosity of the scaffold. There are many methods to create the porosity: direct injection of gas, agitation, gas generation from chemical reaction or thermal decomposition of peroxides [64]. Foaming methods include techniques such as: Gel cast foaming, H₂O₂ foaming or Sol-gel foaming. Even if the final products present acceptable mechanical properties, they also display closed pores, low interconnectivity.

2.3.1.2 Thermal consolidation of particles

These methods are characterized by the use of a sacrificial template that usually is subjected to sintering process. With these techniques can be obtained products of complex shape and with low process costs. The agents to produce porosity are usually natural (eg. Starch, rice husk) or synthetic origin (eg. PE particles) but typically it's difficult to obtain a porosity level < 70% and good interconnectivity [36]. The organic phase burning-out method doesn't need the adding of a sacrificial phase to create the green body and the structural parameters, like the porosity, could be controlled by varying the particle's size during the sintering process. The technique is simple but it allows the production only of low-porosity scaffolds (<50% vol.). In order to obtain high porosity rate scaffolds, a polymeric filler can be added to the inorganic particles but it has to be removed before the sintering process with the aim to obtain clear scaffolds without contamination. Several trials were made with synthetic polymers like camphor [37], polyethylene powders [38] and paraffin wax powders [39] that leads to interconnected porosity rates from 20% for the first, to 70% for the last one.

Even natural origin porogen agent, like starches of different plants or rice husk, were used; they form a gelled system with glass powders and under heat treatments they leave void spaces and pores to use like a template. In general these last methods allows to obtain scaffolds with low porosity but with mechanical properties comparable to that of cancellous bone (5-7 MPa).

2.3.1.3 Porous polymer replication

The basic idea of this technique is to replicate the polymeric foam structure by coating it with glass slurry and then to consolidate it; this allows to create high level porosity structure, more than 90% open porosity, well interconnected. The coating method and the foam replication are part of this technological class. With the coating method can be produced various origins scaffolds and the template could be of different origin too, like polymer, foam or even fibrous bodies. The glass/ ceramic could be deposited on the substrate by several methods like electrophoretic deposition (EPD) or by dipping, but the most important factor is that no thermal treatment is performed in order to maintain the polymeric core stable that leads to an increase of the toughness of the final product. Conversely, for the foam replication, thermal treatment is needed and has a double task. In this method the foam has the role to be a template for the glass slurry and after the coating, the structure is subjected to the double-stage thermal treatment that leads to the total burning-out of the polymeric core structure and to the glass/ ceramic densification. There are some pros and cons for this method too; high levels of porosity (>90% vol.) are reachable but with a decrease of mechanical properties for being implanted into the bone. [40]

2.3.1.4 Freeze-drying

This method was firstly experienced by Fukasawa et al.[41,42] and then optimized by Tomsia et al.[103,104] and consists in rapidly freeze the glass suspension in order to create elongated ice crystals of the solvent, thanks to the directionality of the freezing phase, and after the elimination of the solvent the scaffold could be consolidate. The main advantage of this method is in the oriented microstructure of the pores that confers to the scaffolds much higher compressive strength compared to the other method, but on the other hand high porosity levels are not reachable.

2.3.1.5 Thermally induced phase separation

With the Thermally Induced Phase Separation (TIPS) method it's possible to obtain scaffolds with a porosity >97 vol.%. It is mainly used to obtain polymeric scaffolds but glass nanoparticles can be incorporated to increase scaffold's bioactivity [43]. This method is built on the change of solubility of two polymers after a critical temperature, before which they were totally insoluble. So when the solution is made and cooled under the critical temperature, two phases were formed and with a good chemistry is possible to control the amount of the two phases and their morphologies. In order to obtain porous structure, one of the two phases that will be polymer-poor, will be removed. Some researchers [44] found out some effects related to glass particles, like decreasing of porosity, an increase in the apparent density, changing in shape of the pores and dispersion in particles (more uniform with high content of glass).

2.3.1.6 Solvent-casting and particulate leaching

This method is based on the solvent-casting technique where a polymeric solution is poured into a stamp and consolidated with the elimination of the solvent by evaporation. A water-soluble salt must be added now to the solution in order to obtain macropores in the structure. With this method is possible to obtain only flat sheet or tubes with a porosity up to 90 vol.% but with a not so good pores network; moreover, retention of toxic agent is possible, and if the scaffold must include proteins or biological molecules, they could be denaturated, decreasing scaffold bioactivity. [28]

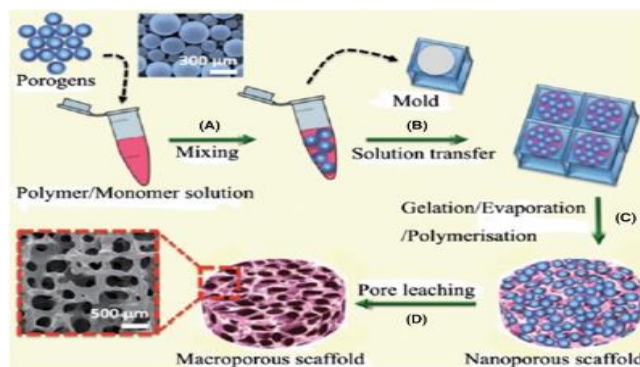


Figure 2: Steps of a porous polymeric scaffold by solvent-casting and particulate leaching

2.4 ADDITIVE MANUFACTURING TECHNOLOGIES

The additive manufacturing technologies (AMT), also known as Rapid Prototyping techniques (RP), was developed for the first time in 1986 by Chuck Hull and took a big change in several industrial sectors by a revolution of the fabrication process. This technique was based on the stereolithography [45] and allows to create structures with an high construction control level by the “layer-by-layer” technique [46] where the starting point of the process is a CAD model or even a computer tomography (CT) of the object that will be reproduced. Every type of material can be used in an AMT process, but regarding this thesis work, AMTs for glass-ceramic materials could be divided into two major groups: direct and indirect techniques. With direct AMT techniques it is possible to obtain the final structure without any post treatment because involves the melting and consolidation on the surface of the final product during the layer-by-layer process. However, if post-treatments like de-binding or sintering are needed, the AMT is referred to indirect methods. Four categories of AMT exist:

1. Laminated object manufacturing: sheets of material are produced and then cut in the desired shape
2. Extrusion-based techniques: a filament of material is extruded by a nozzle (robocasting, fused modelling deposition, dispense plotting)
3. Methods based on stereolithography (SLA) like digital light processing (DLP) and laser-based systems
4. Fusing of bed powders: a binder keeps together particles and is deposited in the bed or melted

Usually, the procedure of the RP techniques is divided into 5 main steps:

Creation of the CAD model

The CAD could be created from magnetic resonance imaging (MRI) or TC that give the possibility to obtain a 3D reconstruction with high resolution, otherwise it allows to create a patient-specific model. CAD could come also from the repetition in the space of a single structure with known properties in order to create simple geometries and shape.

Conversion from CAD to STL and slicing

The CAD model is converted in an STL file in order to discretize the surface with the mesh and cut into layers.[47]

Setting the RP apparatus

After checking possible error, alle the parameters for the printing, like layer thickness, are set due to the type of material and the technique.

Post processing

This last step is not always necessary as wrote before.

A short comparison of commonly used RP technique is now provided:

2.4.1.1 *Selective laser sintering – SLS*

Is a direct AMT and so only one step is needed to create the scaffold. The feedstock powders are prepared in a chamber and then moved by a roll into another chamber where a laser follow the path of the CAD model to create the structure. This steps are repeated until the whole structure is done. [48] For this process is very important to control a lot of parameters like powders granulometry, laser parameters like energy density and distance, and the process temperature that obviously cold lead to an unintended sintering of the powders.

With this technique it's possible to reach a resolution of 500 μm with a strong dependence on laser characteristics.

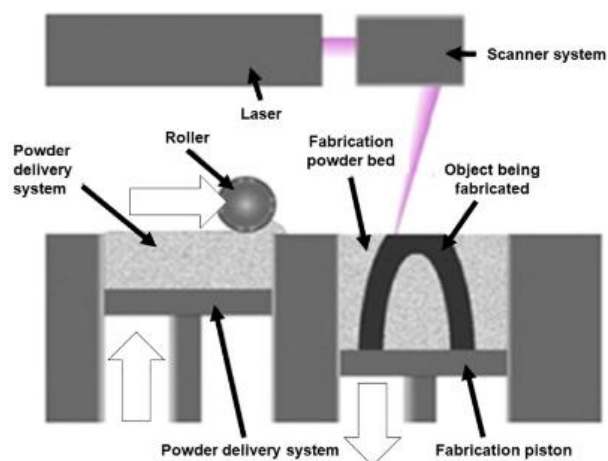


Figure 3: Schematic illustration of the SLS process [49]

2.4.1.2 Stereolithography – SLA

This method, also called vat photopolymerization, presents the higher resolution of 20 μm , for commercially available machines, and could process a large range of materials. For SLA methods is necessary the use of a UV-light curable polymer that is stored in a tank where a building platform relies. The UV light follows the pattern from the CAD model, building the first layer on the platform that then is moved in order to proceed with the layer-by-layer fabrication. This process takes a lot of time and has high production costs, but on the other hand, scaffolds with complex shapes and complex internal structure can be obtained. More details on this technique are reported in a dedicated section (section 2.5).

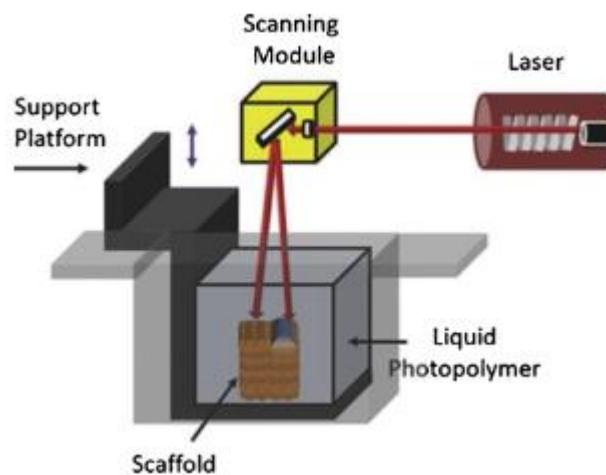


Figure 4: Schematic of SLA. Adapted with permission from [50]. Copyright (2015) Wiley-VCH Verlag GmbH & Co. KGaA

2.4.1.3 Fused deposition modelling – FDM

In this technology the material is extruded from a nozzle that is moving following the CAD model along both x and y-axis. The platform on which the material is settled, moves down according to the layer thickness set before. The feedstock material is partially heated before exit from the nozzle, in fact this technology is more suitable for processing polymers. This technique has an accuracy of 250-370 μm .

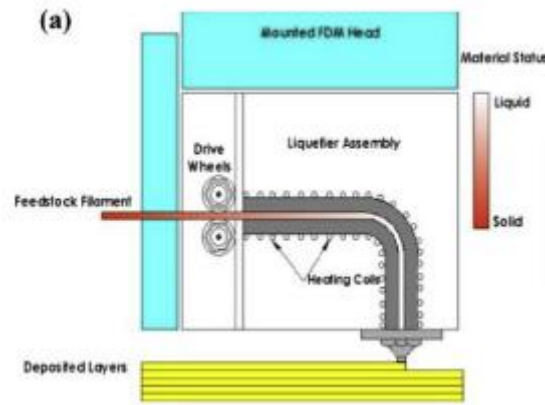


Figure 5: Schematic illustration of the FDM process [51]

2.4.1.4 3D printing

This technique is very similar to the SLS, in fact a powder bed has to be created firstly using rollers or blades. Then the binder, that is commonly water-based or organic-based, is patterned by a print following the CAD model, and after the powders are subjected to heat treatment to consolidate them. This is the process for one layer, so it is repeated until the entire structure is done. With this technique it is possible to obtain a scaffold porosity around 50 vol.% but with low mechanical strength and low quality surface. Even the resolution, 100-200 μm , is low compared to SLA.

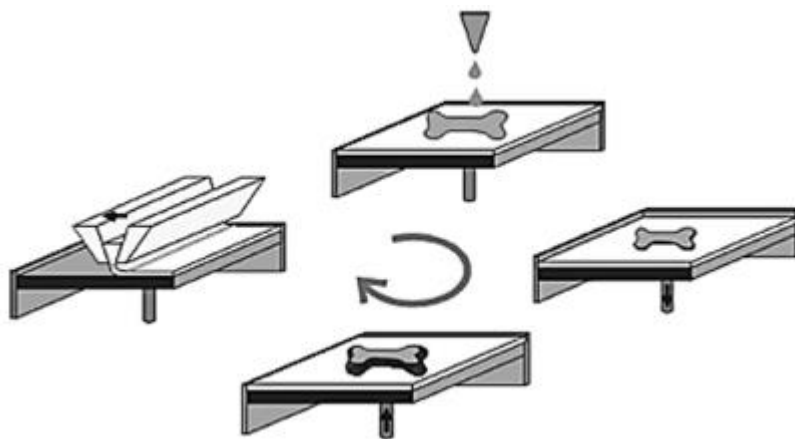


Figure 6: Illustration of the 3D printing process [28]

2.4.1.5 Robocasting

Robocasting is similar to the traditional printing but differs from it because it doesn't require nozzle heating. Moreover, the inks could maintain their properties through the time and this makes these types of materials very suitable for BTE. This technique too has a resolution lower than SLA, 100-1000 μm .

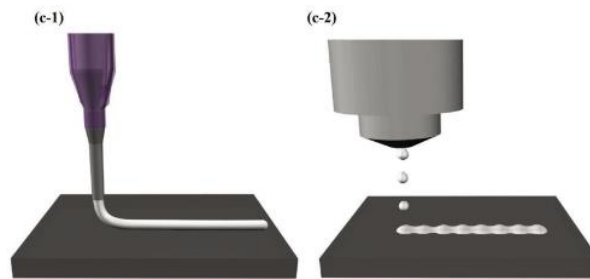


Figure 7: Robocasting technique with single filament writing (c1) and droplet jetting (c2) [52]

2.4.1.6 Low-temperature deposition manufacturing – LDM

This model is a combination of the deposition manufacturing and the phase separation process [53]. It allows to produce only polymeric scaffolds depositing liquid material layer by layer with a lower environment temperature. The lower temperature allows to maintain the bioactivity of biomaterials, but on the other hand there is always a resolution of 400 μm and a limited choice of materials.

Down here a schematic table of the main process in AMT for BTE is given with resolution of every technique and some pros and cons.

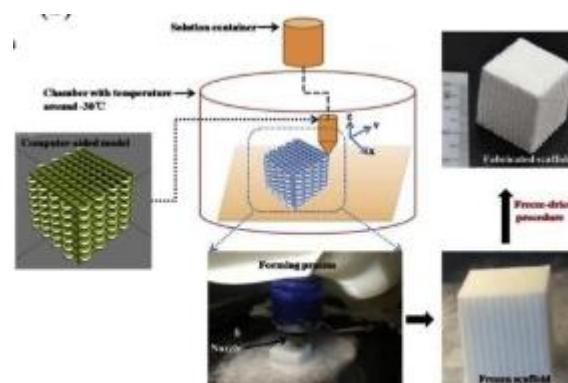


Figure 8: Schematic illustration of LDM technology with permission from [54]

Table 2: Overview of the main AMTs in BTE with some advantages and disadvantages [28,55-57]

Technique	Process details	Resolution (μm)	Material for BTE	Advantages and Disadvantages
SLS	Preparing the powder bed Layer-by-layer addition of powder Sintering each layer according to the CAD file, using a laser source	500	Ceramics Polymers Metals	+ No need for support + No post-processing – Feature resolution depends on laser beam diameter
SLA	Immersion of platform in photopolymer liquid Exposure to focused light according to the desired design Polymer solidifying at the focal point, non-exposed polymer remains liquid Layer-by-layer fabrication	30	Ceramics Bioactive glass Polymers	+ Complex internal features can be obtained + Growth factors, proteins, and cell patterning is possible – Only applicable for photopolymers
FDM	Strands of heated polymer/ceramics extrusion through a nozzle	250	Ceramics Thermoplastic polymers	+ No need for platform/support – Materials restriction due to the need for molten phase
LDM	The scaffold –building cycle is performed in a low –temperature environment under 0°C	300-500	Polymers (PLLA)	+Can incorporate biomolecule -Solvent is used Requires freeze drying
3D printing	Strands of paste/viscous material (in solution form) extrusion based on the pre-designed structure Layer-by-layer deposition of strands at a constant rate, under specific pressure Disruption of strands according to the tear of speed	100-200	Ceramics Polymers	+ Mild condition of the process allows drug and biomolecules plotting – Heating/post-processing needed for some materials restricts the biomolecule incorporation
Robocasting	Direct writing of liquid using a nozzle Consolidation through the liquid-to-gel transition	100-1000	HA/PLA HA/PCL 6P53B glass/PCL	+ Independent 3D nozzle movement + Precise control of the thickness + No need for platform-support (–) Material restriction

2.5 STEREO LITHOGRAPHY (SLA)

2.5.1 Processing

SLA is a technique that involves the use of a UV laser to build layer-by-layer structures, an UV-curable photopolymer, a moving (or building) platform in which the structure is created and a dynamic mirror system. At the starting point of the process, the laser consolidates the surface of the photopolymer bath according to the CAD model, creating the first layer of the structure.

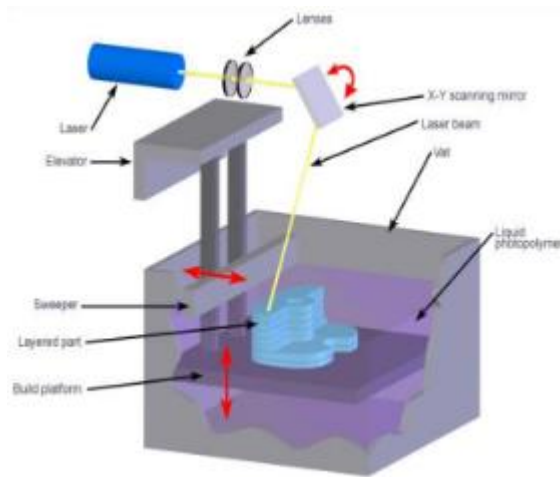


Figure 9: SLA technique

When the irradiation ends the slurry is raised or lowered by the platform that moves along z-axis, depending on the machine configuration (top-down or bottom-up). The layer thickness is established by the movement of the building platform at each cycle and by the irradiation depth.

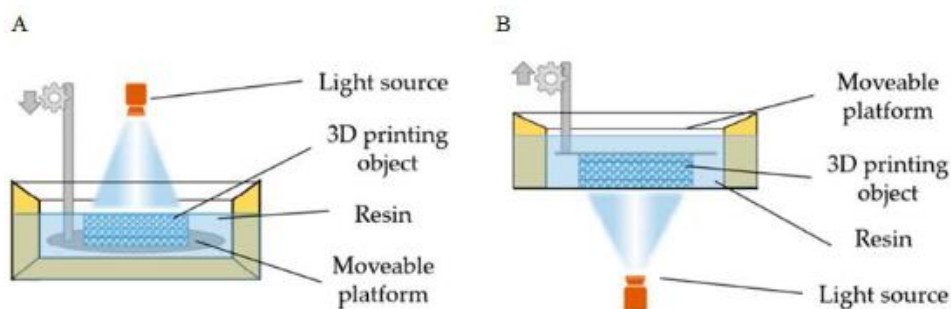


Figure 10: Top-down and bottom-up configurations

2.5.2 Slurry characteristics

Photocurable slurries are the principal component in the SLA technology. Most of the photosensitive slurries used for SLA are acrylate-based with a certain level of photoinitiator [58]. An ideal slurry must have a long-time stability, excellent dispersion in order to obtain high quality green and sintered density, good mechanical properties of the final structure and homogenous microstructure of the ceramics [59,60]. This is the most important challenge in the stereolithography process. Regarding the rheological aspects, the slurry must exhibit a Newtonian flow behaviour and low density value for the purpose to make easier the printing process and avoid the formation of air bubbles. The quantity of ceramic inside the slurry is fundamental: when the ceramic load increase, the viscosity of the slurry increases as well, and for this reason usually there is a limit in the ceramic load that corresponds to the 50 vol% in order to obtain more mobile fluids. Viscosity limit, instead, is around 3 Pa·s with shear rates of 10 s^{-1} [61]. Furthermore, homogeneously dispersed particles size must be smaller than the layer thickness. It is even possible to add to the slurry some dispersant agents in order to ensure better quality, lower viscosity, good homogeneity and at the same time keep a good level of ceramic load. Another important factor is the transparency to UV light. The slurry must ensure the desired penetration depth of the light for the purpose of obtaining the better curing depth of the UV beam.[44]

2.5.2.1 The polymerization process

The stereolithography technology involves the consolidation of a photosensitive polymer thanks to a light source irradiation. This, with the right energy applied induce a chemical reaction, the curing reaction, that leads to highly cross-linked polymer.

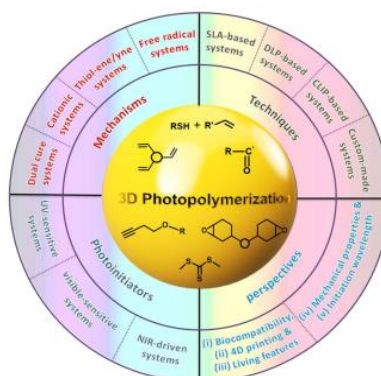
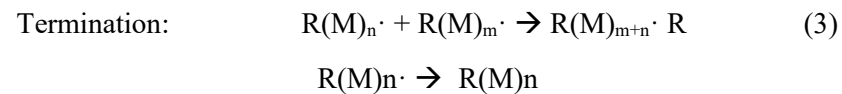
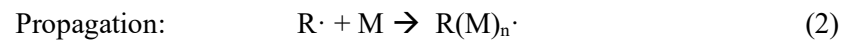


Figure 11: Schematic illustration of photopolymerization

Polymerization start when the ceramic powders, monomer and the photoinitiator are subjected to the UV light (1); cation species or free radical are generated by the photoinitiator, and they attack the double bond of the monomer. The polymeric chains increase their length due to the reactions (2) between the monomer and the active end of the chain, until the termination reaction (3). Two different photopolymerisation may occur: cationic and radical polymerisation, the last one is preferred for the SLA because it is easier to control. Radical polymerization has 3 steps:



M= Monomer, R= Radical, PI= photoiniziator

The kinetic of reaction and the mechanical properties of the final scaffold are influenced by the quantity of photoinitiator. It has been reported that the stiffness of the final product and the polymerization speed are directly proportionate to the PI [44]. However, the quantity of PI must be limited as their intrinsic cytotoxicity could be harmful for tissue ingrowth and regeneration.

2.5.3 Main parameters

Energy of the UV laser

The laser is fundamental for the photopolymerization and typically it's beam is Gaussian, this means that the intensity decrease from the beam centre according to the Gaussian law. It is assumed that photocurable resin obey the Lambert-Beer law of exponential absorption, and so when the Gaussian laser scan the resin surface, a parabolic cylinder is solidified. According to this, the exposed lights has its maximum energy value (E_{max}) at the resin surface and it is exponentially attenuated when it penetrates through the resin. E_{max} is controlled by two parameters: the light power and the scanning speed.

$$E_{max} = \sqrt{\frac{2}{\pi}} \frac{P}{w_0 v_s} \quad \left[\frac{mJ}{cm^2} \right]$$

Where P is the laser power, w_0 is the beam radius and v_s is the scanning speed.

Cure depth (C_d)

Cure depth is defined as the depth at which the light energy brings the resin to the gel point, where it is converted from liquid-state to solid-state. At this level, the energy is called critical energy (E_c). C_d is calculated according to the Jacob's version of Lambert-Beer law:

$$C_d = D_p \ln \left(\frac{E_{max}}{E_c} \right) \quad [\mu m]$$

Where D_p is the penetration depth at which the beam intensity is reduced to $1/e^2$ (37%) of its value at the resin surface.

Cure width (C_w)

The cure width is another key parameter that is directly proportional to the laser spot size and the square root of the ratio of C_d and D_p :

$$C_w = w_0 \sqrt{\frac{2 C_d}{D_p}} \quad [\mu m]$$

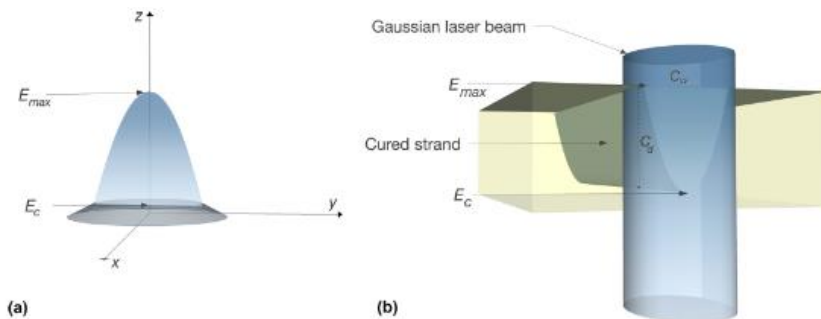


Figure 12: Gaussian distribution of energy (a) and light attenuation in a photocurable slurry (b) [62]

2.5.4 Post Processing

Being the SLA an indirect technique, an additional phase is required in order to obtain the final product.

The post-processing consists of the thermal treatment of the green bodies, thus obtaining ceramic parts.

The green body, in fact, contains a solid load (ceramic powder) and a volatile matrix which has to be eliminated. [63]

Post-processing involves three steps:

- Cleaning and drying
- De-binding
- Sintering

So, for the first step, the bodies are cleaned with specific solvent until the non-polymerized slurry is removed from the cavities of the structure.

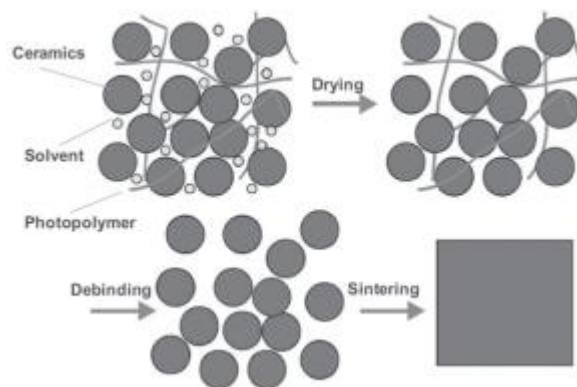


Figure 13: Schematic illustration of the post-processing steps [64]

The de-binding step is a thermal treatment in which the binder is decomposed due to a slow and constant increase of the temperature. It is very important to control the temperature in this phase in order to not create any internal stresses that could lead to cracks in the structure and in mechanical properties loss. The debinding temperature depends on some factors like the quantity of organic components and their composition, granulometry and distribution of the ceramic particles, percentage of solid particle and organic matrix in the slurry [64].

The last step is the sintering process. The temperature for this steps is around 50-75% of the melting temperature of the material. During this phase the scaffolds face a volumetric shrinkage that must be considered before the printing process [28].

2.6 DIGITAL LIGHT PROCESSING (DLP)-BASED STEREO LITHOGRAPHY

DLP-based SLA is a technique that leads to considerable reduction in production time, allows excellent resolution and reduce the processing stresses on the scaffold.[65] DLP refers to the digital mirror device (DMD), that selectively expose the photosensitive slurry to the UV-light. Like the SLA, also the DLP is a layer-by-layer technique that builds the structure from a CAD model. The difference to classical SLA is the use of a series computer-programmable arrays of DMD [66], which allow the simultaneous irradiation of the entire desire section [47,67]. Commonly DLP printers could use two different mechanisms: bottom-up or top-down, depending on the position of the light respect to the vat, as shown in figure 13.

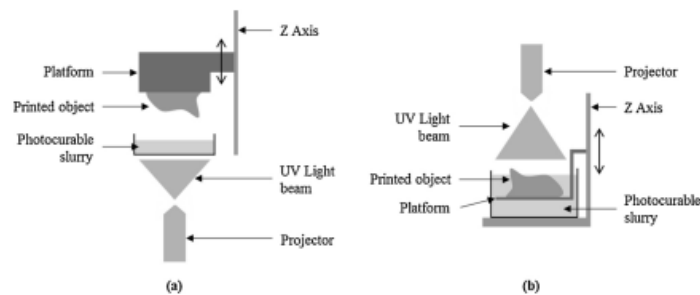


Figure 14: Bottom-up (a) and top down (b) approach for DLP-based stereolithography

2.6.1 Digital Micromirror Device (DMD)

The DMD is an optical semiconductor on which DLP is based. It is composed of thousands of micromirrors that can be oriented by electrical signals and can individually turn of $\pm 10-12^\circ$ from the ON state to the OFF state. The voltage define the micromirrors position, if the micromirror position is in a condition of $< 10^\circ$ (ON state), the light from the source is reflected in the projection lens and the image is created [68]. Vice versa, if the position is $> 10^\circ$ the light is not reflected but it is adsorbed by a light collector.[69] Usually, a DMD chip

contains more than 442,000 mirrors and could process up to 32,000 image frames in one second.[47,68].

With the DMD-based lithography , submicron structure could be achieved.

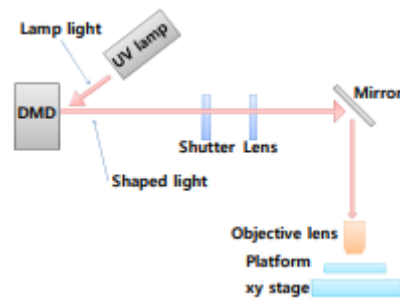


Figure 15: Schematic view of the DMD-based SLA system

2.6.2 Advantages and disadvantages of the DLP-based SLA

DLP-based stereolithography can reach a resolution of $25\ \mu\text{m}$ [70] and also ceramic structures were printed with a layer height of $15\ \mu\text{m}$ and lateral resolution of $40\ \mu\text{m}$ [71]. This technique is based on the work of the DMD, which function is to act as a dynamic mask, tilting every single mirror in an ON or OFF-state. For this reason, the entire surface of the layer is illuminated simultaneously but, thanks to the DMD work, there is the pixels lightening or shutdown, according to the CAD model. [73]

DLP is excellent for illumination of sharp corners but can cause saw-tooth type surface roughness [71]. Moreover, when high resolution is needed, the pixel size needs to be reduced, but having the DMD a fixed number of mirrors, this leads to images shrinkage problems reducing the maximum geometry size. In comparison to the SLA, DLP has lower production costs and faster printing. [72,74]

References

- [1] G. Bouet, D. Marchat, M. Cruel, L. Malaval, L. Vico, In vitro three-dimensional bone tissue models: from cells to controlled and dynamic environment, *Tissue Eng. B Rev.* 21 (2015) 133–156, <http://dx.doi.org/10.1089/ten.TEB.2013.0682>.
- [2] M. Navarro, A. Michiardi, O. Castao, J.A. Planell, Biomaterials in orthopaedics, *J. R. Soc. Interface* 5 (2008) 1137–1158, <http://dx.doi.org/10.1098/rsif.2008.0151>.
- [3] Bone Tissue Engineering: recent advances and challenges A.R. Amini, C.T. Laurencin and S.P. Nukavarapu *Crit. Rev. Biomed. Eng.*, 40 (2012), pp. 363–408, [10.1615/CritRevBiomedEng.v40.i5.10](http://dx.doi.org/10.1615/CritRevBiomedEng.v40.i5.10).
- [4] G. Bouet, D. Marchat, M. Cruel, L. Malaval, L. Vico, In vitro three-dimensional bone tissue models: from cells to controlled and dynamic environment, *Tissue Eng. B Rev.* 21 (2015) 133–156, <http://dx.doi.org/10.1089/ten.TEB.2013.0682>.
- [5] J. Henkel, M.A. Woodruff, D.R. Epari, R. Steck, V. Glatt, I.C. Dickinson, P.F.M. Choong, M.A. Schuetz, D.W. Huttmacher, Bone regeneration based on tissue engineering conceptions – a 21st century perspective, *Bone Res.* 1 (2013) 216–248, <http://dx.doi.org/10.4248/BR201303002>.
- [6] S. Kumbar, C. Laurencin, M. Deng, *Natural and Synthetic Biomedical Polymers*, first ed. Elsevier, Philadelphia, 2014.
- [7] F.J. O'Brien, *Biomaterials & scaffolds for tissue engineering*, *Mater. Today* 14 (2011) 88–95, [http://dx.doi.org/10.1016/S1369-7021\(11\)70058-X](http://dx.doi.org/10.1016/S1369-7021(11)70058-X).
- [8] B.P. Chan, K.W. Leong, Scaffolding in tissue engineering: general approaches and tissue-specific considerations, *Eur. Spine J.* 17 (2008) 467–479, <http://dx.doi.org/10.1007/s00586-008-0745-3>.
- [9] A.R. Amini, C.T. Laurencin, S.P. Nukavarapu, Bone Tissue Engineering: recent advances and challenges, *Crit. Rev. Biomed. Eng.* 40 (2012) 363–408, <http://dx.doi.org/10.1615/CritRevBiomedEng.v40.i5.10>.
- [10] Q. Chen, J.A. Roether, A.R. Boccaccini, Tissue engineering scaffolds from bioactive glass and composite materials, in: N. Ashammakhi, R. Reis, F. Chiellini (Eds.), *Topics in Tissue Engineering 2008*, pp. 1–27.
- [11] S. Hofmann, M. Garcia-Fuentes, Bioactive scaffolds for the controlled formation of complex skeletal tissues, in: Daniel Eberli (Ed.), *Regenerative Medicine and Tissue Engineering - Cells and Biomaterials*, InTech 2011, pp. 393–432, <http://dx.doi.org/10.5772/22061>.
- [12] T.J. Blokhuis, J.J. Arts, Bioactive and osteoinductive bone graft substitutes: definitions, facts and myths, *Injury* 42 (2011) S26–S29, <http://dx.doi.org/10.1016/j.injury.2011.06.010>.
- [13] A.M. Barradas, H. Yuan, C.A. van Blitterswijk, P. Habibovic, Osteoinductive biomaterials: current knowledge of properties, experimental models and biological mechanisms, *Eur. Cell. Mater.* 21 (2011) 407–429.
- [14] P. Habibovic, K. de Groot, Osteoinductive biomaterials—properties and relevance in bone repair, *J. Tissue Eng. Regen. Med.* 1 (2007) 25–32.
- [15] S.R. Motamedian, S. Hosseinpour, M. Ghazizadeh Ahsaie, A. Khojasteh, Smart scaffolds in bone tissue engineering: a systematic review of literature, *World J. Stem Cells* 7 (2015) 657–668, <http://dx.doi.org/10.4252/wjsc.v7.i3.657>.
- [16] ASTM International Standard Guide for Characterization of Ceramic and Mineral Based Scaffolds used for Tissue-Engineered Medical Products (TEMPs) and as Device for Surgical Implant Applications and ASTM Standard F2883 -11, “Standard Guide for Characterization of Ceramic and Mineral Based Scaffolds used for Tissue-Engineered Medical Products (TEMPs) and as Device for Surgical Implant Applications,” ASTM B. Stand., no. January 2012, pp. 1–7, 2011.
- [17] N. Yuan, K.S. Rezzadeh, J.C. Lee, Biomimetic scaffolds for osteogenesis, *Receptors Clin. Investig.* 2 (2015) e898, <http://dx.doi.org/10.14800/rci.898>.
- [18] J. Rouwkema, N.C. Rivron, C.A. van Blitterswijk, Vascularization in tissue engineering, *Trends Biotechnol.* 8 (2008) 434–441, <http://dx.doi.org/10.1016/j.tibtech.2008.04.009>.

- [19] A. Atala, F.K. Kasper, A.G. Mikos, Engineering complex tissues, *Sci. Transl. Med.* 4(2012) 160rv12, <http://dx.doi.org/10.1126/scitranslmed.3004890>.
- [20] E. Ali Abou Neel, W. Chrzanowski, V.M. Salih, H.W. Kim, J.C. Knowles, Tissue engineering in dentistry, *J. Dent.* 42 (2014) 915–928, <http://dx.doi.org/10.1016/j.jdent.2014.05.008>.
- [21] I. Denry and L. T. Kuhn, “Design and characterization of calcium phosphate ceramic scaffolds for bone tissue engineering,” *Dent. Mater.*, vol. 32, no. 1, pp. 43–53, 2016.
- [22] A. R. Amini, C. T. Laurencin, and S. P. Nukavarapu, “Bone tissue engineering: Recent advances and challenges,” *Crit. Rev. Biomed. Eng.*, vol. 40, no. 5, pp. 363–408, 2012.
- [23] J. Henkel et al., “Bone Regeneration Based on Tissue Engineering Conceptions—A 21st Century Perspective,” *Bone Res.*, vol. 1, pp. 216–248, 2013.
- [24] M. L. Griffith and J. W. Halloran, “Ultraviolet curable ceramic suspensions for stereolithography of ceramics,” *Am. Soc. Mech. Eng. Prod. Eng. Div. PED*, vol. 68–2, no. January 1994, pp. 529–534, 1994.
- [25] L. C. Gerhardt and A. R. Boccaccini, “Bioactive glass and glass-ceramic scaffolds for bone tissue engineering,” *Materials (Basel)*, vol. 3, no. 7, pp. 3867–3910, 2010.
- [26] S. Dorozhkin, “Medical Application of Calcium Orthophosphate Bioceramics,” *Bio*, vol. 1, no. 1, pp. 1–51, 2011.
- [27] L. Zhang, G. Yang, B. N. Johnson, and X. Jia, “Three-dimensional (3D) printed scaffold and material selection for bone repair,” *Acta Biomater.*, vol. 84, pp. 16–33, 2019.
- [28] F. Baino et al., “Processing methods for making porous bioactive glass-based scaffolds—A state-of-the-art review,” *Int. J. Appl. Ceram. Technol.*, vol. 16, no. 5, pp. 1762–1796, 2019.
- [29] G. Turnbull et al., “3D bioactive composite scaffolds for bone tissue engineering,” *Bioact. Mater.*, vol. 3, no. 3, pp. 278–314, 2018.
- [30] C.M. Murphy, F. J. O’Brien, D. G. Little, and A. Schindeler, “Cell-scaffold interactions in the bone tissue engineering triad,” *Eur. Cells Mater.*, vol. 26, pp. 120–132, 2013.
- [31] F. Matassi, L. Nistri, D. Chicon Paez, M. Innocenti, New biomaterials for bone regeneration, *Clin. Cases Miner. Bone Metab.* 8 (2011) 21–24.
- [32] N. Zhu, X. Chen, Biofabrication of tissue scaffolds, in: R. Pignatello (Ed.), *Advances in Biomaterials Science and Biomedical Applications*, InTech 2013, pp. 315–328, <http://dx.doi.org/10.5772/54125>.
- [33] B. Dhandayuthapani, Y. Yoshida, T. Maekawa, D. Sakthi Kumar, Polymeric scaffolds in tissue engineering application: a review, *Int. J. Polym. Sci.* 2011 (2011) (19 pp) 10.1155/2011/290602
- [34] C. Gao, Y. Deng, P. Feng, Z. Mao, P. Li, B. Yang, J. Deng, Y. Cao, C. Shuai, S. Peng, Current progress in bioactive ceramic scaffolds for bone repair and regeneration, *Int. J. Mol. Sci.* 15 (2014) 4714–4732, <http://dx.doi.org/10.3390/ijms15034714>.
- [35] R. Grigolato, N. Pizzi, M.C. Brotto, G. Corrocher, G. Desando, B. Grigolo, Magnesium-enriched hydroxyapatite as bone filler in an ameloblastoma mandibular defect, *Int. J. Clin. Exp. Med.* 8 (2015) 281–288.
- [36]. Denes E, Barrière G, Poli E, Lévêque G. Commentary: bio-ceramics and scaffolds: a winning combination for tissue engineering. *Front Bioeng Biotechnol.* 2017;5:1–17
- [37]. Livingston T, Ducheyne P, Garino J. In vivo evaluation of bioactive scaffold for bone tissue engineering. *J Biomed Mater Res.* 2002;62(1):1–13.
- [38]. Brovarone CV, Verné E, Appendino P. Macroporous bioactive glass-ceramic scaffolds for tissue engineering. *J Mater Sci Mater Med.* 2006;17(11):1069–78.
- [39]. Zhang H, Ye XJ, Li JS. Preparation and biocompatibility evaluation of apatite/wollastonite-derived porous bioactive glass ceramic scaffolds. *Biomed Mater.* 2009;4(4):045007
- [40] Fu Q, Saiz E, Rahaman MN, Tomsia AP. Bioactive glass scaffolds for bone tissue engineering: state of the art and future perspectives. *Mater Sci Eng C.* 2011;31(7):1245–56
- [41]. Fukasawa T, Ando M, Ohji T, Kanzaki S. Synthesis of porous ceramics with complex pore structure by freeze-dry processing. *J Am Ceram Soc.* 2001;84:230–2.

- [42]. Fukasawa T, Deng Z, Ando M, Ohji T, Kanzaki S. Synthesis of porous silicon nitride with unidirectionally aligned channels using freeze-drying process. *J Am Ceram Soc.* 2002;85:2151–5.
- [43]. Roseti L, Parisi V, Petretta M, Cavallo C, Desando G, Bartolotti I, et al. Scaffolds for bone tissue engineering: state of the art and new perspectives. *Mater Sci Eng C.* 2017;78:1246–62
- [44]. Maquet V, Boccaccini AR, Pravata L, Notinger I, Jérôme R. Porous poly(α -hydroxyacid)/bioglass® composite scaffolds for bone tissue engineering. I: preparation and in vitro characterization. *Biomaterials.* 2004;25(18):4185–94
- [45]. Bose S, Vahabzadeh S, Bandyopadhyay A. Bone tissue engineering using 3D printing. *Mater Today.* 2013;16(12):496–504
- [46] W.-Y. Yeong et al., “Rapid prototyping in tissue engineering: challenges and potential,” *Trends Biotechnol.*, vol. 22, no. 12, pp. 643–652, 2004][32] R. Gmeiner et al., “Additive manufacturing of bioactive glasses and silicate bioceramics,” *J. Ceram. Sci. Technol.*, vol. 6, no. 2, pp. 75–86, 2015.]
- [47] C. Schmidleithner, “Master Thesis Additive Manufacturing of Tricalcium Phosphate Scaffolds for Bone Tissue Engineering,” Vienna University of Technology]
- [48]. Gmeiner R, Deisinger U, Schönherr J, Lechner B, Detsch R, Boccaccini AR, et al. Additive manufacturing of bioactive glasses and silicate bioceramics. *J Ceram Sci Technol.* 2015;6(2):75–86
- [49]. Shirazi S, Gharekhani S, Mehrli M, Yarmand H, Metselaar H, Adib Kadri N, et al. A review on powder-based additive manufacturing for tissue engineering: selective laser sintering and inkjet 3D printing. *Sci Technol Adv Mater.* 2015;16(3):033502
- [50] A.V. Do, B. Khorsand, S.M. Geary, A.K. Salem, 3D printing of scaffolds for tissue regeneration applications, *Adv. Healthc. Mater.* 4 (12) (2015) 1742–1762
- [51] M. Nikzad, S.H. Masood, I. Sbarski, Thermo-mechanical properties of a highly filled polymeric composite for Fused Deposition Modeling, *Mater. Des.* 32 (6)(2011) 3448–3456]
- [52] J.A. Lewis, G.M. Gratson, Direct writing in three dimensions, *Mater Today* 7 (7–8)(2004) 32–39
- [53] Z. Xiong, Y.N. Yan, S.G. Wang, R.J. Zhang, C. Zhang, Fabrication of porous scaffolds for bone tissue engineering via low-temperature deposition, *Scripta Mater.* 46 (11) (2002) 771–776.]
- [54] W. Liu, D.M. Wang, J.H. Huang, Y. Wei, J.Y. Xiong, W.M. Zhu, et al., Low-temperature deposition manufacturing: a novel and promising rapid prototyping technology for the fabrication of tissue-engineered scaffold, *Mater. Sci. Eng. C-Mater. Biol. Appl.* 70 (2017) 976–982
- [55] K. Lin, R. Sheikh, S. Romanazzo, and I. Roohani, “3D printing of bioceramic scaffolds—barriers to the clinical translation: From promise to reality, and future perspectives,” *Materials (Basel)*, vol. 12, no. 7, pp. 1–20, 2019
- [56] W.-Y. Yeong et al., “Rapid prototyping in tissue engineering: challenges and potential,” *Trends Biotechnol.*, vol. 22, no. 12, pp. 643–652, 2004.
- [57] S. Bose, S. Vahabzadeh, and A. Bandyopadhyay, “Bone tissue engineering using 3D printing,” *Mater. Today*, vol. 16, no. 12, pp. 496–504, 2013.
- [58] Frank B. Löffler, Ethel C. Bucharsky, Karl G. Schell, Stefan Heißler, Michael J. Hoffmann, Development of silica based organic slurries for stereolithographic printing process, *Journal of the European Ceramic Society*, Volume 40, Issue 13, 2020
- [59] N. Travitzky, A. Bonet, B. Dermeik, T. Fey, F. Filbert-Demut, L. Schlier, T. Schlordt, P. Greil, Additive manufacturing of ceramic-based materials, *Adv. Eng. Mater.* 16 (2014) 729–754, <https://doi.org/10.1002/adem.201400097>.
- [60] G.B. Allen, J.W. Halloran, Stereolithography of ceramic suspensions, *Rapid Prototyp. J.* 3 (1997) 61–65, <https://doi.org/10.1108/13552549710176680>
- [61] Ceramic Stereolithography: Additive Manufacturing for 3D Complex Ceramic Structures Chang-Jun Baet , Arathi Ramachandran, Kyeongwoon Chung, and Sujin Park Process Innovation Department, Korea Institute of Materials Science, Changwon 51508 Korea (Received October 10, 2017; Revised November 16, 2017; Accepted November 16, 2017)]

- [62] Setareh Zakeri, Minnamari Vippola, Erkki Levänen, A comprehensive review of the photopolymerization of ceramic resins used in stereolithography, *Additive Manufacturing*, Volume 35, 2020, 101177, ISSN 2214-8604, <https://doi.org/10.1016/j.addma.2020.101177>.
- [63] A. D. Lantada, A. De Blas Romero, M. Schwentenwein, C. Jellinek, and J. Homa, "Lithography-based ceramic manufacture (LCM) of auxetic structures: Present capabilities and challenges," *Smart Mater. Struct.*, vol. 25, no. 5, 2016
- [64] G. Magnaterra "Tesi di Laurea Magistrale Additive Manufacturing of hydroxyapatite scaffolds for bone repair" Politecnico di Torino
- [65] Y. Zeng et al., "3D printing of hydroxyapatite scaffolds with good mechanical and biocompatible properties by digital light processing," *J. Mater. Sci.*, vol. 53, no. 9, pp. 6291–6301, 2018.
- [66] C. Sun, N. Fang, D. M. Wu, and X. Zhang, "Projection micro-stereolithography using digital micro-mirror dynamic mask," *Sensors Actuators, A Phys.*, vol. 121, no. 1, pp. 113–120, 2005
- [67] C. Schmidleithner, S. Malferarri, R. Palgrave, D. Bomze, M. Schwentenwein, and D. M. Kalaskar, "Application of high resolution DLP stereolithography for fabrication of tricalcium phosphate scaffolds for bone regeneration," *Biomed. Mater.*, vol. 14, no. 4, pp. 1–11, 2019
- [68] Y. Lu, G. Mapili, G. Suhali, S. Chen, and K. Roy, "A digital micro-mirror device-based system for the microfabrication of complex, spatially patterned tissue engineering scaffolds," *J. Biomed. Mater. Res. -Part A*, vol. 77, no. 2, pp. 396–405, 2006
- [69] Yasar, O., Dinh, M., Lan, S.-F., & Starly, B. (2008). Fabrication of Micropatterned Hydrogels Using Maskless Photopolymerization for Tissue Engineering Applications. ASME 2008 Summer Bioengineering Conference, Parts A and B. <https://doi.org/10.1115/SBC2008-192377>
- [70] Ligon SC, Liska R, Stampfl J, Gurr M, Mühlaupt R. Polymers for 3D printing and customized additive manufacturing. *Chemical Reviews*. 2017;117(15):10212-10290
- [71] Hatzenbichler M, Geppert M, Seemann R, Stampfl J. Additive manufacturing of photopolymers using the Texas Instruments DLP lightcrafter. In: *Proceedings of SPIE, Emerging Digital Micromirror Device Based Systems and Applications V*. San Francisco: International Society for Optics and Photonics; 2013. pp. 86180A
- [72] Sun C, Fang N, Wu DM, Zhang X. Projection micro-stereolithography using digital micro-mirror dynamic mask. *Sensors and Actuators A: Physical*. 2005;121(1):113-120
- [73] Katal G, Tyagi N, Joshi A. Digital light processing and its future applications. *International Journal of Scientific and Research Publications*. 2013;3(1):2250-3153
- [74] Baumgartner S, Pfaffinger M, Busetti B, Stampfl J. Comparison of Dynamic Mask- And Vector-Based Ceramic Stereolithography. In: *Proceedings of the 41st International Conference on Advanced Ceramics and Composites*. Hoboken: Wiley; 2018. P. 163-173

3 MATERIALS & METHODS

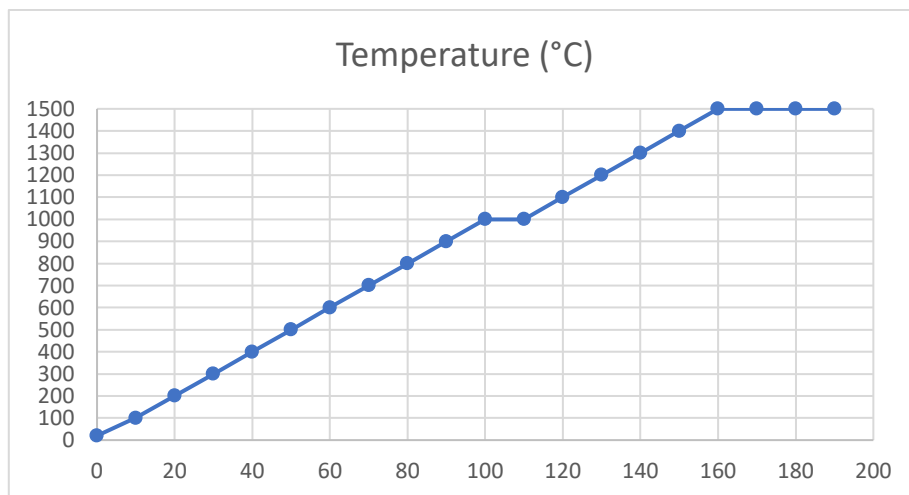
3.1 GLASS PREPARATION

The 47.5B glass has this composition 47.5SiO₂-10Na₂O-10K₂O-10MgO-20CaO-2.5P₂O₅ (mol.%) and was produced using a melting method in standard condition in a platinum crucible. The raw high-purity reagents, all purchased from Sigma-Aldrich and indicated in the table below, were homogeneously mixed in plastic bottles onto rotating rollers overnight to promote the homogeneity of the mix and then were put inside the crucible at room temperature.

<i>Reagent</i>	<i>Chemical formula</i>	<i>Molecular weight (g/mol)</i>	<i>Mass (g)</i>
<i>Silicon Oxide</i>	SiO ₂	60.08	45.34
<i>Calcium Phosphate</i>	Ca ₃ PO ₄	310.18	12.32
<i>Calcium Carbonate</i>	CaCO ₃	100.09	19.87
<i>Magnesium Carbonate hydroxide pentahydrate</i>	(MgCO ₃) ₄ ·Mg(OH) ₂ ·5H ₂ O	485.65	15.43
<i>Sodium Carbonate</i>	Na ₂ CO ₃	105.99	16.84
<i>Potassium Carbonate</i>	K ₂ CO ₃	138.21	21.95

Table 1: Masses of reagents required to produce 100g of 47.5B glass

The powder is well hand pressed to have the minimum quantity of air inside the mix. The crucible is then put inside the furnace Nabertherm (Nabertherm GmbH, Germany) with the lid on top and the temperature goes from the room temperature (20 °C) to 1000 °C increasing constantly of 10 °C/min. After this first step, the temperature is maintained constant for about 10 min, the necessary time that allows the operator to remove the lid from the top of the crucible. The next step leads the temperature from 1000 °C to 1500 °C with an increase ramp of 15 °C and once reached this maximum temperature is maintained constant for 0.5 h. The temperature variation process is showed in the graph below.



The melt is then quenched in water at room temperature to produce the frit, some glass is still adherent to the inside of the crucible and then is manually recovered. The frit is dried and after this, is ball milled in a milling machine with 6 zirconia spheres (Pulverisette 0, Fritsch, Germany) and sieved below 32 μm (Giuliani Technologies Srl, Torino, Italy) because, according to previous experience, this particle size is the most suitable to produce porous glass scaffolds for bone replacement by several technologies like robocasting and foam replica.

3.2 47.5BG SLURRY PREPARATION

The powders prepared at DISAT in Turin were dried for about 24 h at 120 °C and added in 3 steps to the previously prepared organic matrix containing solvent, reactive monomers and photoinitiator (usually less than 1 wt%). At each step, a precise amount of powders was added to the matrix; it was necessary to blend in the material and to ensure that the final result would be a homogeneous slurry. The SpeedMixer™ DAC 400.1 FVZ (Hauschild, Germany) was used for this purpose: it works with a Dual Asymmetric Centrifuge consisting of a mixing arm and a mixing cup, rotating in opposite directions. This combination of forces allows obtaining a fast and effective mixing. The 47.5BG Slurry was mixed for 30 s at 1800 rpm and then for 30 s at 2750 rpm. Once all the powders were added to the binder, the slurry underwent a dispersion process with milling beads for 3 h. Finally, was then placed in storage at a constant temperature of 5°C, ready for use. The main steps performed to prepare the 47.5BG Slurry are shown in Figure 1.

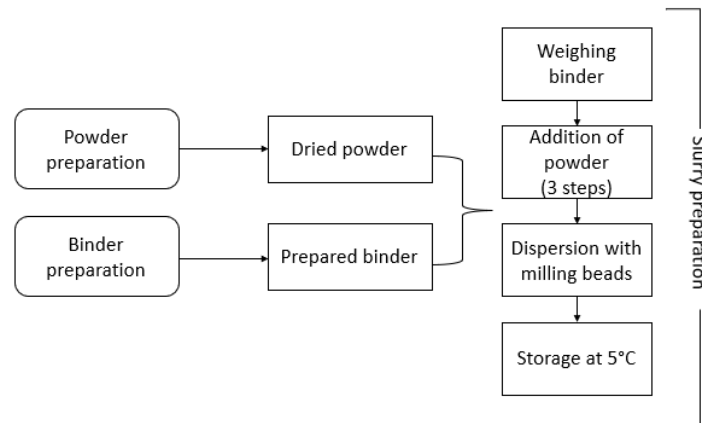


Figure 1: Flowchart for 47.5BG Slurry preparation.

The volumetric ratio between ceramic powder and binder was calculated in order to obtain a slurry with a viscosity that can be used for DLP printing.

3.3 MANUFACTURING

3.3.1 Pre-Processing

The CeraFab system is based on jobs previously created using the CeraFab Control DP (Data Pre-processing) system. Starting from a 3D CAD file in .STL format which, through the software, is modified into fab-file format so that it can be recognized by the CeraFab 7500 machine. Thanks to this, the project may be manipulated through a virtual platform called "tray" (Figure) and all process parameters may be set for the printing, including the number of pieces to be printed for each single job, their position and orientation within the building platform.

The software distinguishes between two types of layers: the "start layers", i.e. the first layers produced during the printing process, and all the subsequent layers, "general layers", which make up the main part of the structure [1]. A summary of the 4 steps needed to completely and correctly define the characteristic of the work is given below:

1. **Machine & Material:** selection of the machine in which the printing job will be done and the material for the structure.
2. **Tray:** organization of the tray. So the number of pieces and their position and relative distance.

3. **Parameters:** selection of the main printing parameters. There are 3 different sets of parameters:
 - a. General settings: layer thickness (μm), exposure time start (s), exposure time general (s), exposure intensity start (mW/cm^2), exposure intensity general (mW/cm^2), shrinkage compensation factor (XY) and shrinkage compensation factor (Z);
 - b. Waiting times: time exposure start (s) and waiting time exposure general (s);
 - c. Velocities and moving distance: rotation speed start (steps/s), rotation speed general (steps/s), tilting down start (steps/s) and rotation angle start ($^\circ$).

4. **Finalization:** error check and data saving. A preview of the project divided into all its individual layers is provided, according to the pre-defined settings and the estimated slurry consumption is provided. Once the project has been checked, the fab-file can be sent to the chosen CeraFab machine.

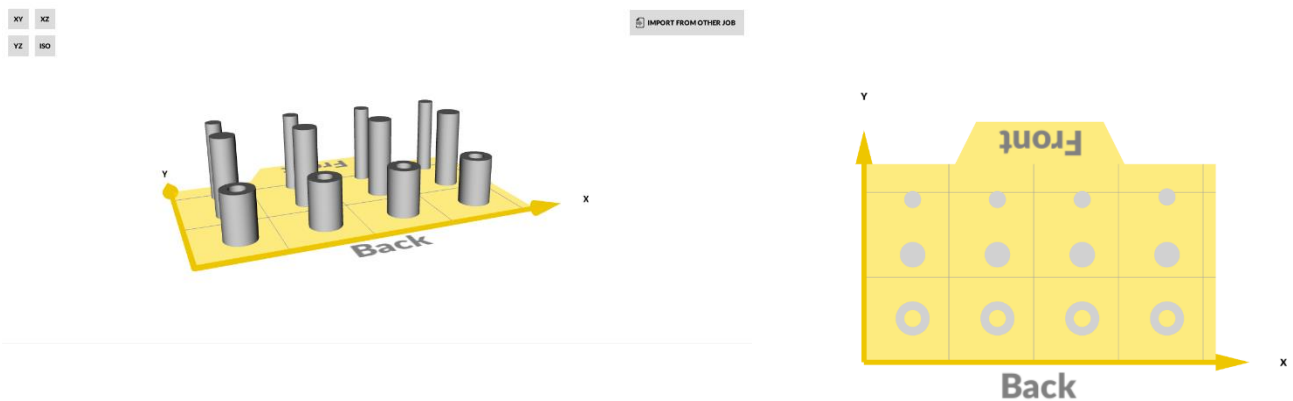


Figure 2: Virtual Tray for “Shrinkage Test” of three sets of cylinders

3.3.2 Processing

The Lithoz CeraFab 7500 (Figure 3) was the machine used for the production of 47.5B bioactive glass scaffolds at Lithoz GmbH.

The CeraFab 7500 uses the Digital Light Processing (DLP)-based stereolithography (SLA) method, previously described in Chapter 2. This system is among the most popular for the manufacture of complex 3D ceramic structures thanks to the opportunity to control the manufacturing of the part in real time,

guarantee great precision of the printed object (in the micrometer range) combined and short production times.



Figure 3: CeraFab 7500 and specifications

The setup is a constrained surface DLP (digital mirror device) system with an LED radiation source in the blue visible light. The light engine utilizes powerful LEDs as a light source and a DMD (digital mirror device) chip as a dynamic mask with a resolution of 1920×1080 pixels and a pixel size of $40 \times 40 \mu\text{m}$ [2]. The DMD - chip of CeraFab 7500 guarantees a selective photopolymerization of the layer; the resolution in the x/y plane is $40 \mu\text{m}$ and a single layer thickness that can vary between 25 - 100 μm , depending on the manufacturer's choice. Layer-by-layer production involves the addition of fresh slurry every time a layer is produced. Figure 3 illustrates how the light source radiates from below the rotating vat.

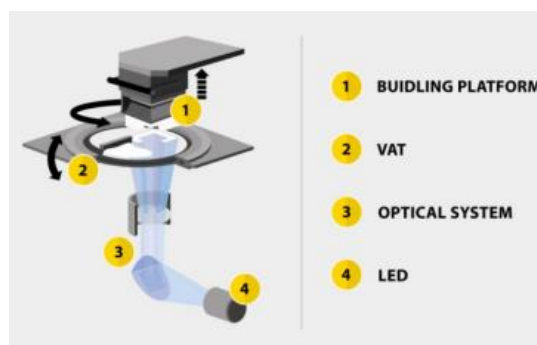


Figure 4: Operation of the Lithoz GmbH DLP system

When the photoinitiator is hit by the light, it forms free radicals which start the polymerization by reacting with the monomers contained in the mixture. The chain reaction forms the desired matrix of monomers that will bind the ceramic particles together in the desired pattern. Compared to other methods of vat photopolymerization, the parts produced are no longer immersed in the slurry and this not only reduces the amount of material required but also the risk of introducing defects during construction [3]

The CeraFab 7500 workspace is composed of:

- **Rotation Vat:** contains the slurry and is coated with new material after each layer is formed. The vat consists of a layer of transparent glass interposed with a layer of silicon. The lower layer of the vat is irradiated by the light. No one of the newly created layer has to remain attached to the surface of the vat, but all the layers are firmly fixed to each other and attached to the building platform. In order to reduce the forces between the structure and the vat, after polymerization of the layer, one side of the vat is slowly lowered before the other, in order to facilitate the detachment of the new layer from the surface.
- **Building Platform:** is placed above the vat and it is the basis for the construction of the structure. It consists of a metal body and a glass plate that can only move along the z axis. To improve the adhesion between the building platform and the scaffold under construction, the glass platform has been coated with a UV-sensitive primer.
- **Cartridge:** contains the slurry. Through a controlled dosing system, new liquid slurry is added to the vat each time the next layer is formed. During the work was never used as the quantity of slurry required was low.
- **Wiper blade:** it is used to distribute the slurry onto the vat after the construction of a layer. When adjusting the position of the wiper blade, the height of the slurry on the vat may be modified; the initial slurry thickness is one of the two parameters which must be checked before the printing process.

3.3.3 CeraFab Hardware Control

CeraFab Hardware Control (HC) is the user interface for direct interaction with the Cerafab 7500 machine. Thanks to the machine's touch screen, the operator can check all the phases of the job, like start printing, the process status, the number of layers being printed and the time required to complete the job; the user can also interact directly with the machine moving the building platform and check the general machine status [1]. The HC control panel provides access to the software directory of the machine to which the fab - file previously created with CeraFab DP has been transferred. The operator can now select it and confirming it and the job starts. During slicing the parts are cut into individual layers, according to the predefined layer thickness. Two mandatory checks must be performed from the control panel before starting to print:

1. Ensure that the slurry evenly covers the vat surface. Set the continuous rotation of the vat to about 1 minute so that the material is distributed on the surface. Measure the initial level of liquid slurry present in the vat and if the height does not reflect the desired level, change the position of the wiper blade below. In the present work, the height of the slurry in the vat was 175 μm .
2. Make sure that vat and building platform are parallel to each other. This alignment is essential for the success of the manufacturing run and the quality of the fabricated parts.

Once the fab-file has been loaded and all aspects of the machine have been checked, printing may begin. The process starts with a complete rotation of the vat, then the building platform moves towards the vat until there is space equal to the height of a single layer. The next step involves the selective exposure of the slurry to visible blue light with consequent polymerization of the desired part. To facilitate the separation between the newly formed layer and the surface of the vat, the latter is slowly tilted downwards and at the same time the building platform is raised as much as the height of a single layer. The sequence of the process is then repeated, as the next layer is formed, and so on until the entire job is completed.

3.3.4 Post-Processing

After printing, some actions like cleaning, drying, remove the binder and sintering are required in order to obtain strong scaffolds.

3.3.4.1 Cleaning

Green samples (Figure 5) were removed from the building platform using razor blades and cleaned meticulously to eliminate the uncured slurry with compressed air and the Lithoz cleaning solution LithaSol

20.



Figure 5: 4a) green samples before cleaning phase; 4b) Lithoz Cera Cleaning Station Ultra; 4c) green samples after cleaning

3.3.4.2 Drying

After cleaning, green samples were stored at 40°C for no longer than 5 days and then sintered.

3.3.4.3 Sintering

After the cleaning and drying phases, the green samples were subjected to the heat treatment to remove the total amount of the organic part and obtain ceramic solid parts. Removing the organic binder is a very important phase in order to obtain more biocompatible scaffolds, in fact, harmful substances for human body are contained in the binder. Four temperature treatment were tested: the first treatment was 48 hours long and provided a heat ramp from room temperature to 430 °C with a heating rate of 0.2 °C/min. The 430 °C temperature was then kept for 6.5 hours to complete the de-binding phase where the binder is gradually

eliminated and internal stresses resulting from high temperature gases are avoided. Then, with a heating rate of 5 °C/min the temperature was increased until 700 °C and maintained for 3 hours before the cooling stage until room temperature is reached again. At this maximum temperature the scaffolds are expected to be in a glass-ceramic state. The entire treatment was 48 hours long. In the figure 6 the graph of temperature treatment is exposed.

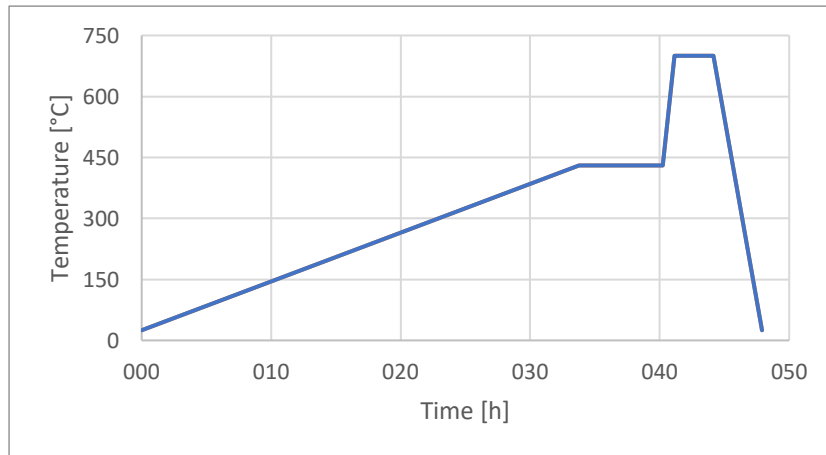


Figure 6: Sintering curve temperature of the first trial

This first treatment did not give good results as the parts melted and were full of cracks. Furthermore, the parts presented a grey colour that is associated to residual carbon in the bodies.



Figure 7: Results of the first trial

The second trial on heat treatment included a maximum sintering temperature lower than the first trial, in fact, after the same de-binding phase, a temperature of 650 °C were reached with the same heating rate and maintained for 3 hours before the cooling stage.

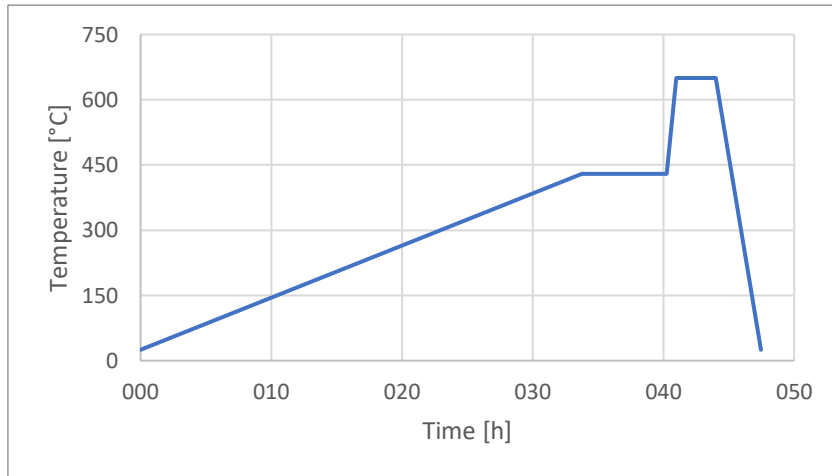


Figure 8: Sintering curve temperature of the second trial

This trial was 47.6 hours long, but the results were still not good enough as the grey colour appeared again on the surface and there were geometry modifications. These results suggested that the de-binding stage was too fast.



Figure 9: Results of the second trial

For the third trial, a step de-binding phase (a succession of increasing and constant phase of temperature) was imposed and a maximum temperature of 650 °C was reached to try to avoid the grey colour surfaces. This trial was 56 hours long and produced the same results as the second trial.

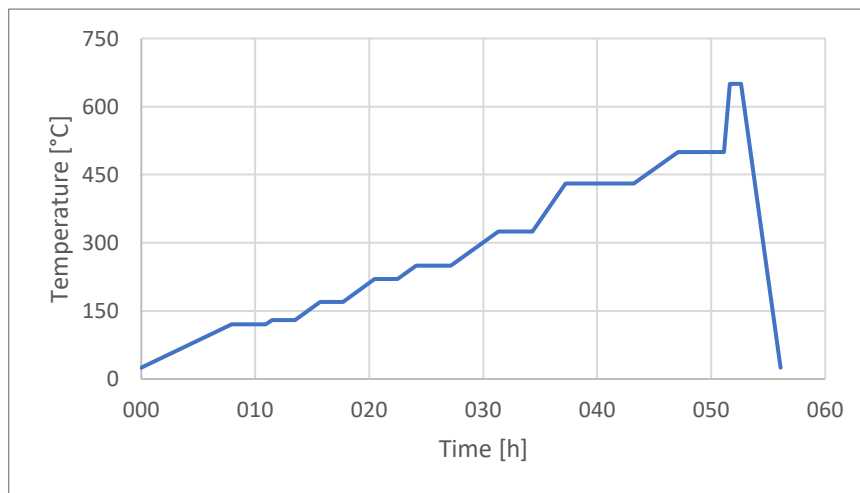


Figure 10: Sintering curve temperature of the third trial



Figure 11: Results of the third trial

Before doing the fourth trial, other tests were approached: the camera-oven heating treatment and the TGA (Thermogravimetric Analysis). The camera-oven test is a test in which the sample is heated in an open oven with a heating curve decided by the user, and a camera takes a photo of the sample every minute. With this test it was noticed that the grey colour appears when the temperature goes over 430 °C. At the end of this test the sample appeared white, and the geometry was kept even if there were some cracks in the structure.



Figure 12: Green bodies after the camera-oven test

The fourth trial presented good results in terms of stability and shape retention. The temperature curve was the same as the third trial but was eliminated the last step at 500°C for 4 hours.

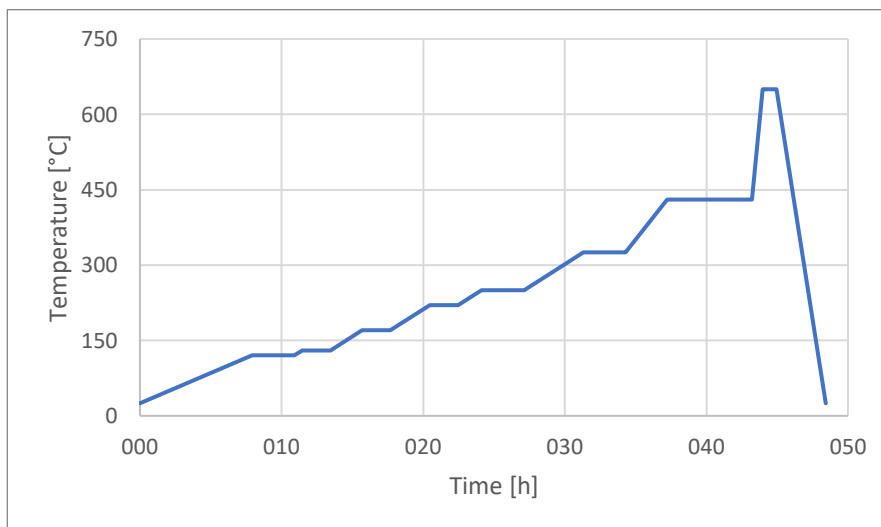


Figure 13: Sintering curve temperature of the fourth trial

3.4 SLURRY CHARACTERIZATION

3.4.1 Viscosity test

In order to optimize the printing parameters for the DLP process, having a good slurry viscosity is an essential aspect. In fact, it's necessary to find a compromise between good mechanical properties of the final product and the ease of printing. High solid load means high density and viscosity and subsequently good mechanical properties but with an increasing printing difficulty.

Viscosity is a physical quantity that measures the resistance of a fluid to slide when a tangential force is applied. If the shear rate is directly proportional to the shear stress (the applied stress) and independent of time the fluid is Newtonian and respects the Newton's law (1).

The tangential stress is:

$$\tau = \frac{F}{S} \text{ (Pa)} \quad (1)$$

Where F (N) is the applied force and S (m²) is the surface in which the force is applied. The viscosity is defined as (2):

$$\eta = \frac{\tau}{\dot{\gamma}} \text{ (Pa}\cdot\text{s)} \quad (2)$$

Where τ is the shear stress (Pa) and $\dot{\gamma}$ is the shear rate (s⁻¹).

If the fluid doesn't obey to the Newton's law, it is called non-Newtonian fluid and the viscosity could exhibit a time-dependent behaviour. Non-Newtonian fluids are divided into [4]:

- **Pseudoplastic fluid** (shear thinning fluids): viscosity decrease under shear stress increasing. For high shear rate values, the viscosity decrease
- **Dilatant fluid** (shear thickening fluid): opposite of dilatant fluid. For high shear stress values the viscosity increase

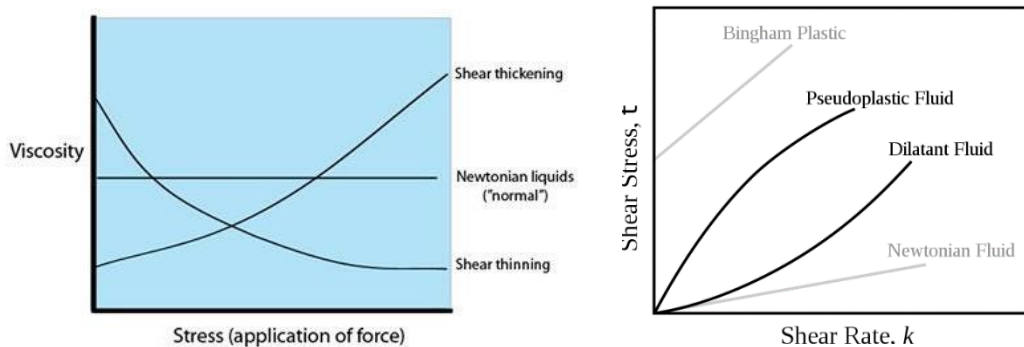


Figure 14: Fluids behaviour in Viscosity vs. Stress and Shear stress vs. Shear rate chart

For the study of the viscosity, two tests could be approached with rheometers that could be used for shear tests and torsional tests. A continuous rotation or a rotational oscillation could be settled to obtain flow

curves or viscosity curves. For rotational tests can be settled two different preset parameters: the shear rate (CSR, controlled shear rate) or the shear stress (CSS, controlled shear stress).

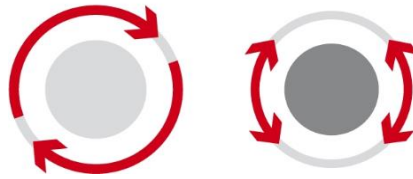


Figure 15: Measuring principle of rheometer for rotational test with continuous rotation (left) and rotational oscillation (right)

From the first test, the rheometer's output is the torque (Nm) that leads to the shear stress, instead for the CSS test, the rheometer's output is the rotational speed (min^{-1}) that allows to calculate the shear rate.



Figure 16: Rheometer used for the viscosity test

Rheological tests are very important to understand the slurry stability over the time and the possibility to the solid load into the slurry to sediment, varying subsequently the viscosity and influencing the printing process. Moreover, is important to continuously check the testing temperature that could influence the viscosity measurements. For the rheological test at Lithoz GmbH was chosen a rotational test in order to better control the viscosity curve and save material, and was performed by the MCR 92 Rheometer, Anton Paar, Italy. [5]

3.4.2 Photorheology test

Photorheology is an instrument for measuring rapid changes in mechanical properties that occur during photopolymerization or photocuring reactions. Through application of small-amplitude, sinusoidal deformations coupled with simultaneous light exposure, rheological properties can be measured in situ without affecting or damaging the sample of interest. [6]

In fact, this test was performed using the same instrument as the viscosity test, with the addition of a UV-light source to the setup. This technique allows to monitoring of modulus changes as well as of sol-to-gel transitions that occur in response to light and, when employed in conjunction with RTFTIR, can be used to relate mechanical properties to degree of chemical conversion. Photorheology has predominantly been applied to systems undergoing simultaneous photopolymerization and chemical cross-linking. [7-9] This approach has been used to characterize the light-responsive behaviour of a variety of materials.

3.4.3 Curing depth test

As described in the previous chapter, the curing depth is defined as the maximum depth at which the slurry modifies its behaviour from visco-plastic to rigid-elastic. This test was performed in the X9.2 machine at Lithoz GmbH and was set an UV-light intensity of 80 mW/cm². On the machine vat was spread a uniform layer of slurry and irradiated in 18 different spots with increasing energy value from 47 mJ/cm² to a maximum energy level of 800 mJ/cm². At the end of the irradiation process the solid spot thickness was measured and thanks to the Jacob's version of Labert-Beer law, the Cd-Energy curve was obtained.

3.4.4 Shrinkage test

The shrinkage factor is an important pre-printing process that determines the volume reduction of the final part after the sintering process. Including this parameter in the pre-set parameters, the printing machine calibrates the required slurry quantity for each layer by itself, offsetting the subsequent contraction of the pieces, in order that the final part dimensions remain those specified from the CAD model. For this test a set of 8 solid cylinders and 4 hollow cylinders was printed.

	<i>Outer diameter (μm)</i>	<i>Inner diameter (μm)</i>	<i>Height (μm)</i>
<i>Solid cylinders 1</i>	2		10
<i>Solid cylinders 2</i>	3		10
<i>Hollow cylinders</i>	4	2	6

Table 2: Design specifications of green bodies for the shrinkage test



Figure 17: Virtual Tray of the cylinders set for the shrinkage test

The green bodies were measured in order to obtain the real dimension of the pieces and then subjected to the sintering process, following the sintering program of the fourth trial. Once the sintering ends, the final parts were measured again to evaluate the contraction percentage.

3.5 SCAFFOLD DESIGN & PRINTING JOB

For this work of thesis, in order to obtain a 3D porous matrix like the architecture of cancellous bone, a CAD file from a 45 ppi commercial polymeric sponge μ -CT images was used. The import process of the images was already done by Lithoz in the past years, so the geometry used was already done. However, thanks to the InVesalius software, it was possible to recreate the 3D cubic profile of the sponge, with high porosity rate, and then modify it in order to obtain a cylindrical shape with an aspect ratio of 2:1 (5mm x 10mm). This structure would be too fragile, so a contour offset was added, and the thickness of the structure was increased by 40% leading to a decreasing of the internal porosity. Moreover, the energy value was increased during the trials.

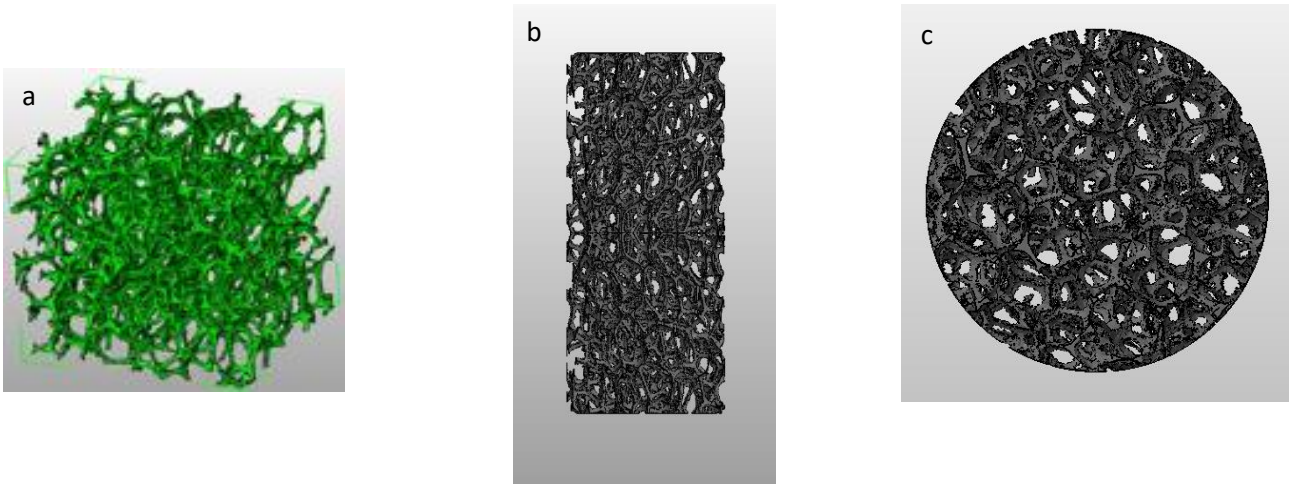


Figure 18: CAD model of the (a) polymeric cubic sponge and (b,c) porous cylindric sponge with aspect ratio 2:1

The used setup in the printing machine CeraFab 7500 for the printing process was a DLP system that uses a LED source in the blue visible region. Before printing the vat glass conditions are checked in order to eliminate every type of scratch or damage that could negatively affect the light beam, and so the photopolymerization of the layers. A UV-sensitive primer was spread on the building platform surface in order to increase the adhesion with the first layer of the structure. Figure 19 shows the Lithoz CeraFab Control tray for porous scaffold job.

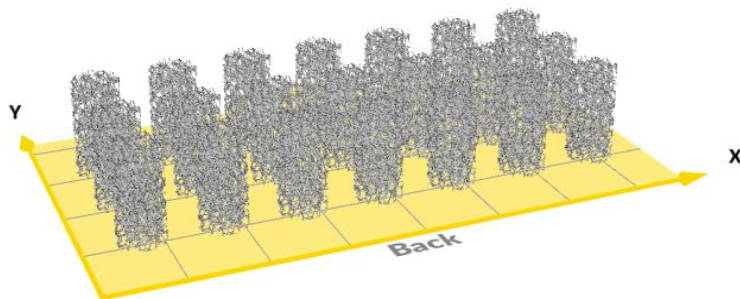


Figure 19: Lithoz CeraFab Control virtual tray showing the porous scaffold printing job

Every job counts the printing of 21 scaffolds; the entire work at Lithoz GmbH counts a total of 76 printed scaffolds.

Due to the high difficulty of the job, the shrinkage compensation (S.C.xy=1.258 and S.C.z=1.437) was directly added to the CAD model, in fact we can see in the parameters a shrinkage compensation of 1, so the machine exactly replied the CAD geometry. Moreover, the DLP energy was increased from 200 mJ/cm² to 400 mJ/cm² due to the high fragility of the scaffolds.

	Parameters	Value
General Job	Layer height	25 μm
	Slurry height	200 μm
	Shrinkage compensation XY	1
	Shrinkage compensation Z	1
	Pixel alignment	Yes
	Contour offset	40 μm
Adhesive Layer	Coat	
	Rotation speed	80 °/s
	Angle of rotation	1080°
	Contact	
	Viscosity offset	10
	Tilt up speed	12 °/s
	Settling time	120 s
	Expose	
	Use DLP instead of backlight	Yes
	DLP energy	400 mJ/cm ²
DLP intensity	71.3 mW/cm ²	
Backlight exposure time	2 s	
First Starting Layer & Other Starting Layers (5 layers)	Coat	
	Rotation speed	80 °/s
	Angle of rotation	1080°
	Contact	
	Viscosity offset	10
	Tilt up speed	12 °/s
	Settling time	60 s
	Expose	
	Use DLP instead of backlight	No
	DLP energy	400 mJ/cm ²
DLP intensity	71.3 mW/cm ²	

Table 3: Main parameters for the printing job

3.6 SCAFFOLD CHARACTERIZATION

3.6.1 X-Ray Diffraction

The X-Ray analysis is a non-destructive technique for the surface characterization e structural analysis of the sample and allows to obtain information about the crystalline structure, about the surface layer and is a qualitative analysis of the stress state of the material. X-Rays are high energy electromagnetic radiations with a wavelength between 10⁻⁹ and 10⁻¹² m. When an electromagnetic radiation interacts with the substance, some phenomenon can occur:

- Reflection of the light
- Transmission
- Diffraction
- Absorption

The diffraction consists in the wave propagation direction change when it hits a slit with dimensions like the electromagnetic wave wavelength. When a X-Ray beam hits a solid material with crystalline structure, it produces the electrons vibration, which emits a electromagnetic radiation with a wavelength λ in all directions. Diffused waves can interact in a destructive or constructive way. This condition is described by the Bragg's Law:

$$n\lambda = 2d_{khl}\sin\theta$$

Where n indicates the reflection order, λ is the x-rays wavelength, d is the interplanar distance and θ is the incident angle.

When the X-rays reach the surface of the sample, they are processed and counted to produce a diffraction spectrum according to position 2θ . Since each material has a unique set of d-spaces, the conversion of diffraction peaks into d-spaces allows the identification of the material [10]. Generally, d-spaces are compared with standard reference models. The device used to determine the diffraction spectrum and to analyse the crystalline structures of the materials is called X-ray diffractometer.

Standard X-ray diffractometers are based on the Bragg-Mentano scheme, where the X-ray source position is fixed and sample and detectors turn around with an angular frequency of θ/min^{-1} and $2\theta/\text{min}^{-1}$. [11]

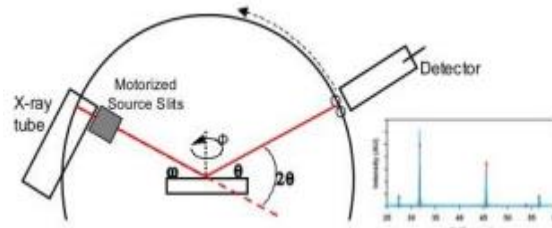


Figure 24: Schematic representation of the Bragg-Mentano diffractometer

3.6.2 Morphological analysis

3.6.2.1 Scanning Electron Microscopy (SEM)

The electron microscopy is a technique that use the interaction between an electron beam and the sample's atoms. The electrons have shorter wavelength than photons and this allows to create images with higher resolution than the optic microscopy, reaching atomic resolution. From the electrons source, when the thermic electrons energy reaches the material source emission energy, the electrons are accelerated and attracted to an anode with positive charge.

The SEM is composed of:

- Electron source
- Lens column
- Detectors that collect the signal from the interaction between the electron beam and the sample
- Stage for the sample
- Vacuum system

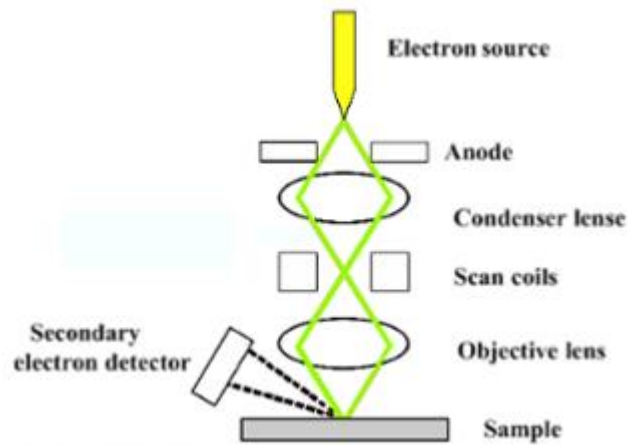


Figure 22: Schematic SEM representation

The interaction of the electron beam generates different types of electrons, photons or irradiations. For the SEM, two types of electron are generated in order to use them for imaging: backscattered electrons (BSE) and secondary electrons (SE). The first ones, are generated due to the elastic collision between the electron beam and the sample. The SE are generated by the sample atoms and are the result of an anelastic interaction between the beam and the sample. The BSE comes from a deeper region of the sample instead of the SE that comes from a more superficial zone of the sample as shown in figure, and display more detailed information about the sample surface. In some microscopes, are revealed X-ray too. These are generated from the electron-matter and allows an elementary analysis of the sample in terms of energy spectrums that leads to a compositional analysis.

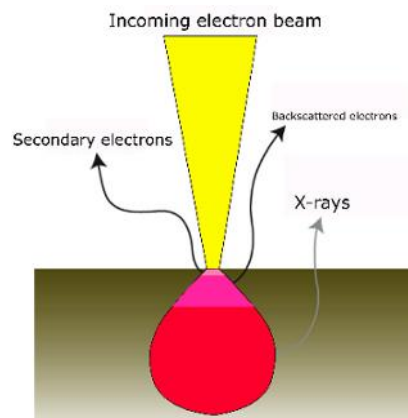


Figure 23: Different types of electrons generated by the electron beam

The SEM-EDS analysis allows to obtain both a qualitative and semi-quantitative analysis of the sample, and thanks to the EDS spectrometers is possible to acquire the complete emission spectrum and differentiate the elements and their proportions that constitute the sample. [10]

3.6.2.2 μ -CT

The X-ray microtomography system allows to analyse trabecular samples with a spatial resolution in the order of 50 μ m and can provides both qualitative and quantitative information on the 3D morphology of the sample. In the μ -CT scanning the specimen is divided into a series of 2D slices which are irradiated with X-rays . The irradiation is attenuated by the sample and the emergent X-ray is captured by a detector array. From the detector measurements, the X-rays path is calculated and the attenuation coefficients are derived, obtaining a reconstruction of the 2D pixel map. The quality of the pixel map depends on the scanning resolution.[12,13]

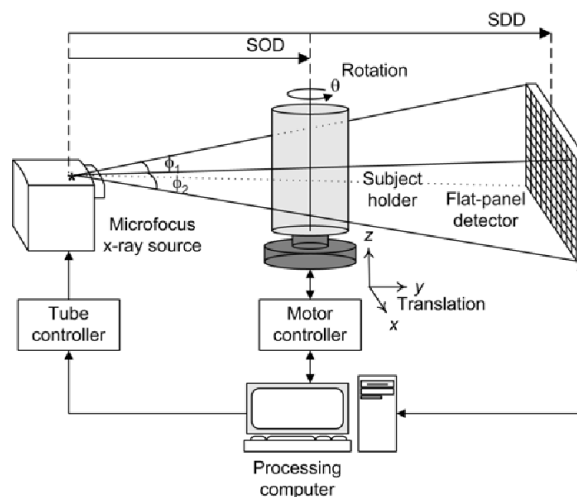


Figure X: micro-CT setup for the bioglass scaffold porosity characterization

3D modelling program is then used to create 3D models from the 2D slice stack and obtain a visualization of the complex structure of the scaffold thanks to the possibility to digitally isolate every geometric structure of the sample. In contrast with the medical CT, for the scaffold analysis the X-rays source and detector position is fixed and the sample spin over a moveable platform.

The flexibility of micro-CT allows the evaluation of foam-like scaffold like the these produced via DLP-based stereolithography and provides an optimal characterization method of the structure porosity.[14] It is possible to evaluate the entire volume and surface of the sample, with a specific view on the pore size, shape and position as well as wall thickness. It is also possible to recreate the total pores volume inverting the threshold and then derive the interconnectivity. [15]

3.6.3 Mechanical tests

Mechanical tests allow studying the material behaviour under applied loads. The main stresses are the traction, the shear stress and the compression. Scaffolds were subjected to uniaxial compression perpendicular to the bases of the cylindrical specimen. This test is very important because one of the key tasks of the scaffold is to ensure the load transfer at which the bone is constantly subjected. The scaffold compression strength is given as:

$$\sigma = \frac{P}{A}$$

Where σ is the compressive strength in MPa, P is the load in N and A is the contact surface (i.e., resistant cross-sectional area) with the load in mm².

This test was performed by using the MTS Criterion Model 43 setup imposing a load application velocity of 0.5 mm/s to 22 samples. These samples were manually treated before in order to obtain a perfect parallelism between the two bases. The results were next analysed by the software MTS TestSuite.

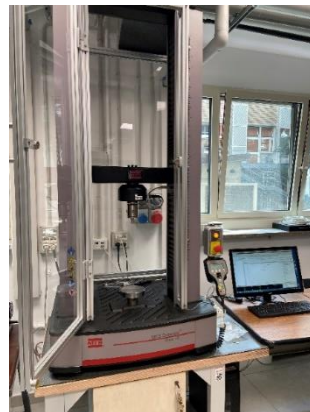


Figure 20: Compression test setup

3.6.3.1 Determination of Weibull's modulus

Generally, the results of fracture tests are reported in terms of mean value +/- the standard deviation of the failure stresses and so an average strength. This doesn't represent an objective measure of the inherent strength because σ_i depends on the test mode and on the volume or the area under the stress.[16] In order to face this problem, it is a common technique to interpret the results on the basis of the distribution:

$$P(\sigma) = 1 - \exp \left[-\left(\frac{\sigma}{\sigma_N}\right)^m \right]$$

Where $P(\sigma)$ is the failure probability, σ_N is the nominal strength and m is the shape parameter. These last two parameters can be obtained by the failure probability fit. The procedure consist of a least-square fit of the linearized version of the Eq.X:

$$\ln\{-\ln[1 - P(\sigma)]\} = -m \ln(\sigma_N) + m \ln(\sigma)$$

Which yields an approximate number for the shape parameter and for the nominal strength. [17]

The Weibull modulus determination counts 3 steps:

- **Step 1:** Estimate the cumulative failure probability from the stress data. The failure stresses must be ordered in ascending order and the failure probability must be assigned like:

$$P_i = \frac{(i - 0.5)}{n}$$

Where n is the number of samples (22) and $i=1,2,\dots,n$

- **Step 2:** fit the $\ln\{-\ln[1 - P_i]\}$ vs. $\ln(\sigma_i)$ data points to a straight line.
- **Step 3:** from the equation of the straight line, obtain the Weibull parameters.

3.6.3.2 Determination of the fracture energy

The fracture energy per unit volume E_v is defined as the necessary energy to deform the sample from the unloaded condition to the failure strain ε_f , and was calculated by the analysis of the area under the stress-strain curve until the breaking point as [18]:

$$E_v = \int_0^{\varepsilon_f} \sigma(\varepsilon) d\varepsilon$$

3.6.4 Bioactivity test

Scaffold bioactivity was tested *in-vitro* by immersing them in Simulated Body Fluid (SBF) solution in order to evaluate the apatite formation on the scaffolds surface and obtain a correlation with the *in-vivo* bone bioactivity. The test was carried out for five different period of time: 24 h, 48 h, 7 days, 15 days and 1 month. Before starting the test, 1 L of SBF was prepared following the Kokubo protocol [19] and checking the pH of the solution once the scaffold ends their test. For every time window, three scaffolds were tested. The bioactivity test was conducted under specific conditions: for every sample was calculated the exact amount of SBF as:

$$V_{sol} = \frac{M_{sample}}{1.5}$$

Where V_{sol} is the SBF volume in mL necessary for testing a sample of mass M (mg). The mass-to-liquid ratio of 1.5 mg/mL is commonly adopted for *in vitro* bioactivity test in SBF when specimens with high surface area are testes, including powders and porous scaffolds [20]. Moreover, the samples are subjected to an orbital movement with a velocity of 100 rpm and at a temperature of 37 °C. The test was led without any refresh of the solution. In the Table 4 the reagents (all purchased from Sigma-Aldrich) necessary for the preparation of the SBF are shown.

Order	Reagent name	Formula	Amount
1	Sodium chloride	NaCl	8.035 g
2	Sodium hydrogen carbonate	NaHCO ₃	0.355 g
3	Potassium chloride	KCl	0.225 g
4	di-potassium hydrogen phosphate trihydrate	K ₂ HPO ₄ · 3H ₂ O	0.231 g
5	Magnesium chloride hexahydrate	MgCl ₂ · 6H ₂ O	0.311 g
6	1M Hydrochloric acid	HCl	39 mL
7	Calcium chloride	CaCl ₂	0.292 g
8	Sodium sulfate	Na ₂ SO ₄	0.072 g
9	Tris-hydroxymethyl aminomethane	Tris	6.118 g
10	1M Hydrochloric acid	HCl	0-5 mL

Table 4: Reagents for 1000 mL of SBF solution

The SBF solution replicates the human plasma blood ions concentration as shown in the figure below:

Ion	Ion concentrations (mM)	
	Blood plasma	SBF
Na ⁺	142.0	142.0
K ⁺	5.0	5.0
Mg ²⁺	1.5	1.5
Ca ²⁺	2.5	2.5
Cl ⁻	103.0	147.8
HCO ₃ ⁻	27.0	4.2
HPO ₄ ²⁻	1.0	1.0
SO ₄ ²⁻	0.5	0.5
pH	7.2-7.4	7.40

Figure 21: Ion concentration of SBF in comparison with those in human blood plasma [18]

References

- [1] A. R. L. Francisco, "User guide CeraFab 7500," *J. Chem. Inf. Model.*, vol. 53, no. 9, pp. 1689–1699, 2013.
- [2] A. D. Lantada, A. De Blas Romero, M. Schwentenwein, C. Jellinek, and J. Homa, "Lithography-based ceramic manufacture (LCM) of auxetic structures: Present capabilities and challenges," *Smart Mater. Struct.*, vol. 25, no. 5, 2016.
- [3] I. Potestio, "Lithoz: How lithography-based ceramic AM is expanding the opportunities for technical ceramics," *Powder Inject. Mould. Int.*, vol. 13, no. 2, pp. 2–5, 2019.
- [4] "<https://it.wikipedia.org/wiki/Viscosit%C3%A0>" [Online]. [Accessed:10-May-2022]
- [5] "<https://wiki.anton-paar.com/it-it/fondamenti-della-reologia/#rotational-tests>" [Online]. [Accessed:10-May-2022].
- [6] "Photorheology and Gelation during Polymerization of Coordinated Ionic Liquids" Ria D. Corder, Sumner C. Dudick, Jason E. Bara, and Saad A. Khan, *ACS Applied Polymer Materials* 2020 2 (6), 2397-2405, DOI: 10.1021/acscpm.0c00343
- [7] Chiou, B.-S.; Khan, S. A. Real-Time FTIR and in Situ Rheological Studies on the UV Curing Kinetics of Thiol-Ene Polymers. *Macromolecules* 1997, 30 (23), 7322–7328.
- [8] Chiou, B.-S.; Raghavan, S. R.; Khan, S. A. Effect of Colloidal Fillers on the Cross-Linking of a UV-Curable Polymer: Gel Point Rheology and the Winter-Chambon Criterion. *Macromolecules* 2001, 34, 4526–4533.
- [9] Gorsche, C.; Harikrishna, R.; Baudis, S.; Knaack, P.; Husar, B.; Laeuger, J.; Hoffmann, H.; Liska, R. Real Time-NIR/MIR-Photorheology: A Versatile Tool for the in Situ Characterization of Photopolymerization Reactions. *Anal. Chem.* 2017, 89 (9), 4958– 4968.]
- [10] "Microscopia elettronica da banco" [Online]. Available:<https://www.microscopiaelettronica.dabanco.it/come-funziona-il-sem> [Accessed: 05-May-2022]
- [11] "Diffrazione di raggi X in polvere(XRD)."[Online]. Available:https://serc.carleton.edu/research_education/geochemsheets/techniques/XRD.html. [Accessed:06-May-2022].
- [12] Feldkamp LA, Goldstein SA, Parfitt AM, Jesion G, Kleerekope M. The direct examination of three-dimensional bone architecture in vitro by computed tomography. *J Bone Min Res* 1989;4:3–11.
- [13] Weiss P, Obadia L, Magne D, Bourges X, Rau C, Weitkamp T, et al. Synchrotron X-ray microtomography (on a micro scale) provides three-dimensional imaging representation of bone ingrowth in calcium phosphate biomaterials. *Biomaterials* 2003;24:4591–601
- [14] Saey Tuan Ho, Dietmar W. Hutmacher, "A comparison of micro CT with other techniques used in the characterization of scaffolds", *Biomaterials*, Volume 27, Issue 8, 2006, Pages 1362-1376, ISSN 0142-9612
- [15] Wang F, Shor L, Darling A, Khalil S, Sun W, Guceri S, et al. Precision extruding deposition and characterization of cellular poly ϵ -caprolactone tissue scaffolds. *Rapid Prototyping J* 2004;10(1):42–9]
- [16] D. Green, *An Introduction to the Mechanical Properties of Ceramics*, Cambridge Univ. Press, New York (1998)76]
- [17] Claude A. Klein, "Characteristic strength, Weibull modulus, and failure probability of fused silica glass", *Optical Engineering* 48(11), 113401 (November 2009)]76.
- [18] Kenesei P., Kádár C., Rajkovits Z., Lendvai J., The influence of cell-size distribution on the plastic deformation in metal foams, *Scripta Mater.*, 2004, 50, 295-300.
- [19] *Biomaterials* 27 (2006) 2907–2915," How useful is SBF in predicting in vivo bone bioactivity?", Tadashi Kokubo, Hiroaki Takadama. Received 6 September 2005; accepted 13 January 2006
- [20] Macon et al, *J Mater Sci Mater Med* 2015

4 RESULTS & DISCUSSION

During the period in Lithoz, the rheological behaviour of the 47.5BG-slurry was studied in order to obtain information about its viscosity. Thanks to the study of its photo-rheological behaviour, a better understanding about its stiffness and viscosity modulus was given. The tests about the sintering program, shown in the previous section, conducted to the choice of the best thermal treatment to obtain porous structures with the best mechanical features. Moreover, the curing depth test was approached with the aim of finding the best UV beam energy to print with the Lithoz DLP system CeraFab 7500. Afterwards, at the DISAT laboratories of the Politecnico di Torino, the scaffolds morphology and composition were evaluated by X-ray, SEM and EDS analysis. In order to understand the maximum scaffolds load strength, the compression tests were approached. From the mechanical tests were derived information about the Young's modulus, Weibull modulus and about the fracture energy. Moreover, the in-vitro bioactivity was evaluated by soaking the scaffolds in SBF for 5 different time periods and evaluating the formation of the HA layer on the surface of the scaffold, essential for the osteogenic process of new bone.

1.1 SLURRY CHARACTERIZATION

1.1.1 Viscosity test

The viscosity test of the 47.5BG Slurry was carried out with an RCM Rotational Rheometer, setting a constant shear rate of 100 s^{-1} and a rotational time of 2 minutes at room temperature ($T=25 \text{ }^{\circ}\text{C}$). The average viscosity, when the shear rate is constant after the first transitory period (30 s), was recorded equal to 5.52 Pa.s.

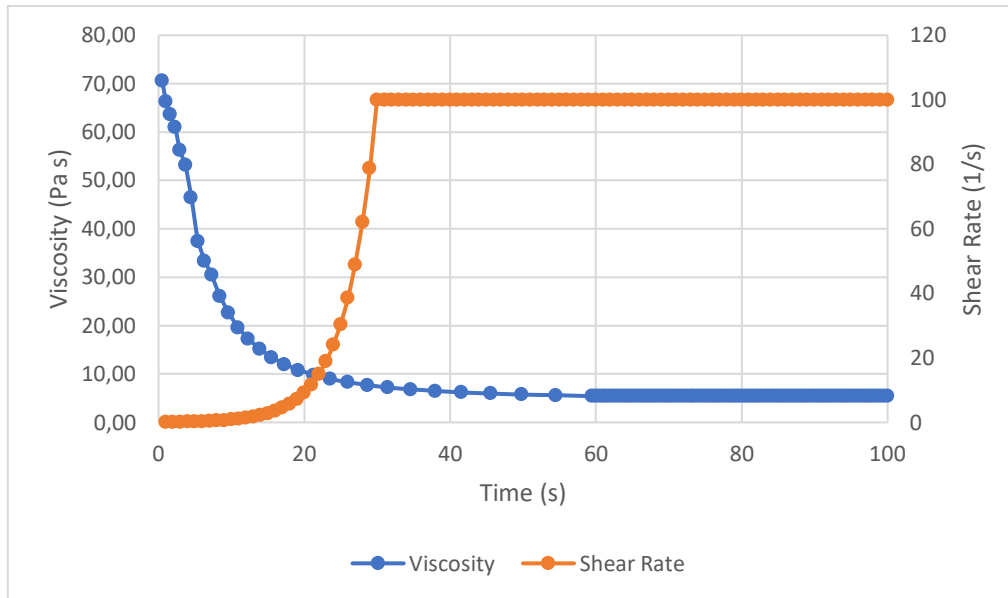


Figure 1: Graph illustrating 47.5BG slurry viscosity vs. time “Viscosity test”

The relationship between viscosity and shear rate in the first 30 s of the test, where the shear rate increases and the viscosity decreases, highlights a pseudoplastic behaviour of the slurry. Moreover, these results are comparable to other materials used by Lithoz for other DLP job. They display a viscosity between 5 and 12 Pa·s but in different test conditions: shear rate of 50 s⁻¹ and T=20°C.[1]

Viscosity is important for optimization of the printing process: if the viscosity is too high, printing of complex structures like microporous scaffolds could be difficult. Viscosity is directly correlated to the solid load in the slurry composition, in fact, the more the solid load in the slurry, the higher the viscosity. For having a more reliability of the test, other viscosity tests could be approached varying the temperature, the solid load and the shear rate, in order to make a comparison between the different conditions and have a wide slurry composition range of choices for DLP printing.

1.1.2 Photo-rheology test

In order to analyse the slurry reaction to the photopolymerization, the photo-rheology test was carried out 6 times for a time period of 2'55". This test, despite the variability of the results, allow obtaining the maximum stiffness of the material (50684 kPa) and the curing speed as shown below.

For this test, the slurry sample was subjected to a constant shear stress of 250 kPa and exposed to the UV-light of 80 mW/cm² after 30 seconds from the beginning of the test. The best results were given from the sample 2 and 5, that show a similar trend to the ideal one in which the storage (elastic) modulus G' , once the maximum is reached, is maintained constant in the time. In the graph below is shown the trend of every test.

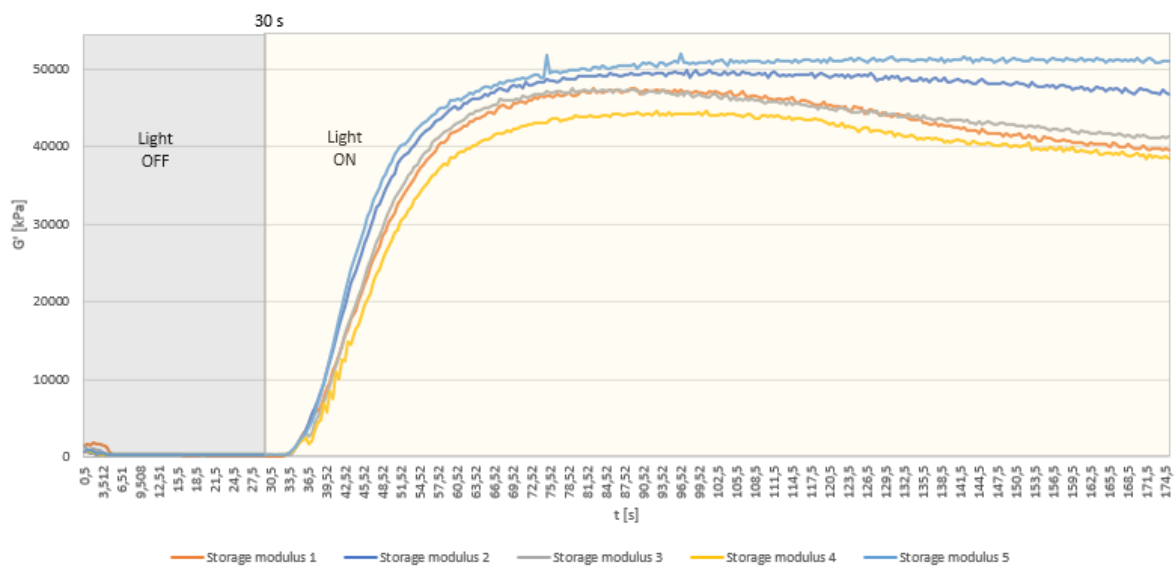
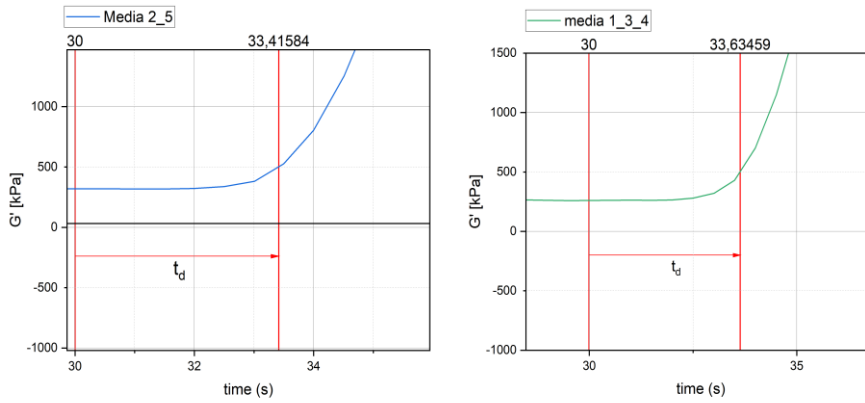


Figure 2: Storage modulus G' vs time of the 5 photo-rheology tests.

Moreover, the delay time and the curing speed were evaluated for the two sets of samples.

The first one, also called gelation time, is a measure of the necessary time of the material to reach the gel point from the onset of the UV-light irradiation. It depends on the binder, in fact, the two delay times are almost equal as shown in the graph below.



The curing speed (R_p) is the G' first derivative in time and gives an indication about the maximum DLP energy in order to obtain the best mechanical properties from the material. In fact, from the maximum R_p value, it is possible to calculate the energy necessary to the written before purpose. The maximum value of curing speed is reached after 11'' from the UV-light onset and this, knowing the intensity value of the light, allows to obtain an energy of 881.6 mJ/cm^2 .

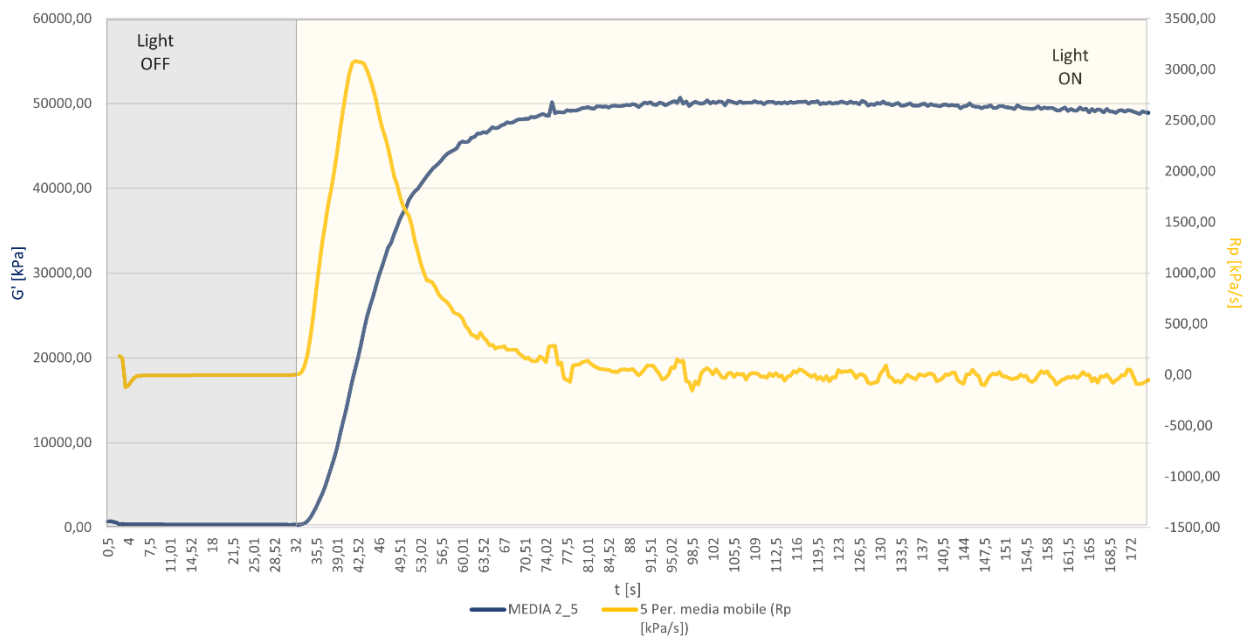


Figure 3: Storage modulus and curing speed during time graph

The rheological time sweep experiment output includes one more quantity over G' : the viscous/loss modulus G'' . Generally, for a typical solution, G'' dominates on G' ; but for gels the inverse situation typically takes place. Analysing the relationship between G' and G'' it is possible to evaluate the gelation rate thanks to the complex shear modulus defined as:

$$G^* [kPa] = \sqrt{(G'')^2 + (G')^2}$$

and from the ratio:

$$\frac{G''}{G'}$$

Rapid growth in time of G^* and high values of it indicate that the material gel faster with a consequently energy reduction. Moreover, from the ratio value it is possible to comprehend how elastic, if $G''/G' < 1$, or plastic, $G''/G' > 1$, a material is.[2-4] The graph below shows the trend of G^* and of the ratio G''/G' .

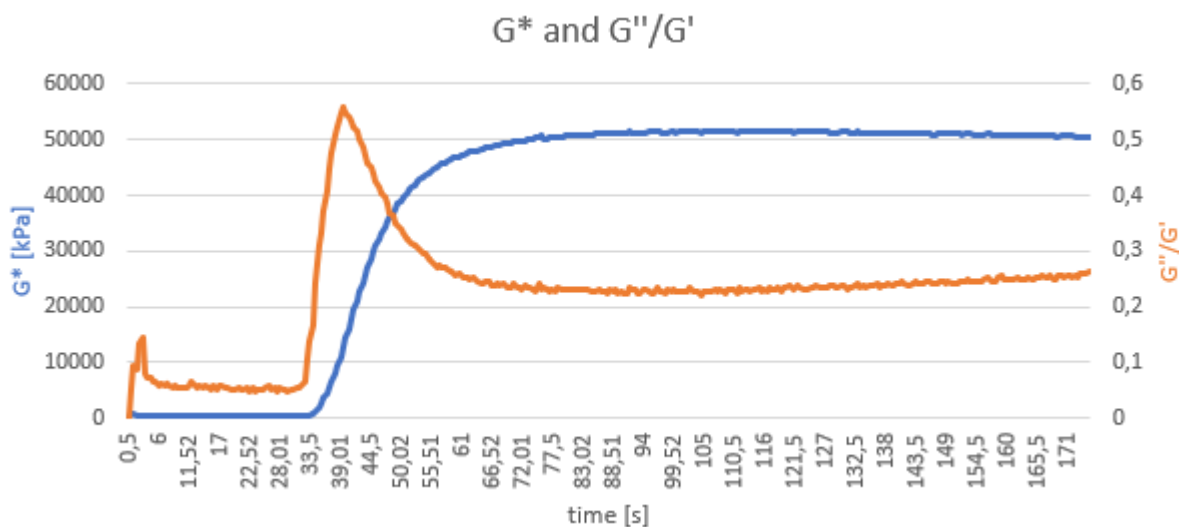


Figure 4: G^* vs time and G''/G' vs time graph showing the elastic behaviour of the slurry under photopolymerization

1.1.3 Curing depth test

With the curing depth test is investigated the maximum depth at which the slurry modifies its behaviour from visco-plastic to rigid-elastic. The test was performed setting an UV-light intensity of the machine of 80 mW/cm² and irradiating the slurry in 18 different spots with increasing energy (calculated on a grey scale).

The 18 plates were measured after, and the results are presented below:

Machine: X9.2			Intensity: 80 mW/cm ²			
Energy [mJ/cm ²]	800	411	220	122	72	47
Curing depth [μm]	300	223	183	122	93	/
	298	222.5	176	120	84	/
	292	224.5	173	132	71	/

Table 1: Parameters of the curing depth test

It is noteworthy that for an energy of 47 mJ/cm² it was not possible to calculate the curing depth because the three plates were too fragile and they broke right after the end of the test.

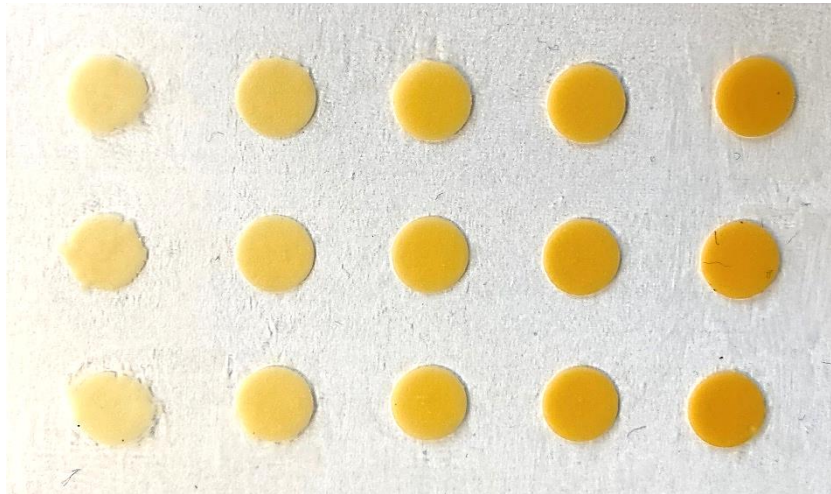


Figure 5: Plates obtained after the curing depth test where it can be seen that those in the first column were irradiated by a 800 mJ/cm² energy and those in the last one by an energy of 72 mJ/cm².

Thanks to the Lambert-Beer law with these results, it was possible to obtain the Cd-Energy curve shown below.

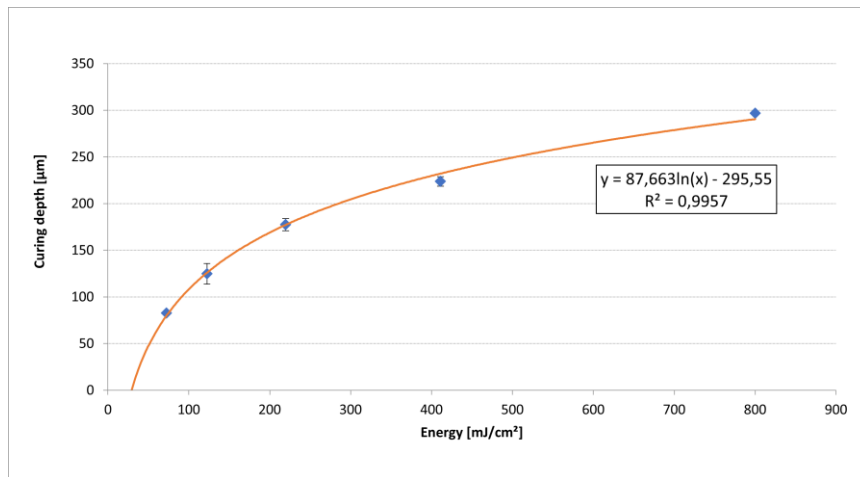


Figure 6: Cd-Energy logarithmic curve

1.2 CHARACTERIZATION OF POROUS SCAFFOLDS

The green bodies in the image below were thermally treated with the last sintering trial with a sintering temperature of 650 °C and 76 porous cylindrical scaffolds were obtained from the printing process.

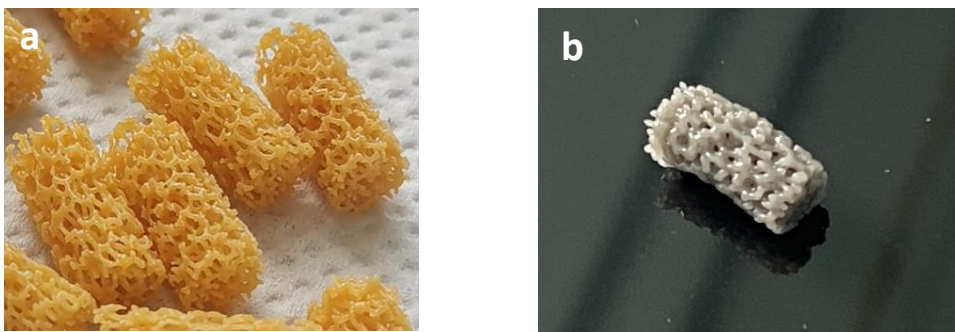


Figure 7: Green bodies (a) before and (b) after the sintering process

Next, they were morphologically and compositionally analysed by SEM and XRD analysis, evaluating their macroporosity and the presence of a crystalline phase.

1.2.1 Porosity

The total porosity P (vol.%) was assessed by the calculation of mass-to-volume ratio using the apparent density and the bulk density.

$$P = \left(1 - \frac{\rho}{\rho_0}\right) * 100$$

where ρ is the apparent density and ρ_0 is the bulk density.

The calculation was performed considering the 24 scaffolds used for the mechanical test, and has been obtained a total porosity (vol.%) P of $34.48 \pm 5,57$. This value is much lower than the porosity of an ideal scaffold which should have above 50 vol.% of porosity [5]. This range would have been achieved if in the processing phase the structure general thickness had not been increased to deal with softening problems. From μ -CT analysis it was possible to calculate the average pores diameter on the scaffold surface.

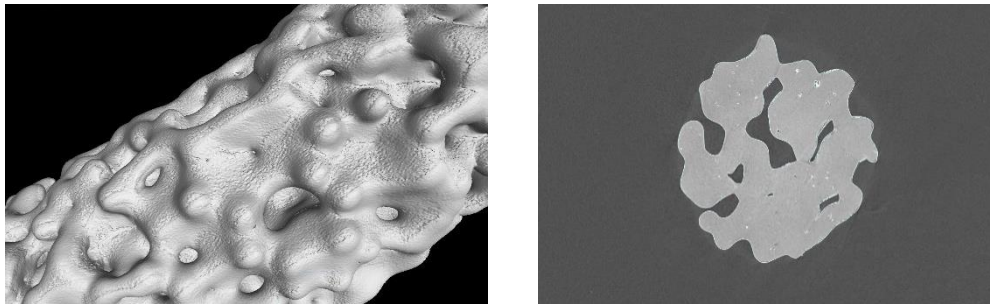


Figure 8: μ -CT images of the as-such scaffold (a) surface and (b) slice from the scan that shows pores interconnectivity.

The best pores size for bone regeneration is considered to be between 200 – 500 μm ; for the as-such scaffold was calculated an average pore size of **150 – 600 μm** that perfectly fit the size range for vascularisation, mineralization and formation of new bone tissue. [6-8]

1.2.2 XRD

For the XRD analysis, a scaffold after sintering was crushed in order to obtain fine powder and was analysed by using a PANalytic diffractometer with Bragg-Brentano chamber for the identification of the crystalline phases in the sample. In the Figure 9 are shown both the XRD patterns obtained from the analysis of the powders before the sintering process and after. It can be seen how, before the heating treatment, the material is in an amorphous state but after the sintering process at 650 °C for 1 h, some low-intensity diffraction peaks are detected, suggesting the formation of crystalline phases (main peaks in the range 32°-35°). However, the material still is predominantly amorphous, as confirmed by the “amorphous broad halo” that is well visible in the 25-35° range.

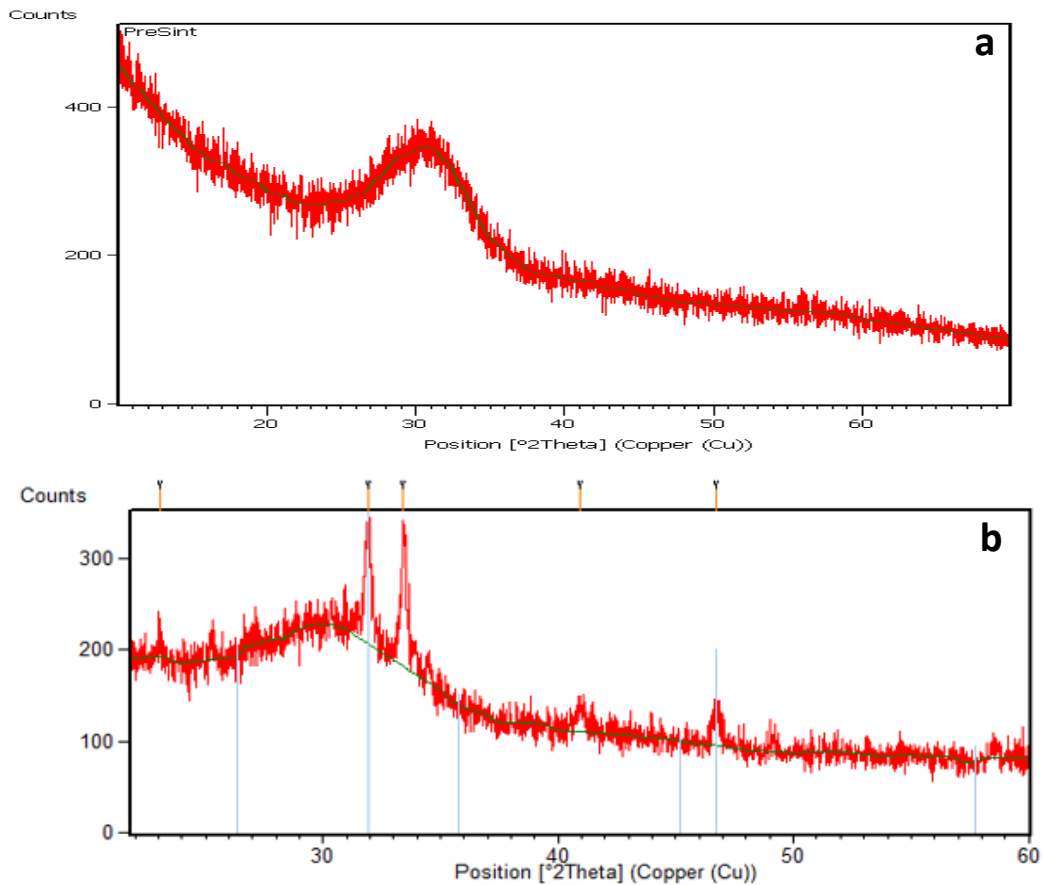
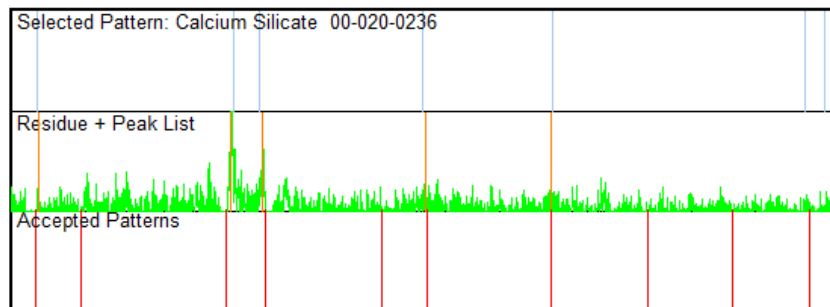


Figure 9: XRD patterns of (a) pre-sintering process powders and (b) after.

The detected peaks are related to the formation of the Calcium Silicate (Ca_2SiO_4) crystalline phase (Ref.code: 00-020-0236) after the sintering process and in the *Figure 8* below its spectrum is compared to



the sintered scaffold one.

Even if in other studies it's reported that the presence of a crystalline phase could decrease the bioactivity ability to form HA on the scaffold surface [9] , this doesn't affect the bioactivity in-vitro test, in *Section 4.5*, that show excellent results.

1.3 MECHANICAL TESTS

For the evaluation of the scaffold mechanical properties, the compression test was approached. The sample was fixed between the fixed platform and the moveable load. A constant velocity of 1 mm/min was imposed to the moveable load and the stress-strain plot was obtained for the 22 samples.

Is reported an example of the stress-strain curve obtained from the compression test in which can be seen a multi-peaks profile, typical of brittle cellular materials like porous glasses.[10] This profile reflects the sequential fracture of the inner trabeculae of the scaffold during the compression, which generate the peaks in the curve.

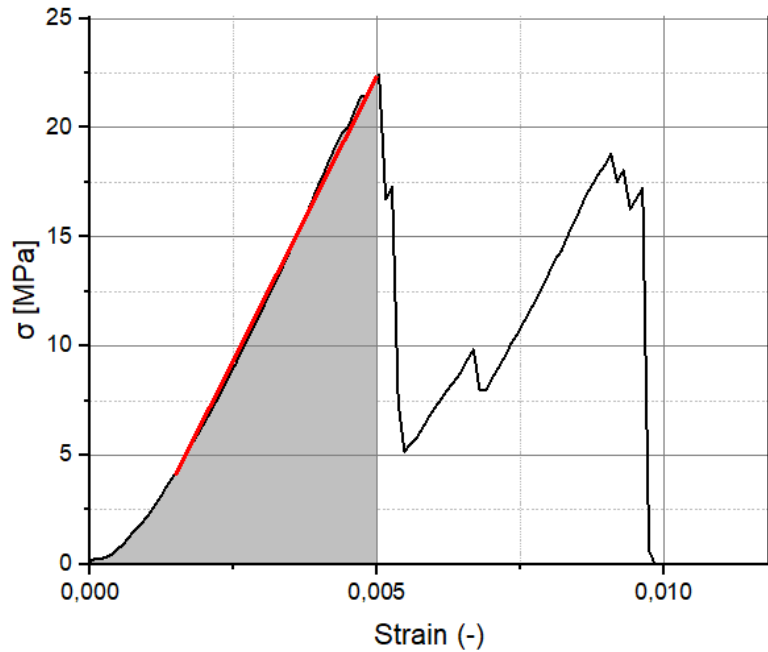


Figure 10: stress-strain curve of 47.5B scaffold. The red line is the fitting used for the Young's modulus calculation and the grey area under the curve is the one used for the fracture energy analysis

The curve start with a positive slope until the first peak that correspond to the first trabeculae cracking. This induce a decreasing of the stress (negative slope) but the material is still able to sustain the load and so, we can see another positive slope. The repetition of this behaviour results in the formation of the serrated profile, typical of foam-like material. [11-14] The ultimate negative slope occurs when also the stronger trabecula cracks and the failure of the scaffold happens. The scaffolds elastic modulus was 4.79 ± 0.1 GPa, reflects the order of the cortical bone, was calculated in the first linear region of the curve before of the first peak.

The scaffold compressive strength was 21.9 ± 6.2 MPa, a little bit higher than the standard references for trabecular bone (2-12 MPa).[15] This could be related to the increase of the trabeculae thickness during the printing process, done in order to avoid breaking phenomena in the sintering process. As said in the *Chapter 3.5* the structure thickness was increased by 40% thus leading to lower porosity but an increasing in the mechanical properties of the final scaffolds.

The Weibull modulus is a key mechanical parameter for evaluating the scaffold reliability. There are few studies reporting the Weibull modulus for other glasses composition or other production techniques; in one of these, the same glass was printed by robocasting, obtaining an m value of 3.1 and a Weibull scale parameter $\sigma_0=0.14$ [16]. Higher values of m , 3 to 9, were obtained in compression tests of hydroxyapatite scaffold [18-20], and $m=4$ and $m=6$ for glass-ceramic foams produced from $\text{SiO}_2\text{-CaO-Na}_2\text{O-Al}_2\text{O}_3$ (SCNA) glass [17] and 45S5 Bioglass powders [21] respectively. In this study was obtained a Weibull modulus of 3.9 and a related Weibull scale parameter $\sigma_0=23.4$ MPa determined by knowing the intercept of the linear fit (-12.3).

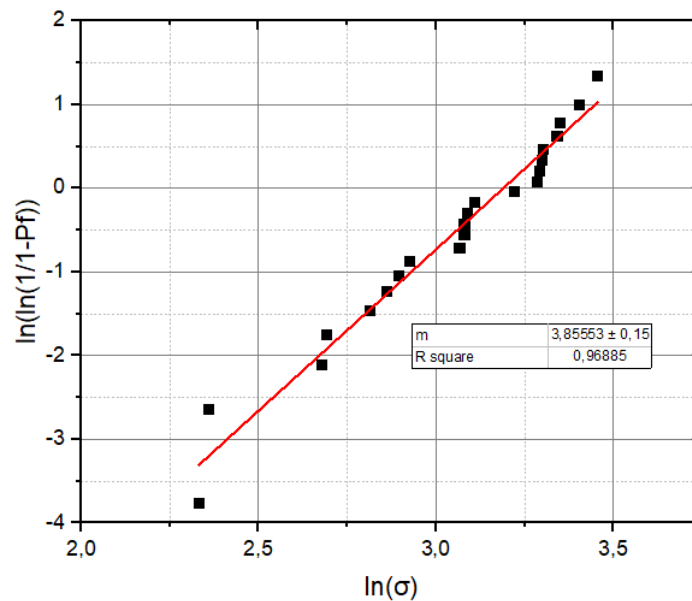


Figure 11: Weibull plot of the experimental data and linear interpolation.

The fracture energy of the scaffolds was 71.07 ± 33.48 kJ/m³; this parameter is hard to find in literature for glass-derived scaffolds, so it makes a comparison really difficult to carry out. An energy value of 150 kJ/m³ was found out for glass scaffold produced by the burn-off method [22] and a higher value of 544 kJ/m³ for $\text{SiO}_2\text{-CaO-Na}_2\text{O-Al}_2\text{O}_3$ -based glass-ceramic scaffolds produced via sponge replication.[17]

1.4 BIOACTIVITY TEST

The bioactivity *in vitro* test was performed without any refresh of the solution on 15 scaffolds, 3 samples for each time period, in order to obtain a minimum number to assess a statistical approach of the results. In the table below, the test parameters are shown:

Number of scaffolds	Test duration	Temperature [°C]	Movement [rpm]
3	28 days	37.5	100
3	14 days	37.5	100
3	7 days	37.5	100
3	48 hours	37.5	100
3	24 hours	37.5	100

The pH value of the SBF solution was checked once the tests ended for every sample solution and was observed a rapid increase in the first 24 hours and a more constant increasing of the value during the residual period of immersion and a settling down at the plateau value of about 7.71 ± 0.008 as shown in the plot below.

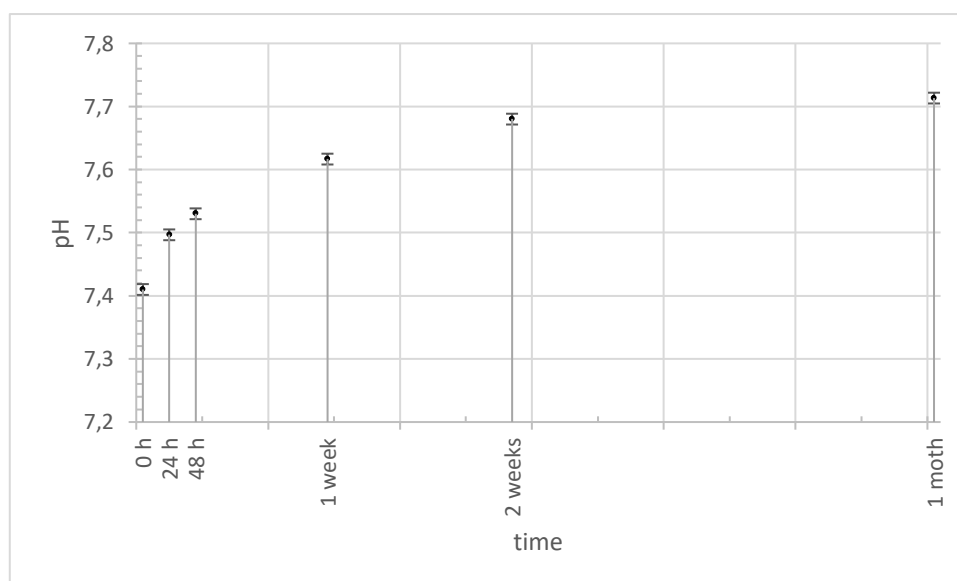


Figure 12: pH trend during the entire bioactivity test period

This pH value falls within the range (< 7.9) in which the osteogenic differentiation of the cells is not affected; therefore, the moderate alkaline environment is beneficial for the beginning and continuation of the osteogenic process. [23]

Morphological and semi-quantitative analysis were approached by X-rays, SEM and EDS analysis, evaluating the formation of the hydroxyapatite layer on the surface. By comparing the samples before and after soaking in SBF, it can be seen that two new peaks are revealed in the 14 days soaked sample. These wide and short peaks are typical of crystalline hydroxyapatite (Ref.code: 00-001-1008) at 2θ position of 26° and 32° and referred to the (0 0 2) and (2 1 1) reflections, respectively. The peaks became wider and shorter after 1 month of soaking in SBF, confirming the formation of a crystalline hydroxyapatite layer on the scaffold surface.

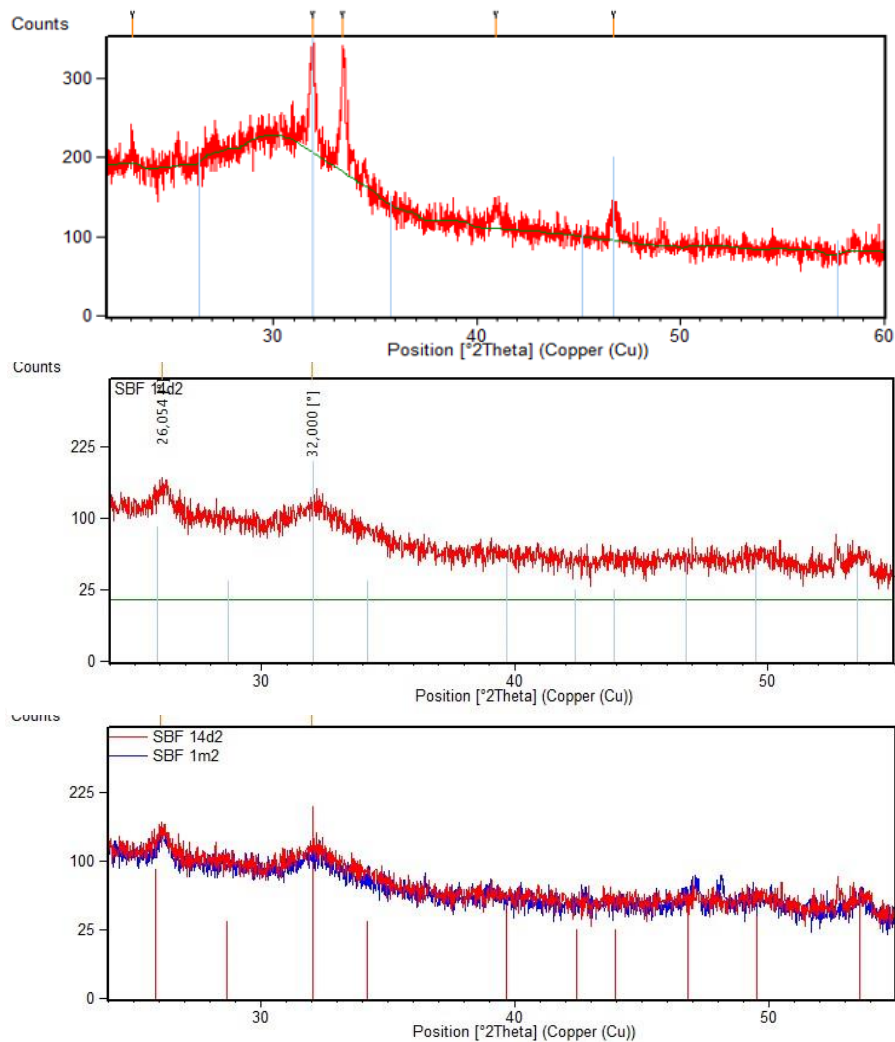


Figure 13: XRD spectra of as-such scaffold, 14 days in SBF and 28 days in SBF

SEM topographic shows the formation of the HA layer following the 5-step bioactivity process proposed by Hench.

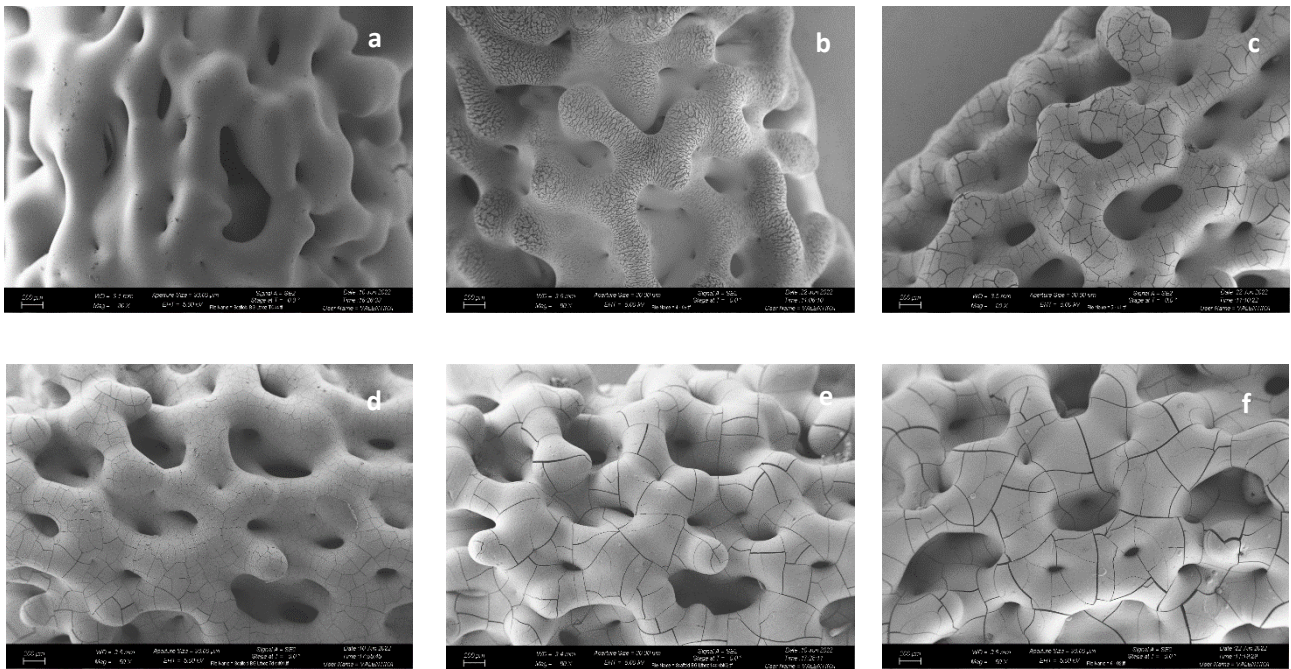


Figure 14: low magnification (80x) SEM images of (a) as-such scaffold, and soaked in SBF for (b) 1 day, (c) 2 days, (d) 7 days, (e) 14 days and (f) 28 days. Scale bar 200 μm

At low magnification it is possible to see the cracked surface due to the formation of the silica gel layer during the first days of soaking and the smoothing during the immersion period. At 30k x magnification it is possible to see, in the first days of soaking, the HA nuclei show a not-round shape.

Already after 2 days of soaking they grow up and join together forming the typical “cauliflower” shape, typical of the bone-like apatite. The surface is then levelled after 1 month.

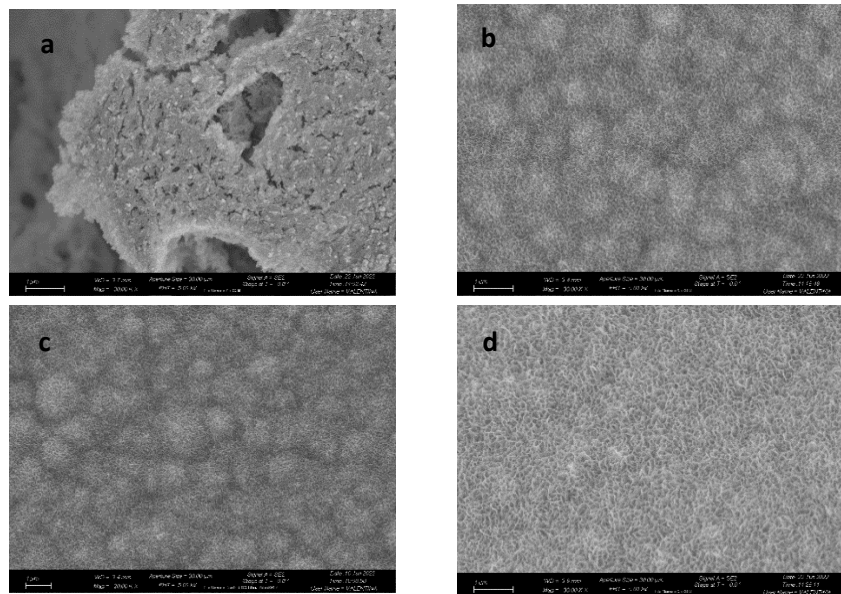


Figure 15: 30kx magnification SEM images of (a) 1 day, (b) 2 days, (c) 1 week and (d) 1 month soaked in SBF. Scale bar 1µm

The Ca/P ratio, assessed by the energy dispersive spectroscopy (EDS) analysis, was stable around at 1.4 after been soaked for 1 month in SBF, under the theoretical value of stoichiometric HA (1.67). This is coherent with other in vitro studies on the scaffold bioactivity that show a Ca-deficient HA layer on the surface.[24,25]

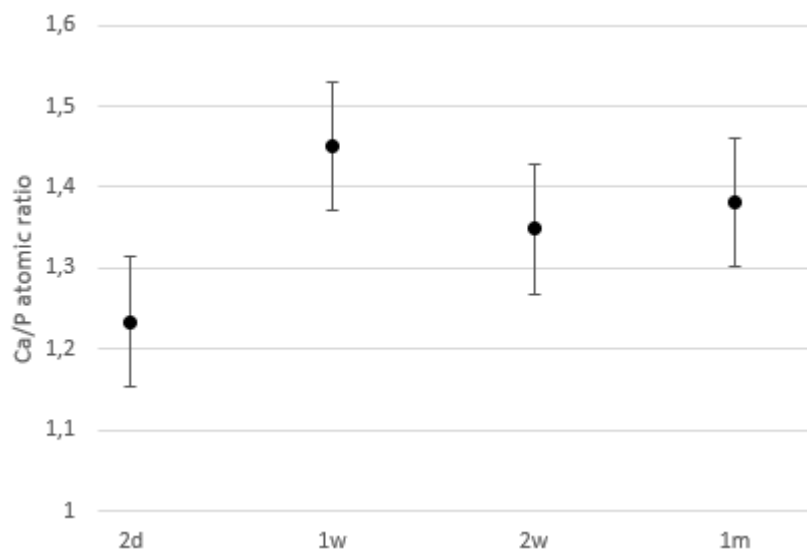


Figure 16: Ca/P ratio variation during in vitro bioactivity test

Moreover, the other compositional ions (Si, Mg, Na and K) atomic percentage decreased over time and were slightly detectable during compositional analysis at 1 month. This confirms the formation and thickening of the HA layer on the surface with no contamination of external agents. The EDS spectra are reported below for the 1 day-soaked, 2 weeks and 1 month samples with their relative summary table.

Element	Atomic %		
	<i>1 day</i>	<i>14 days</i>	<i>28 days</i>
<i>Si</i>	4.15	0	0
<i>Ca</i>	11.69	9.32	7.46
<i>Mg</i>	1.14	0.84	0.67
<i>P</i>	7.44	6.15	5.70
<i>Na</i>	1.17	/	0.43
<i>K</i>	0.38	/	/

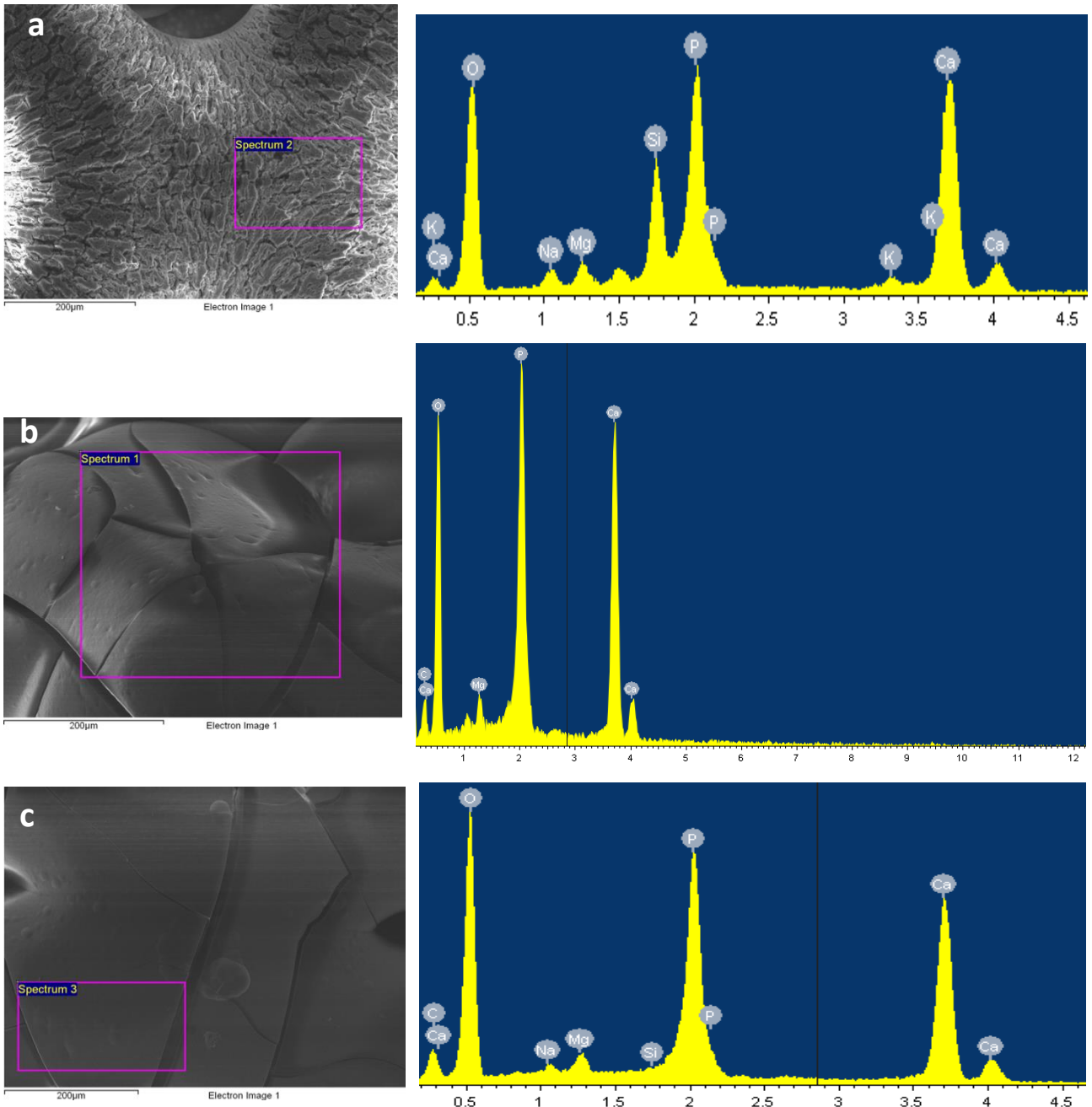


Figure 17: EDS spectra and related calculation area for the samples at (a) 1 day, (b) 2 weeks and (c) 1 month soaked in SBF

The new HA layer, and its thickening during the time, is also possible to see from μ -CT images of the scaffold section that also show the different density of the HA gel (inner) and crystalline layer (outer) on the surface. Additionally, calculation on the pore size of the soaked scaffold display a decreasing of it from 200-500 μm of the as-such sample, to **50-500 μm** for the scaffold after 14 days in SBF and lastly, **30-450 μm** after 28 days soaking.

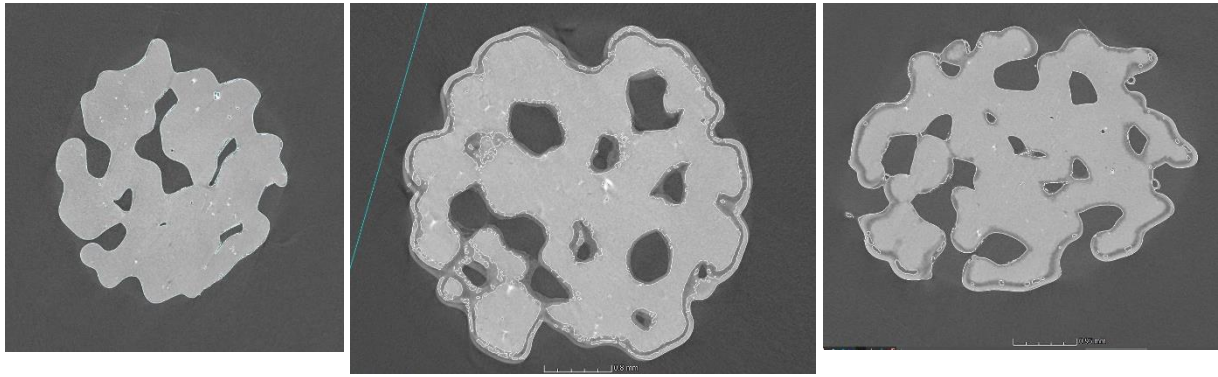


Figure 18: μ -CT section of (a) as-such scaffold, (b) 14 days of immersion and (c) 28 days of immersion in SBF.

References

- [1] https://www.lithoz.com/application/files/7416/3273/1351/LITHOZ_Materialfolder_EN_web.pdf
- [2] <https://www.stevenabbott.co.uk/practical-rheology/G-Values.php>
- [3] Photorheology and Gelation during Polymerization of Coordinated Ionic Liquids Ria D. Corder, Sumner C. Dudick, Jason E. Bara, and Saad A. Khan ACS Applied Polymer Materials 2020 2 (6), 2397-2405 DOI: 10.1021/acsapm.0c00343]
- [4] Chambon, F.; Winter, H. H. Linear Viscoelasticity at the Gel Point of a Crosslinking PDMS with Imbalanced Stoichiometry. *J. Rheol.* 1987, 31 (8), 683–697].
- [5] Karageorgiou V, Kaplan D. Porosity of 3D biomaterial scaffolds and osteogenesis. *Biomaterials.* 2005 Sep;26(27):5474-91. doi: 10.1016/j.biomaterials.2005.02.002. PMID: 15860204.
- [6] “Normal Bone -Bone Research Society.” <https://boneresearchsociety.org/resources/gallery/12/#top>. [Accessed: 12/07/22]
- [7] R. A. Perez and G. Mestres, “Role of pore size and morphology in musculo-skeletal tissue regeneration,” *Mater. Sci. Eng. C*, vol. 61, pp. 922–939, 2016
- [8] R. Z. LeGeros, “Properties of osteoconductive biomaterials: Calcium phosphates,” *Clin. Orthop. Relat. Res.*, no. 395, pp. 81–98, 2002
- [6] Filho O. P., La Torre G. P., Hench L. L. Effect of crystallization on apatite-layer formation of bioactive glass 45S5. *Journal of Biomedical Materials Research.* 1996;30(4):509–514. doi: 10.1002/(sici)1097-4636(199604)30:4<509::aid-jbm9>3.0.co;2-t
- [7] Gibson L.J., Modelling the mechanical behavior of cellular materials, *Mater. Sci. Eng. A*, 1989, 110, 1-36.
- [8] Mohammad J. Mirzaali, J. Jakob Schwiedrzik, Suwanwadee Thaiwichai, James P. Best, Johann Michler, Philippe K. Zysset, Uwe Wolfram, “Mechanical properties of cortical bone and their relationships with age, gender, composition and microindentation properties in the elderly”, *Bone*, Volume 93, 2016, Pages 196-211, ISSN 8756-3282, <https://doi.org/10.1016/j.bone.2015.11.018>.]
- [9] Vitale-Brovarone C., Baino F., Verné E., High strength bioactive glass-ceramic scaffolds for bone regeneration, *J. Mater. Sci. Mater. Med.*, 2009, 20, 643-53.
- [10] Vitale-Brovarone C., Baino F., Bretcanu O., Verné E., Foam-like scaffolds for bone tissue engineering based on a novel couple of silicate-phosphate specular glasses: Synthesis and properties, *J. Mater. Sci. Mater. Med.*, 2009, 20, 2197-205.
- [11] Poologasundarampillai G., Lee P.D., Lam C., Kourkouta A.M., Jones J.R., Compressive strength of bioactive sol-gel glass foamscaffolds, *Int. J. Appl. Glass Sci.*, 2016, 7, 229-37.
- [12] D. Tomas, S. Saroash, H.R. Graham, Apatite glass-ceramics: a review, *Frontiers in Materials* 3 (2017) (article 59). [21] M.C. Crovace, M.T. Souza, C.R. Chinaglia, O. Peitl, E.D. Zanotto, Biosilicate®-amultipurpose, highly bioactive glass-ceramic. In vitro, in vivo and clinical trials, *J. Non-Cryst. Solids* 432 (2016) 90–110. [22] M. Wang, Bioactive glasses and glass-ceramics, in: D. Shi (Ed.), *Biomaterials and Tissue Engineering*, Springer-Verlag, Berlin Heidelberg New York, 2004, pp.27–40 (Chapter 1.3)]
- [13] Barberi, J., Nommeots-Nomm, A., Fiume, E., Verné, E., Massera, J., & Baino, F. (2019). Mechanical characterization of pore-graded bioactive glass scaffolds produced by robocasting. *Biomedical Glasses*, 140–147. <https://doi.org/10.1515/bglass-2019-0012>
- [14] Baino F., Vitale-Brovarone C., Mechanical properties and reliability of glass-ceramic foam scaffolds for bone repair, *Mater. Lett.*, 2014, 118, 27-30.

- [15] Miranda P., Pajares A., Saiz E., Tomsia A.P., Guiberteau F., Mechanical properties of calcium phosphate scaffolds fabricated by robocasting, *J. Biomed. Mater. Res. A*, 2008, 85, 218-27.
- [16] Martínez-Vázquez F.J., Perera F.H., Miranda P., Pajares A., Guiberteau F., Improving the compressive strength of bioceramic robocast scaffolds by polymer infiltration, *Acta Biomater.*, 2010, 6, 4361-8.
- [17] Shanjani Y., Hu Y., Pilliar R.M., Toyserkani E., Mechanical characteristics of solid-freeform-fabricated porous calcium polyphosphate structures with oriented stacked layers, *Acta Biomater.*, 2011, 1788-96.
- [18] Bairo F., Fiume E., Mechanical characterization of 45S5 bioactive glass-derived scaffolds, *Mater. Lett.*, 2019, 245, 14-7
- [19] Bretcanu O., Bairo F., Verné E., Vitale-Brovarone C., Novel re-sorbable glass-ceramic scaffolds for hard tissue engineering: From the parent phosphate glass to its bone-like macroporous derivatives, *J. Biomater. Appl.*, 2014, 28, 1287-303.[
- [20] Laurent-Emmanuel Monfoulet, Pierre Becquart, David Marchat, Katleen Vandamme, Marianne Bourguignon, Elodie Pacard, Véronique Viateau, Herve Petite, and Delphine Logeart-Avramoglou “The pH in the Microenvironment of Human Mesenchymal Stem Cells Is a Critical Factor for Optimal Osteogenesis in Tissue-Engineered Constructs”, *Tissue Engineering Part A* 2014 20:13-14, 1827-1840]
- [21] Karageorgiou, V.; Kaplan, D. Porosity of 3D biomaterial scaffolds and osteogenesis. *Biomaterials* 2005, 26, 5474–5491. [CrossRef] [PubMed]
- [22] Chatzistavrou, X.; Newby, P.; Boccaccini, A.R. Bioactive glass and glass-ceramic scaffolds for bone tissue engineering. In *Bioactive Glasses: Materials, Properties and Applications*; Woodhead Publishing: Cambridge, UK, 2011; Volume 3, pp. 107–128. ISBN 9781845697686].

5 CONCLUSIONS & FUTURE DEVELOPMENT

This thesis project has been carried out in collaboration with Lithoz GmbH (Wien, Austria) and then in DISAT laboratory of the Politecnico di Torino (Turin, Italy), in order to obtain and characterized porous ceramic scaffolds which can simulate the porous structure of the cancellous human bone. Using the CeraFab 7500 system based on DLP process, 76 porous cylindrical scaffolds were printed. During the period in Lithoz, much work has been dedicated to the study of the slurry behaviour (47.5BG-slurry) and its characterization. In particular, slurry viscosity ($\eta=5.52 \text{ Pa}\cdot\text{s}$ at $T=25 \text{ }^\circ\text{C}$) and photo-rheological properties were evaluated. Moreover, the curing depth test was approached to assess the optimal UV beam energy for the printing process. Were also conducted test on the post processing step, especially for the sintering treatment. 4 possible treatments were analysed, choosing the one which that allows the mechanical properties and shape maintenance. Microstructural, compositional, and morphological characterization of the scaffolds was carried out at the DISAT laboratory of the Politecnico di Torino. Before the sintering, the scaffold was in an amorphous state, however, after the heat treatment, Calcium Silicate (Ca_2SiO_4) was the only crystalline phase detected by X-ray diffraction (XRD). Scanning Electron Microscopy (SEM) morphological analysis revealed the presence of interconnected macropores in the range 200-800 μm . Mechanical tests were approached on 22 samples in order to evaluate the scaffolds mechanical properties. A compression load test was performed, obtaining the stress-strain plot and giving the possibility to achieve information about the Young's modulus ($4.79 \pm 0.1 \text{ GPa}$), the compressive strength ($21.9 \pm 6.2 \text{ MPa}$), the fracture energy ($71.07 \pm 33.48 \text{ kJ/m}^3$), the Weibull modulus of 3.9 and its scale parameter $\sigma_0=23.4 \text{ MPa}$. The in-vitro bioactivity of the scaffolds was, furthermore, evaluated by soaking the samples in SBF solution for 5 different times (24 hours, 48 hours, 7 days, 14 days and 28 days) in order to evaluate the HA formation on the surface. SBF solution replicates the human plasma blood ions concentration, simulating the in-vivo bone bioactivity. SEM analysis have proved the presence of a HA layer on the scaffold surface already after 24 hours of immersion, and the typical "cauliflower" shape after 14 days. From the EDS analysis it was possible to verify the thickening of the HA layer during the time; thanks to the spectra that shown an increasing of the Ca and P peaks (final Ca/P ratio of 1.4) and a decreasing of any other elements peaks. The formation of the HA layer

was also confirmed by the X-rays analysis that display the presence of the two characteristics peaks of crystalline hydroxyapatite after 14 days of soaking in SBF.

On the basis of these reported results, further studies and in-depth analysis deserve to be carried out in order to optimize the DLP printing process and the solid load-binder ratio into the slurry composition in order avoid structural defects and shape troubles related to the sintering process. Moreover, study the scaffold permeability could be very helpful for a better understanding over the relationship between the scaffold pores interconnectivity and the osteogenesis process after implantation.

Ringraziamenti

I primi ringraziamenti vanno al Professor Francesco Baino e alla Professoressa Enrica Verné per avermi dato la possibilità di svolgere questo lavoro di tesi per me di grande stimolo e interesse; per essere sempre stati estremamente disponibili e per avermi sempre fornito grande supporto sin dal primo giorno.

Un enorme grazie va inoltre a tutte le persone del DISAT che mi hanno accompagnato, aiutato e supportato durante tutto il periodo di lavoro. In particolare, vorrei ringraziare Daniele per la grande disponibilità, l'aiuto che costantemente ha sempre dimostrato e per il bel rapporto che si è instaurato.

Vorrei ringraziare, inoltre, il Dr. Martin Schwentenwein per avermi dato la possibilità di poter lavorare in un ambiente efficiente e stimolante come Lithoz. L'esperienza trascorsa in azienda mi ha fatto crescere sia dal punto di vista professionale che da quello umano.

Un grazie particolare va a Joana che con estrema pazienza, grande disponibilità e professionalità, mi ha supportato per tutto il periodo di lavoro in Lithoz. Il suo aiuto e i suoi consigli sono stati fondamentali.